International Communications in Heat and Mass Transfer 125 (2021) 105341

Contents lists available at ScienceDirect

International Communications in Heat and Mass Transfer

journal homepage: www.elsevier.com/locate/ichmt

Role of hybrid-nanofluid in heat transfer enhancement – A review

M. Muneeshwaran [a,b], G. Srinivasan [c], P. Muthukumar [c,*], Chi-Chuan Wang [a,b,*]

[a] Department of Mechanical Engineering, National Yang Ming Chiao Tung University, Hsinchu 300, Taiwan
[b] Department of Mechanical Engineering, National Chiao Tung University, Hsinchu 300, Taiwan
[c] Department of Mechanical Engineering, Indian Institute of Technology –, Guwahati, Assam, India

ARTICLE INFO

Keywords:
Hybrid nanofluids
Synthesis
Mono nanofluids
Thermophysical properties
Heat transfer enhancement
Heat transfer applications

ABSTRACT

The promising thermophysical properties of mono nanofluids show great potential in various heat transfer applications. The properties of mono nanofluids can be tailored by varying the proportion/concentration of the nanoparticles. However, the mono nanofluids, employing only single-type nanoparticles (metallic or non-metallic), revealed the stable thermophysical properties in the limited range. To tailor this shortcoming, in recent years, hybrid nanofluids have been synthesized to improve the base fluid's thermophysical properties and heat transfer characteristics. In this paper, a state-of-the-art review on the use of hybrid nanofluid in various heat transfer applications is presented. The first part of the article summarizes the existing research works on the preparation and synthesis of various hybrid nanocomposites and hybrid nanofluids. Subsequently, density, specific heat, viscosity, and thermal conductivity values of different hybrid nanofluids are tabulated, serving as a database. The collection of thermophysical properties correlations is also presented. The later part of the article covers the hydrothermal behavior of hybrid nanofluids in various heat transfer applications such as heat exchangers, heat sinks, heat pipes, solar panels, natural convection enclosures/cavities, air conditioning systems, impingement jet cooling, thermal energy storage, and boiling-related applications. In addition, the Nusselt number and friction factor correlations are tabulated for different heat transfer applications. Finally, the challenges associated with hybrid nanofluids and future research scopes are presented.

1. Introduction

Science and technology have made continuous growth and significant advancements in every aspect of human activity, including power generation [1,2], heating and cooling, electronics [3,4], manufacturing industries [5], biomedical applications [6], food industries [7], and pharmaceutical industries [8]. Effective thermal management is necessary for the reliable and efficient operation of these thermal systems [9]. The exponential growth in manufacturing capabilities and the miniaturization of components dramatically increased the power density (i.e., heat flux), which challenges the existing cooling technologies. In the past, extensive research works have been carried out to augment the heat transfer rate via various active or passive techniques such as extended surfaces [10,11], vortex generators [12], multiphase cooling [13,14], mini and microchannels [15,16], porous media [17], and natural convection techniques [18,19]. Even though the above methods have provided a considerable heat transfer augmentation, the low thermal conductivity of working fluid (e.g., water, ethylene glycol) limits their heat transfer capability. Alternatively, improving thermophysical properties of the working fluid can greatly augment the heat transfer. Hamilton and Crosser [20] introduced the concept of enhancing the thermal conductivity of base fluid by dispersing the micro-sized solid particles. The coagulation issue associated with the micro-sized particles has deterred its usage in practical applications. Later, Choi and Eastman [21] introduced nanofluids in which the nanoparticles are dispersed in base fluid to prevent agglomeration and enhance thermal conductivity. Adding surfactants in nanofluids can significantly reduce the agglomeration issue. In nanofluids preparation, single nanoparticles (e.g., Au, Ag, Cu, Al_2O_3, CuO, TiO_2, SiO_2, Fe_3O_4, SiN, SiC, CNT, MWCNT, graphite, diamond) are dispersed in base fluid (e.g., water, ethylene glycol, a mixture of water and ethylene glycol, transformer oil, Polymer solutions). This type of fluid is referred to as mono nanofluid (MoNF) [22–25]. A further examination of various nanoparticles reveals that the metal particles (e.g., Ag, Cu, Au) have high thermal conductivity and less chemical inertness and stability; whereas, the metal oxide particles (e.g., Al_2O_3, CuO) exhibit greater stability but offer lower thermal conductivity. The facts mentioned above indicate that the MoNF can provide either higher thermal

* Corresponding author at: Department of Mechanical Engineering, National Yang Ming Chiao Tung University, Hsinchu 300, Taiwan.
E-mail addresses: pmkumar@iitg.ac.in (P. Muthukumar), ccwang@nctu.edu.tw (C.-C. Wang).

https://doi.org/10.1016/j.icheatmasstransfer.2021.105341

conductivity or better stability in one go [26–31]. However, most of the engineering applications require a trade-off among the several characteristics of mono nanofluids. A new kind of fluid called hybrid nanofluid (HyNF) is developed to harvest the blend of favorable features of various nanoparticles in a single fluid. In HyNF, two or more nanoparticles are thoroughly mixed in the base fluid to attain good thermophysical and rheological properties. The composition of metal and metal oxide particles is mostly dispersed in the base fluid. Through the combination of metal and metal oxide nanoparticles, hybrid nanofluid can attain the synergistic effect of high thermal conductivity and better chemical inertness and stability [32–35].

The use of mono nanofluids in heat transfer applications is extensively studied and reviewed by numerous researchers. The concept of using hybrid nanofluids is relatively new, and recently, it gained more research attention. Limited reviews on the HyNF applications are reported. Moreover, the previous review articles described the synthesis and preparation methods of selected HyNFs, and they are more focused on very few applications, namely heat exchanger-related applications. Besides, the thermophysical properties database for the collection of HyNFs is not available in the open literatures. Therefore, in this review article, synthesis and preparation techniques of various HyNF are presented along with their thermophysical properties database. Then, the widely adopted relationships for estimating density, specific heat, viscosity, and thermal conductivity are summarized. The use of hybrid nanofluids in a range of heat transfer applications is comprehensively reviewed, including heat exchangers, heat sinks, heat pipes, photovoltaic modules, natural convection enclosures, refrigeration and air-conditioning systems, boiling applications, jet impingement cooling systems, and thermal energy storage systems. Finally, the challenges associated with HyNF and the future research directions are discussed.

2. Preparation and synthesis of nanofluids

Advancement in fabrication techniques has enabled the preparation of nano-sized particles. The nanoparticles of less than 100 nm offer better mechanical, thermal, optical, magnetic, and electrical properties. This enhancement is attributed to the higher surface area to volume ratio due to a larger cluster of atoms at the grain boundaries [21]. MoNF is the mixture of the base fluid and a single type of nanoparticle; whereas, the HyNF is the mixture of the base fluid and two or more types of nanoparticles. The performance of hybrid nanofluids depends on the chemical properties such as purity, dispersibility and compatibility, and the geometrical parameters of the nanoparticles, such as size and shape. The hybrid nanoparticles are produced either by the single-step (small scale production) or by the multi-step method (mass production), as shown in Fig. 1. In the single-step process, the simultaneous preparation and dispersion of nanoparticles are carried out. In the multi-step process, the nanoparticles are prepared and dispersed into the base fluid one after another.

2.1. Synthesis of hybrid nanoparticles

The details of various synthesis methods for different hybrid nanocomposites are described in this section, and the advantages and limitations of different synthesis techniques are listed in Table 1.

2.1.1. Synthesis of Silica – MWCNT hybrid nanocomposite

Baghbanzadeh [36,37] prepared a silica and MWCNT based hybrid nanocomposite using a wet chemical method. COOH based functional groups were adopted to increase the dispersibility of MWCNT in the solvent. At first, the mixture of sodium silicate (15 g) and distilled water (95 ml) was prepared, and then 4 g of MWCNT was added to that solution. The solution containing 4 g of MWCNT was sonicated for 45 min. in an ultrasonic bath. Then, 11.7 g of CTAB was added to the mixture of 86 ml distilled water and 300 ml dimethylformamide, and it was well mixed using a magnetic stirrer for about 15 min. Then, the later solution was mixed with the ultrasonicated solution, which contains MWCNT. The combined solution was agitated using a magnetic stirrer for three hours at 25 °C, and the solution was maintained at pH12. Finally, the products were dried in a vacuum oven for 12 h at 60 °C to produce the silica-MWCNT based hybrid nanocomposites.

2.1.2. Synthesis of Ag – MWNT hybrid nanocomposite

Chen et al. [38] adopted a green method to synthesize Ag/MWNT hybrid nanocomposite. To attain a functionalized MWNT, a mixture of 0.5 g MWNT and 3.2 g NH_4HCO_3 were rolled in a cylindrical ball milling machine operated at a speed of 250 rpm for 5 h. Then, it was dried in a vacuum oven for 24 h at 100 °C to remove the residual gases. Subsequently, the mixture was subjected to a silver mirror reaction and followed by introducing a Tollens reagent ($[Ag(NH_3)_2]^+$) in 50 ml of 0.1% sodium dodecyl sulfate (SDS) solution with 0.2 g of MWNT under stirring. The reducer formaldehyde (0.5 g) was dipped into the mixture and stirred for 0.5 h at 60 °C. Finally, the Ag/MWNT composite was collected using centrifugation. The ball milling process helped control the length of MWNTs, and this process can be used for mass production at a low cost.

Munkhbayar et al. [39] prepared an Ag-MWCNT nanofluid by the one-step physical technique. The MWCNT was prepared first by purifying in nitric and sulphuric acid, followed by 5 h of ultra-sonication to remove the impurities and amorphous carbon. This process can increase the exterior activity of the nanotubes. The MWCNT (0.7g) was ball-milled using spherical zirconia balls at 500 rpm for 1 h, followed by

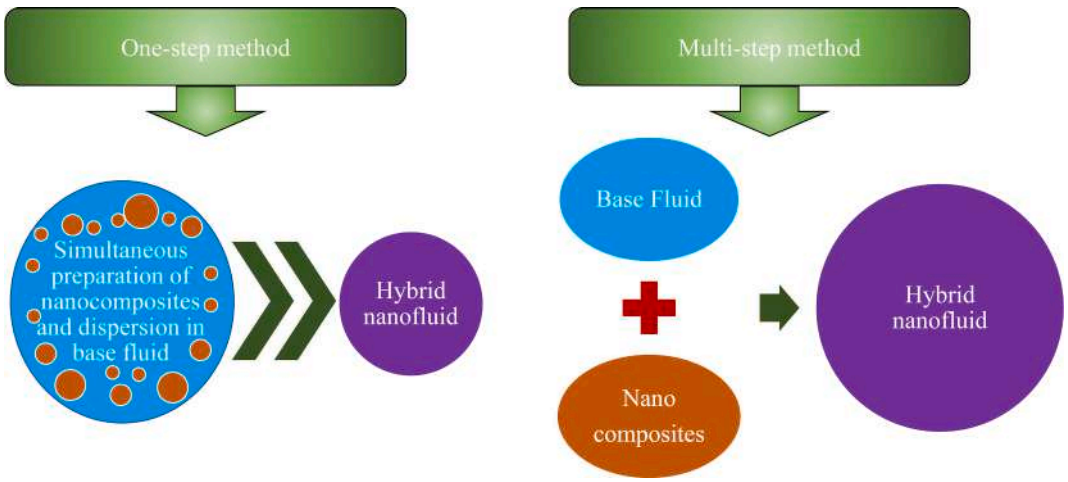

Fig. 1. Comparison of single-step method and multi-step method.

Table 1
Advantages and limitations of various synthesis techniques.

SI. No	Reference	Synthesizing methods	Advantages	Limitations
1	[57]	Physical phase gas condensation / Inert gas condensation process	• Produces equiaxed crystals • Suitable for oxide, nitrate, and carbide particles • High concentration of inert gas atoms can control the collision rate and coalescence rate	• Controls the growth of nanoparticle and prevent the particles from agglomeration
2	[58,59]	Spray drying process	• High product-quality reliability • The dried particle size, shape, crystal form, moisture content, and porosity can be controlled • Low operating cost and energy-efficient	• The size depends on the concentration of the spray drying solution used. • The overall yield of spray dryers used in the laboratory is around 50 to 70 %
3	[58]	Magnetron sputter deposition technique	• Elements having different vapor pressure can be synthesized • Achieves better compositional homogeneity • Particles with a higher melting point can be synthesized	• In the case of thermal evaporation, the gas pressure can be varied to obtain different particle size, and it is not possible in the magnetron sputter technique • The sputtering process is only suitable for producing particles in a cluster of small sizes
4	[60–62]	Pulse wire evaporation method	• Higher efficiency and production rate • Particle size can be controlled precisely	• Results in a broader range of particle size distribution and hence filters are attached to obtain particles in similar size
5	[63]	Vacuum based submerged arc	• Both ductile and brittle metallic materials can be synthesized • Ultrasonic vibration is used to enhance the arc discharge	• Cost increases due to usage of the vacuum pump to maintain the vacuum condition in the synthesizing method • Maintaining a clean vacuum environment is difficult
6	[64,65]	Acetylene flame synthesis system (AFSS)	• Higher temperature can be achieved • It can cover a larger area during synthesis by using single or multiple flames	• Toxic chemical usage and longer processing time are the drawbacks

ultra-sonication. Deionized water-based Ag (2 wt.%) nanofluid was prepared by employing the pulse wire evaporation method (PWE). The previously prepared MWCNT (0.05 wt.%) was poured in a 500 ml exploding bottle and was installed in the PWE unit. The Ag was synthesized by making direct contact with the base fluid using the PWE unit, and thus Ag-MWCNT/water hybrid nanofluid was prepared.

2.1.3. Synthesis of MWCNT- Fe_3O_4 hybrid nanocomposite

Sundar et al. [40] used an in-situ method to synthesize MWCNT-Fe_3O_4 composite. At first, the MWCNT was dispersed in a strong acidic medium (hydrochloric and nitric acid at a ratio of 1:3 on a molar basis), and it was stirred for 72 h at 60 °C. The solution was thoroughly washed using acetone and distilled water, and it was dried in an oven for 24 hours at 100 °C. The above process generates carboxyl groups on the MWCNTs surface, which helps attaching the Fe_3O_4 particle onto the surface of the nanotubes. The prepared carboxylated MWCNT (0.35 g) was mixed with 50 ml of distilled water and stirred for an hour. Then, $FeCl^{3+}$ /$FeCl^{2+}$ salts in the molar ratio of 2:1 were further added to the solution, and then aqueous sodium hydroxide solution was mixed with the above solution to yield a pH value of 12. The solution was continuously stirred for about 0.5 h, which resulted in a change of color into black, indicating the completion of the reaction. The precipitate was further cleaned by acetone and distilled water and dried in an oven at 80 °C for 24 h.

2.1.4. Synthesis of Al_2O_3 – Cu hybrid nanocomposite

Suresh et al. [41,42] prepared an Al_2O_3 – Cu hybrid nanocomposite using the thermochemical synthesis method. A water-based solution contains the salts of Cu $(NO3)_2.3H_2O$ and Al $(NO_3)_3.9H_2O$ was spray-dried at 180 °C to obtain the precursor powder. It was heated at 900 °C for 60 min. at atmospheric conditions. Followed by heating to 400 °C and maintained for an hour in the hydrogen atmosphere. The proportion of each salt was taken such that the final powder mixture would have the 90:10 ratio of alumina and copper oxides. After this process, the CuO was reduced to metallic copper, whereas the Al_2O_3 remains unchanged. The obtained powder was ball milled for 1 h at 400 rpm. Then it was dispersed in deionized water with sodium lauryl sulfate (SLS) as a dispersant and was ultra-sonicated for 6 h.

2.1.5. Synthesis of Cu-TiO_2 hybrid nanocomposite

Madhesh et al. [43] prepared Cu-TiO_2 based hybrid nanocomposite. Initially, Titania (5 g) aqueous solution was prepared using the ultra-sonication method, and then Cu acetate (0.5 g) solution containing the reducing agents (sodium borohydride and ascorbic acid) was mixed with the previous solution. The mixture was continuously stirred for 2 h at 45 °C to form the hybrid nanocomposite (HyNC) colloids.

2.1.6. Synthesis of Graphene – MWCNT hybrid nanocomposite

Aravind et al. [44] developed graphene - MWCNT based hybrid nanocomposites. The graphene was obtained from the graphitic oxide prepared by the Hummer method [45]. The graphene oxide was exposed to solar radiation through a convex lens, and then the solar graphene was refluxed in HNO_3 for an hour to enable easy dispersion in the base fluid. The catalytic chemical vapor deposition technique (CCVDT) was used to prepare the MWCNT, and it was kept at 350 °C for 2 h for processing air oxidation. Further, it was refluxed in HNO_3 for 2 h to remove the amorphous carbon and impurities. The prepared GO and f-MWCNT were refluxed in concentrated HNO_3 for 2 h in the ratio of 1:1 and then dried thoroughly to become a fine powder of GO-f-MWCNT composite.

2.1.7. Synthesis of Au – CNT hybrid nanocomposite

Jana et al. [46] prepared CNT nanocomposite and Au nanocomposite separately. The CNT (1 g) was dispersed in a 40 ml mixture of concentrated acids (nitric and sulfuric acid at a volume ratio of 1:3) and then refluxed for 1 h at 140 °C. Then, the filtered CNTs from the solution were cleaned using deionized water, followed by drying in a vacuum oven for

12 h at 150 °C to obtain a CNT composite. The prepared CNTs were dispersed in water to attain a CNT solution. The Au nanocomposites were mixed with deionized water at a ratio of 1.4:1 to obtain an Au solution. The Au solution and CNT solution were proportionally mixed to get hybrid nanofluid.

2.1.8. Synthesis of γ-Al_2O_3/MWCNT hybrid nanocomposite

Abbasi et al. [47] produced γ-Al_2O_3/MWCNT hybrid nanocomposite using the solvothermal method. The functionalization of MWCNT is similar to the procedure explained in section 2.1.3. The alumina acetate powder was dispersed in ethanol and stirred for 30 min. The functionalized MWCNT particles were added to the prepared acetate solution and sonicated continuously. Then 25% of ammonium solution was added to the previous solution to maintain a pH of 9, and the solution was kept in vacuum condition for 24 h. The solution was subjected to a solvothermal process in an environment of 200 °C and 16 bar pressure for 24 h, during which the nanocomposites formed. The precipitate was washed with ethanol, followed by drying at 60 °C for 6 h, and then it was calcined at 500 °C for 1 h in an inert (argon) atmosphere.

2.1.9. Synthesis of TiO_2-CNT hybrid nanocomposite

Magetif et al. [48] prepared a TiO_2-CNT hybrid nanocomposite by functionalizing the CNTs in an HNO_3-H_2SO_4 acid mixture (1:3 v/v) for 3 h at a temperature of 70 °C [49]. The functionalized CNTs were dispersed in 40 ml distilled water using an ultra-sonicator. Then, 1.5 ml of ethylene glycol and 20 ml 2-propanol were added to the CNTs solution under the N_2 atmosphere. Subsequently, 1 mL of $Ti(OBu)_4$ was slowly suspended with the previous solution and then stirred for 15 h at 80 °C. Finally, the vacuum filtered precipitates were washed using 2-propanol solution followed by drying for 12 h at 60 °C.

2.1.10. Synthesis of MWCNT – HEG hybrid nanocomposite

Baby and Ramaprabhu [50] synthesized MWCNT – hydrogen exfoliated graphene (HEG) using catalytic chemical vapor deposition (CCVD) and exfoliating graphite oxide, respectively. The graphene was obtained from the graphitic oxide prepared by the Hummer method [45], in which 2g graphite was treated with 46 ml sulfuric acid in an ice bath. Then, 1g sodium nitrate and 6g potassium permanganate were mixed with the solution to accelerate the reaction at ambient temperature. Subsequently, hydrogen peroxide was added after 15 min in the suspension. Finally, the solution was washed with distilled water, followed by vacuum drying for 8 h at 40 °C.

2.1.11. Synthesis of Al- Zn based hybrid nanocomposite

Paul et al. [51] prepared hybrid nanoparticles through a two-stage process (mechanical alloying method followed by ultra-sonication). Initially, the aluminum and zinc powders were blended (Al - 5wt.% Zn). The sample at room temperature was subjected to ball milling at a speed of 300 rpm, and at 10:1 ball to powder ratio. The oxidation, agglomeration, and coating of balls and vials with powder was prevented by using toluene as a wet medium. The milling process was carried out to achieve ultra-fine particles with similar compositions, and these particles were mixed with base fluid (ethylene glycol). This mixture was kept in an ultrasonicator, followed by magnetic stirring.

2.1.12. Synthesis of Al_2O_3- microencapsulated PCM based hybrid nanocomposite

Ho et al. [52] prepared hybrid nanofluid using Al_2O_3 nanoparticles and microencapsulated PCM particles. The PCM suspension was prepared by the emulsion technique along with the interfacial polycondensation. The PCM n-eicosane particle was used, and it was emulsified in water-based urea-formaldehyde per polymer solution and consisted of 60% MEMPCM particles. The MEMPCM particles were mixed with the ultra-pure Mill-Q water in a container and were ultrasonicated for 2 h. Further Al_2O_3 nanoparticles in the weight range of 2 to 10 % were mixed with the ultra-pure Mill-Q water and were stirred for 4 h. Then the above two solutions were mixed to obtain the hybrid nanofluid.

2.1.13. Synthesis of Fe_3 $(NO)_3$/ $Al(NO_3)_3$ with CNT based hybrid nanocomposite

Han et al. [53] studied the application of hybrid nanotube produced through the spray pyrolysis method. An aqueous solution with the ratio of 1:1 with 3 wt.% of Fe_3 $(NO)_3$ and $Al(NO_3)_3$ was prepared. The aluminum and iron nanoparticles were formed by the thermal decompression process. The nebulizer was used to generate the aerosol droplets with nitrogen as the carrier gas. The presence of water in the particles was removed by passing through a silica gel dryer. The pyrolytic process was carried out in a furnace at 1000 °C to convert metallic nitrate to oxide, and the nitrate was mixed with hydrogen gas at the entrance. Besides, it was routed to another furnace at 750 °C to initiate a reaction with hydrogen and acetylene to produce CNT growth at the surface.

2.1.14. Synthesis of Ag-HEG based hybrid nanocomposite

Baby and Ramaprabhu [54] synthesized Ag-HEG hybrid nanocomposites. Graphene oxide (GO) was used to synthesize HEG, and subsequently, its functional groups were removed from GO. As polar solvents cannot disperse the as-synthesized HEG, the carboxyl and hydroxyl FG were used for dispersion. The residue was treated in an acid medium, consisting of $3(H_2SO_4)$: $1(HNO_3)$ followed by ultrasonication, filtering, and drying at vacuum conditions. The Ag-HEG nanocomposite was then dispersed in deionized water and ultrasonicated. Further, it was kept in a magnetic stirrer for 5 h, and then silver nitrate was added to the solution. After 24 h, $NaBH_4$ NaOH (40 ml) was added to the solution.

2.1.15. Synthesis of CuO-HEG based hybrid nanocomposite

Sidik et al. [55] used a two-step method to prepare CuO-HEG/water-based hybrid nanofluid. The process consists of synthesis, functionalization, chemical reduction, and ultrasonication. The graphene was synthesized using HEG (hydrogen-induced exfoliation). The CuO was synthesized through chemical reduction followed by calcination at low temperatures.

2.1.16. Synthesis of ND-Fe_3O_4 based hybrid nanocomposite

Sundar et al. [56] used the in-situ growth and chemical co-precipitation method to synthesize ND- Fe_3O_4 nanoparticles. The ND (1.5g) was treated in an acid medium and dispersed in distilled water (50 ml), and stirred for 2 h. Two salts ($FeCl_3{\cdot}6H_2O$ and $FeCl_2{\cdot}4H_2O$) in the mole ratio of 2:1 were added to the ND suspensions. Further, NaOH was added until the PH value reached to 12 and stirred for 2 h. Then, the residue was washed to remove the Fe^+, Na^+, Cl^{2+} ions and dried at 80 °C for 12 h.

2.2. Preparation of hybrid nanofluids

The nanoparticles are commonly developed using two main techniques: the one-step and two-step method, as shown in Fig. 2. In the one-step method, the nanoparticle preparation and their dispersion into the base fluid are completed simultaneously. The nanofluid synthesis can be carried out either by a physical or chemical process in the one-step approach. The physical method includes evaporation and physical phase gas condensation, magnetron sputter deposition technique, pulse wire evaporation, laser ablation, vacuum-based submerged arc, and dual plasma synthesis. At the same time, the chemical method involves sol-gel, polyol, microemulsion, and chemical reduction techniques [55,63,66–76]. The metal nanoparticles (high thermal conductivity) are commonly synthesized using the one-step method to avoid oxidation; however, the one-step process is not suitable for mass production.

In comparison, the two-step method is ideal for mass production. In the two-step method, nanoparticles are produced in the first step and

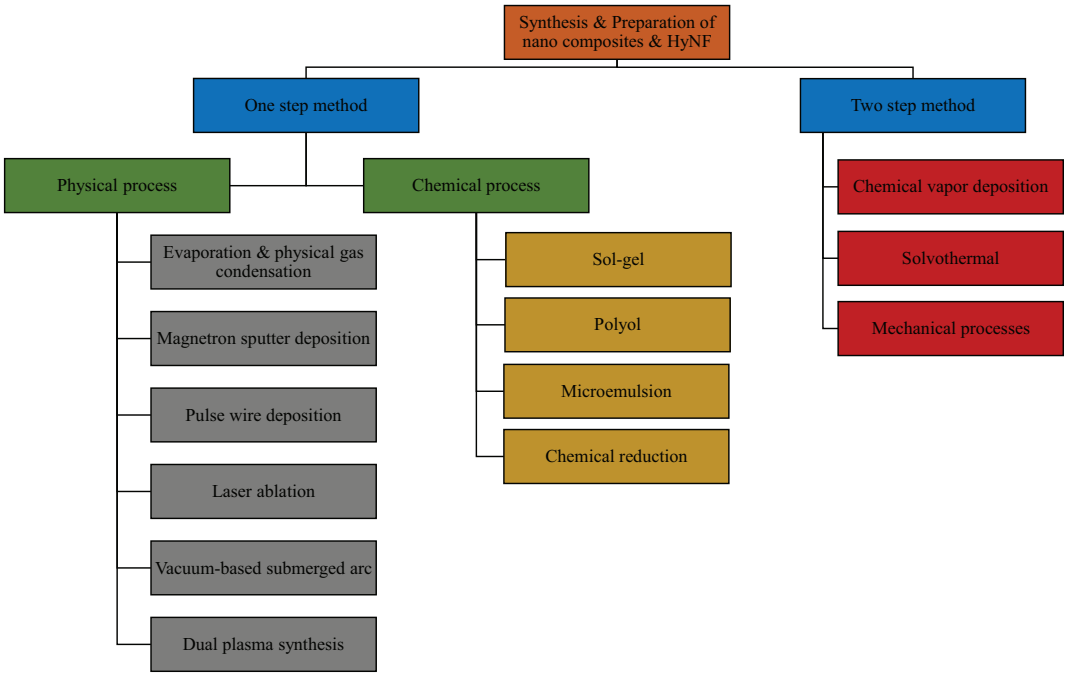

Fig. 2. Synthesis and preparation techniques used in the one step and two step method.

then suspended in the base fluid in the subsequent steps. In the two-step method, the nanocomposites can be prepared using various techniques, such as chemical vapor deposition, solvothermal method, and mechanical processes (e.g., grinding, milling, sintering). Subsequently, the dispersion can be carried out using an ultra sonicator and a magnetic stirrer.

Most importantly, in nanofluid preparation, stability is the primary concern for practical applications [77]. The stability of different hybrid nanofluids [40,78–90] is reported in Fig. 3. Most of the HyNF's exhibited stability for just two weeks or less; however, MWCNT-Fe_3O_4/water and AlN/EG showed stability for two months. Nevertheless, the long-term stability of HyNF's is demanded for realistic applications. The stability of HyNF's is dependent on many factors, including the base fluids, types of nanoparticles, nanoparticles shape and size, nanoparticles concentration, pH value, the temperature of HyNF, dispersion techniques, sonication techniques, sonication time, surfactants, and the combinations of above, as represented in Fig. 4. The list of factors that influence the stability is more exhaustive; however, all the above factors can critically affect the HyNF's stability. For instance, the TiO_2-SiO_2/EG-Water sample undergone 90 min sonication demonstrated 360 hours of stability, while the same sample with 60- and 120-min sonication time showed just 120 hours of stability [87].

To achieve better stability, the dielectric constant of the base fluid must be higher. The repulsive potential is directly proportional to the dielectric constant. Water has the highest dielectric constant value of 78.5 when compared to other base fluids like acetone (21.01), ethanol (24.6), ethylene glycol (24.6), hexane (1.89), and benzene (2.28) at 20

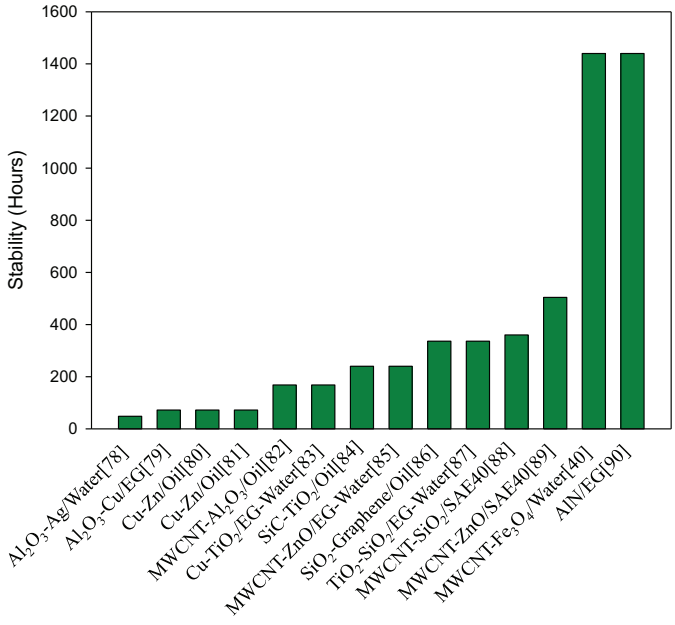

Fig. 3. Stability period of different hybrid nanofluids.

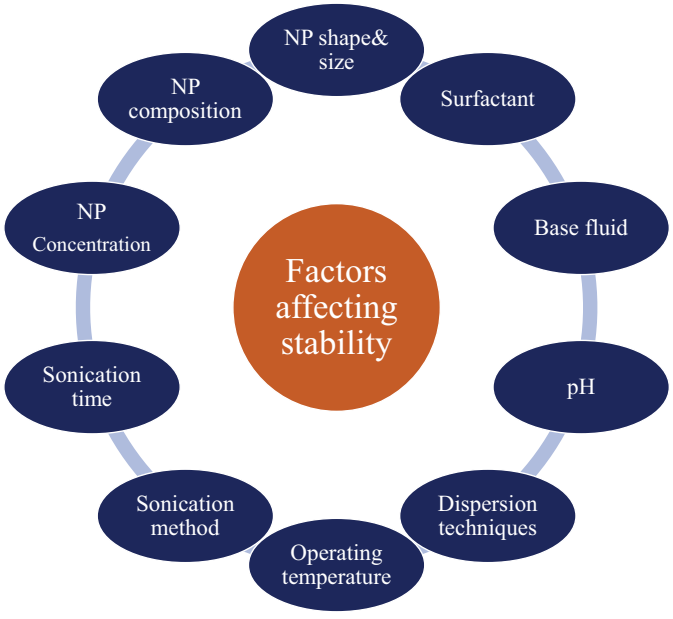

Fig. 4. Graphical illustration of factors influencing stability of hybrid nanofluid.

°C [91]. It is reported that a higher density difference between the nanoparticle and base fluid leads to sedimentation even if the particle has a higher zeta potential. At zero zeta potential value, no repulsive forces are observed, and the pH value of nanofluid at that point is termed as isoelectric point (IEP). IEP is the reference point to check stability. At IEP, the suspension must have greater than ±2 pH to achieve stability [92–94]. Thus, by altering the pH value, stability in nanofluid can be improved.

The nanoparticle size, shape, and concentration play a significant role in controlling stability. The repulsive force and Van der Waal force depend on the particle size. Smaller particle size and minimal density difference between base fluid and nanoparticle result in higher stability due to lower settling velocity. An increase in particle concentration decreases the separation distance between atoms and increases the Van der Waal forces. The agglomeration of particles starts when the Van der Waal force is higher than the repulsive force. Thus, an increase in particle concentration decreases the stability [95,96].

Operating parameters like temperature, salinity, confinement, and shear affect the stability of nanofluids. The stability of nanofluids decreases when used at high temperatures. The Brownian motion of nanoparticles increases when the temperature rises and results in frequent collisions, and subsequently, agglomeration is initiated. The nanoparticles get deposited on the surface due to agglomeration and increase the heat transfer resistance. Further stabilizing the nanofluid with surfactant and polymer solution is difficult when operated at high temperatures [97]. Thus, the thermophysical properties of nanofluids are altered. A stable nanofluid has higher thermal conductivity than an unstable nanofluid [98,99]. Similarly, when the particle concentration increases, the specific heat capacity decreases with stability [100–102].

Moreover, agglomeration and clogging should also be avoided for using HyNF in real-world applications. The instability and agglomeration issues are inevitable in nanofluids due to the high cohesive and Vander Waals forces between each nanoparticle. It is well known that one of the heat transfer mechanisms in nanofluids is the Brownian motion of nanoparticles in working fluids. However, the agglomeration hinders the Brownian motion, thereby deteriorating the heat transfer augmentation. In addition, it can also increase the pressure drop due to clogging phenomena. Therefore, it is essential to avoid agglomeration and to enhance stability of nanofluids. The commonly used methods to minimize the agglomeration are electrostatic stabilization, ultrasonic vibration, and use of surfactants such as Sodium Dodecyl sulphate (SDS), Gum Arabic, Sodium Dodecyl Benzene Sulfonate (SDBS), and Cetyl Trimethyl Ammonium Bromide (CTAB) [32,51,103–110]. The listed factors that could influence the stability of nanofluids is exhaustive. However, stability is the main criterion that determines its usage in practical applications. Therefore, comprehensive works on stability are further required in terms of stability improvement and nanomaterial selection.

Although improved stability is essential, stability measurement is another central aspect. The following measurement techniques are widely adopted for measuring stability,

(1) Zeta potential method
(2) Spectral absorbance analysis
(3) Centrifugation method
(4) Sedimentation method

Most of the researchers used the zeta potential value to characterize the stability of nanofluid. The repulsive force between nanoparticles increases at a higher zeta potential value, improving the stability. The absolute zeta potential (AZP) value of 60mV indicates a higher level of stability. The AZP of 30 mV denotes good stability, whereas the AZP of 15 mV implies instability [77,111–113].

2.2.1. Physical phase gas condensation/inert gas condensation process

This technique involves evaporation and rapid condensation. The selected material is evaporated by heating, and the vapor is rapidly condensed into nano-size particles. This process is carried out in an inert gas atmosphere or at a pressure lower than atmosphere.

2.2.2. Spray drying process

A solution with the water-soluble materials is prepared and made into an aerosol. In the spray drying process, hot air is blown to vaporize the solvent, which turns into powder accordingly. The powder is then evenly pyrolyzed in a fluidized bed reactor, creating porous powder with an evenly distributed structure without any volatile constituents.

2.2.3. Magnetron sputter deposition technique

The material is placed in a magnetron sputter under the inert gas atmosphere. The supplied heat energy turns the material into ionized plasma and directs it towards the confinement area with the assistance of the magnetic field. Then vapor is condensed into nanoclusters. The maintained pressure difference between the deposition chamber and aggregation zone helps to deposit the nanoclusters on the substrate [68].

2.2.4. Pulse wire evaporation method

It is a commonly used method to produce a low-cost hybrid nanofluid. In this method, a high voltage (300 V) is supplied to the source material (wire), forming plasma. Then, it is condensed in an inert gas atmosphere resulting in the formation of nanoscale powder [55].

2.2.5. Vacuum based submerged arc nanoparticles

An electric arc with high temperature is used to melt the material and to vaporize with the presence of dielectric fluid in the vacuum chamber. An ultrasonic device is used to divert the vaporized metal from the fusion zone, and it assists in stabilizing the arc. This vapor present in the dielectric fluid starts to nucleate and forms as nanoparticles [63].

2.2.6. Acetylene flame synthesis system (AFSS)

The AFSS system consists of a nebulizer, synthesizer, torch, collector, carbon source (acetylene flame), and pipelines. The filtered water is passed through the nebulizer to generate the mist, and it is passed through the synthesizer. In the collector section, the water mist from the synthesizer and the hybrid carbon produced from acetylene flame is combined to form hybrid carbon nanofluids, as shown in Fig. 5. The suspension and dispersion of hybrid carbon nanofluids are improved by dispersing in a hot plate stirrer [114].

3. Thermophysical properties

Determination of thermophysical properties such as density, viscosity, thermal conductivity, and specific heat is essential to quantify the hydraulic and thermal performance of the systems. In this section, the determination of the aforementioned thermophysical properties of the hybrid nanofluids is discussed in detail. The density of the HyNF plays a crucial role in controlling the stability and determining the volume of hybrid nanofluid required in a thermal system. Similarly, viscosity and density help in assessing the pumping power requirement [115]. Thermal conductivity decides the rate of heat transfer of a thermal system. The exergy and energy parameters can be determined by estimating the specific heat values.

3.1. Density

Density is the ratio of the mass to volume. The density of nanoparticles depends on the type of nanoparticles and it is independent of the geometric parameters (shape and size), zeta potential, and additives [116]. Usually, the density of solid particles is higher than the base fluids. Hence, the addition of nanoparticles increases the density of the prepared nanofluid. Density varies with the temperature of nanofluid [117], and it decreases with an increase in temperature. The nanoparticles density is determined either by weighing a known volume

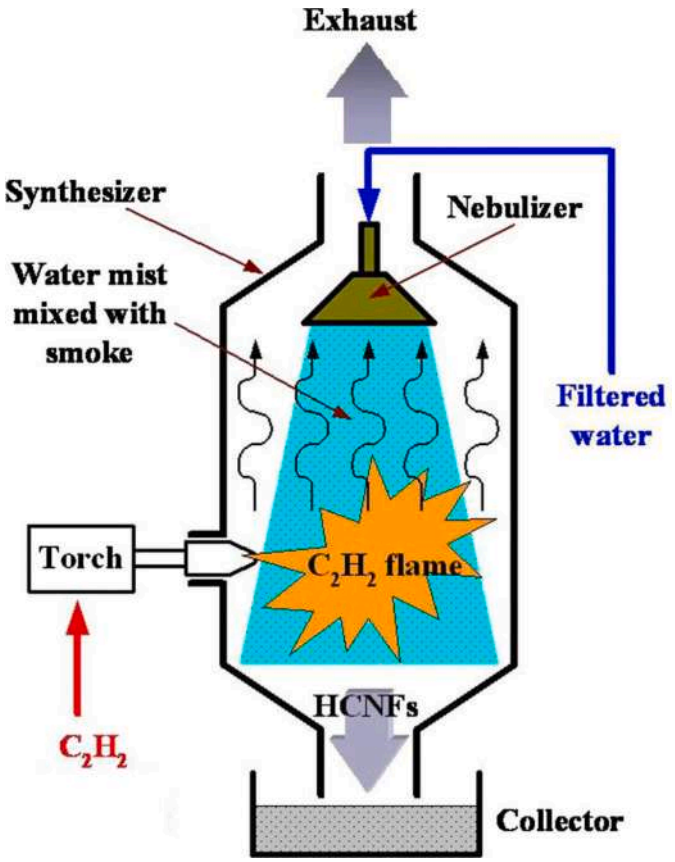

Fig. 5. Acetylene flame synthesis procedure [114].

(weighing the fluid volume in a standard container) or using a digital density meter or using the mixing theory or the combinations of the above methods [6,118–120]. It is observed that prolonged ultrasonication can increase nanofluid density [121]. The density of hybrid nanoparticles can be determined using the mixing rule and derived from the mono nanofluid density equations [56,99,122]. The density of hybrid nanoparticles can be determined by measuring the density, weight percentage, and volume fraction of individual nanoparticles given in Eqs. (1-3),

$$\rho_{hnp} = \frac{\rho_{np1} w_{np1} + \rho_{np2} w_{np2}}{w_{np1} + w_{np2}} \tag{1}$$

$$\rho_{hnf} = \phi_{np1}\rho_{np1} + \phi_{np2}\rho_{np2} + (1 - \phi_{hnp})\rho_{bf} \tag{2}$$

$$\phi_{hnp} = \phi_{np1} + \phi_{np2} \tag{3}$$

where, $\rho_{hnp}$and ρ_{np} are the density of hybrid nanoparticle and single nanoparticle, respectively, $w_{np}$is the weight percentage of single nanoparticle, and ϕ_{hnp},and $\varphi_{np}$are the volume fraction of hybrid nanoparticle and single nanoparticle, respectively.

3.2. Viscosity

It is defined as the internal resistance offered to the fluid flow. The viscosity of hybrid nanofluid depends on the synthesis and preparation methods, nanoparticles size and shape, volume fraction, concentration, and temperature. The kinematic viscosity is inversely proportional to the temperature of the hybrid nanofluid [123]. Viscosity is measured using a cone, disk (plate/parallel), cylindrical viscometers, rheometer, micromachined capillary viscometer [124,125].

Batchelor [126] considered the Brownian motion effects in evaluating the viscosity of the particles dispersed fluid and proposed a viscosity relationship, as given in Eq. (4).

$$\mu_{nf} = (1 + 2.5\varphi + 6.5\varphi^2)\mu_{bf} \tag{4}$$

Nguyen et al. [127] predicted the dynamic viscosity of nanofluids for various nanoparticle sizes using Eqs. (5-7); and the proposed dynamic viscosity relationship is a function of temperature, as given in Eq. (8). The following expressions are also used for predicting the viscosity of nanofluids [128].

$$\frac{\mu_{nf}}{\mu_{bf}} = 1.475\text{-}0.319\varphi + 0.051\varphi^2 + 0.009\varphi^3 \text{ for } d_p = 29\text{nm} \tag{5}$$

$$\frac{\mu_{nf}}{\mu_{bf}} = 1 + 0.025\varphi + 0.015\varphi^2 \text{ for } d_p = 36\text{nm} \tag{6}$$

$$\frac{\mu_{nf}}{\mu_{bf}} = 0.904exp(0.1483\varphi) \text{ for } d_p = 47 \text{ nm} \tag{7}$$

$$\frac{\mu_{nf}}{\mu_{bf}} = (2.1275 - 0.0215T + 0.00027T^2) \tag{8}$$

Brinkman model is also used to determine the viscosity of HyNF as shown below [129,130],

$$\mu_{hnf} = \frac{\mu_{bf}}{(1 - \phi_{np1})^{2.5}(1 - \phi_{np2})^{2.5}} \tag{9}$$

Where, $\mu_{nf}$and $\mu_{bf}$are the dynamic viscosity of nanofluid and basefluid respectively, φ is the volume fraction of the nanoparticle, d_p is the nanoparticle's average diameter, and T is the temperature.

3.3. Specific heat

The specific heat of nanofluid is determined using various techniques like differential scanning calorimeter (DSC) and mixing rule. Few researchers have developed the correlations from their self-fabricated experimental setup [99,131–134]. The specific heat depends on the temperature, nanoparticle size and shape, and material. The specific heat increases as the nanoparticle diameter increases.

Pak et al. [99] developed a relationship (Eq. 10) to predict the specific heat of nanofluid using the mixing rule assuming the suspended nanoparticles and the basefluid are in thermal equilibrium. And the reported values were found in good agreement with the experimental data [52,56]. The specific heat of the hybrid nanofluid can be determined by measuring density, specific heat, and volume fraction of individual nanoparticles and base fluid, as given in Eq. (11) [135].

$$Cp_{nf} = \frac{\phi\rho_{np}Cp_{np} + (1 - \phi)\rho_{bf}Cp_{bf}}{\rho_{nf}} \tag{10}$$

$$Cp_{hnf} = \frac{\phi\rho_{np1}Cp_{np1} + \phi\rho_{np2}Cp_{np2} + (1 - \phi_h)Cp_{bf}}{\rho_{hnf}} \tag{11}$$

Where, $Cp_{hnf}$is the specific heat of hybrid nanofluid and $Cp_{np}$is the specific heat of nanoparticles, and $\varphi_{np}$is the volume fraction of nanoparticle.

3.4. Thermal conductivity

Thermal conductivity is a significant thermophysical property that determines the heat transfer characteristic of the hybrid nanofluid. Thermal conductivity of the HyNF is a strong function of the type of nanoparticles and their concentration, type of base fluid , and the operating temperature [136,137]. Besides, it is reported that the preparation method (particularly the ultrasonication period) can also affect the conductivity of HyNF. Thermal conductivity can be measured using a KD2 pro thermal analyzer, transient hot-wire, insulated wire, and liquid metal wire methods [121,138–140]. Usually, thermal

conductivity of nanofluids is higher than that of the basefluids due to the convection current occurring between the suspended nanoparticles and basefluid [141]. Thermal conductivity of HyNF increases as the temperature increases, making the HyNF quite attractive in high-temperature applications such as heat exchangers, heat pipes, and heat sinks.

Einstein [142] proposed (Eq. 12) a relationship for the Brownian diffusion coefficient. From Eq. (12), it is clear that the number of collisions among the nanoparticles increase as the temperature increase; which in turn leads to higher thermal conductivity.

$$D_B = \frac{k_B T}{\left(\frac{3\pi\mu}{d_p/10^9}\right)} \tag{12}$$

Where, D_B is the Brownian diffusivity, K_B is the Boltzmann's constant, T is the temperature, d_p is the particle average diameter, and μ is the dynamic viscosity

The correlation proposed by Maxwell [143] to measure the thermal conductivity of solid particles suspended in fluids is used as the base equation to determine nanofluids' conductivity.

$$k_{stat} = k_{bf}\left(\frac{k_{np} + 2k_{bf} + 2\phi(k_{np} - k_{bf})}{k_{np} + 2k_{bf} - \phi(k_{np} - k_{bf})}\right) \tag{13}$$

Where, k_{stat}, k_{bf} and k_{np} are the thermal conductivity of a static suspension, base fluid, and nanoparticle, respectively, and φ is the volume fraction of the nano particle.

Hamilton and Crosser [20] modified the Maxwell equation by introducing the shape factor of nanoparticles as follows,

$$k_{stat} = k_{bf}\left(\frac{k_{np} + (ns-1)k_{bf} - (ns-1)\phi_p(k_{np} - k_{bf})}{k_{np} + (ns-1)k_{bf} + \phi_p(k_{np} - k_{bf})}\right) \tag{14}$$

Where, ns (shape factor) = 3 for spherical shape and ns = 0.5 to 6 for other shapes.

Bruggeman [144] proposed a correlation for the spherical shape nanoparticles as follows,

$$\frac{k_{nf}}{k_{bf}} = \frac{1}{4}(3\phi - 1)k_{np} + (2 - 3\phi)k_{bf} + \frac{k_{bf}}{4}\sqrt{\Delta}$$
$$where, \Delta = (3\phi - 1)^2\left(\frac{k_{np}}{k_{bf}}\right)^2 + (2 - 3\phi)^2 + 2(2 + 9\phi - 9\phi)^2\frac{k_{np}}{k_{bf}} \tag{15}$$

Koo and Kleinstreuer [145] combined the static influence equation (Eq. 13) and the Brownian motion (Eq. 17) to predict the thermal conductivity of the nanofluid using Eq.16,

$$k_{nf} = k_{stat} + k_{brown} \quad (16)$$

$$k_{brown} = 5{*}10^4{*}\beta{*}\varphi{*}\rho_{cp}{*}Cp_{bf}\sqrt{\frac{K_B T}{\rho_{np}{*}d_{np}}}f \tag{17}$$

$$\beta = 0.0137(100\varphi)^{-0.8229} \quad \varphi < 1\% \tag{18}$$

$$\beta = 0.0037(100\varphi)^{-0.0841} \quad \varphi > 1\% \tag{19}$$

$$f = (-134.63 + 1722.3\varphi) + (0.4075 - 6.04\varphi)T \tag{20}$$

The Maxwell model is also used to determine the thermal conductivity of HyNF as shown below [143],

$$k_{hnf} = k_{bf}\left(\frac{\left(\frac{k_{np1}\phi_{np1} + k_{np2}\phi_{np2}}{\phi_{np1} + \phi_{np2}} + 2k_{bf}\right) - 2(\phi_{np1} + \phi_{np2})\left(k_{bf} - \frac{k_{np1}\phi_{np1} + k_{np2}\phi_{np2}}{\phi_{np1} + \phi_{np2}}\right)}{\left(\frac{k_{np1}\phi_{np1} + k_{np2}\phi_{np2}}{\phi_{np1} + \phi_{np2}} + 2k_{bf}\right) + (\phi_{np1} + \phi_{np2})\left(k_{bf} - \frac{k_{np1}\phi_{np1} + k_{np2}\phi_{np2}}{\phi_{np1} + \phi_{np2}}\right)}\right) \tag{21}$$

Where k_{brown} and k_{nf} are the thermal conductivity of Brownian motion and nano fluid, respectively, and d_{np} is the diameter of the nanoparticle. f and β are the factorial function and the fraction of liquid volume, respectively.

Further, thermal expansion coefficient, heat capacitance, and thermal diffusivity of HyNF can be determined using the following relationships [146–150],

$$(\rho\beta)_{hnf} = (1 - \phi_{np1} - \phi_{np2})(\rho\beta)_{bf} + (\rho\beta)_{np1}\phi_{np1} + (\rho\beta)_{np2}\phi_{np2} \tag{22}$$

$$(\rho Cp)_{hnf} = (1 - \phi_{np1} - \phi_{np2})(\rho Cp)_{bf} + (\rho Cp)_{np1}\phi_{np1} + (\rho Cp)_{np2}\phi_{np2} \tag{23}$$

$$\alpha_{hnf} = \frac{k_{hnf}}{(\rho Cp)_{hnf}} \tag{24}$$

3.5. Overview of thermophysical properties for various HyNF

Farhana et al. [151] studied the thermophysical properties of various HyNF, such as Al_2O_3.TiO_2, TiO_2-ZnO, and ZnO-Al_2O_3/water (0.1 vol.%). It was observed that the viscosity and thermal conductivity values were identical for the above-mentioned HyNFs. Bellos and Tzivanidis [152] studied the thermal behavior of hybrid nanofluid (1.5 % Al_2O_3 +1.5% TiO_2) with oil as a base fluid. The inlet temperature of hybrid nanofluid was varied from 300 to 650 K, and the corresponding variation in thermophysical properties was reported. It was observed that the specific heat capacity was increased, whereas the density, dynamic viscosity, and thermal conductivity were decreased with an increase in temperature from 300 to 650 K.

Yarmand et al. [128] studied the thermophysical properties of hybrid GNP-Ag nanocomposite. Water is selected as base fluid. The density, specific heat, viscosity, and thermal conductivity variations with temperature (20 – 40 °C) and concentration (0 – 0.1 wt.%) were reported. It was observed that as the nanoparticle concentration increases, density, viscosity, and thermal conductivity values were found to increase. The viscosity and density value decreases with a rise in temperature, and thermal conductivity increases as the temperature increases. Minea and El-Maghlany [153] and Esfe et al. [154] studied the thermophysical properties of Ag–MgO/water hybrid nanofluid at two different volume concentrations 1.5 % and 2 %. It is observed that as the volume concentration increases, the density, viscosity, and thermal conductivity value increases, and the specific heat value decreases.

Sundar et al. [40,155,156] studied the influence of temperature (20 and 40 °C) and volume concentration (0 to 0.3 %) on the thermophysical properties of hybrid nanofluid consisted of 0.26 g of MWCNT - 0.74 g of Fe_3O_4 with distilled water as base fluid. As the temperature increases, the density, specific heat, and viscosity decreases, whereas the thermal conductivity increases. The density, specific heat, thermal conductivity, and viscosity increase with the rise of the volume concentration. Hameed et al. [157] studied the thermophysical properties of Alumina – Cu/water and Alumina –CNT/water hybrid nanofluids for two different volume concentrations (0.1 % and 0.3 %). The density, viscosity, and thermal conductivity of both the HyNFs increases slightly with the volume concentration, whereas the specific heat values remain unchanged. Kumar et al. [158] estimated the thermophysical properties of various hybrid nanofluids of Al_2O_3-MWCNT, TiO_2-MWCNT, ZnO-MWCNT, and CeO_2-MWCNT/water at different concentrations ranging from 0.25 to 2 %. It was observed that as the volume concentration increases, the density increases, and the specific heat decreases. Kumar and Sarkar [159] estimated the thermophysical properties of Al_2O_3-CNT/water HyNF for the various mixing ratios such as Al_2O_3-CNT (5:0), Al_2O_3-CNT (4:1), Al_2O_3-CNT (3:2), Al_2O_3-CNT (2:3), Al_2O_3-CNT (1:4), and Al_2O_3-CNT (0:5). The variations in density, specific heat, viscosity, and thermal conductivity subject to different volume mixing ratios were minimal. Verma et al. [160] studied the thermophysical properties of MgO-MWCNT/water and CuO-MWCNT/water-based HyNFs by varying the particle volume concentration (0.0 to 2 %) and temperature (25 to 50 °C). As the temperature increases, the specific heat and thermal

conductivity of the HyNFs increases, and the viscosity decreases with volume concentration.

Minea and El-Maghlany [153] and Sundar et al. [161] examined the accuracy of correlations used to determine the thermal conductivity and dynamic viscosity of HyNF (0.15% GO-Co_3O_4 dispersed in water, 0.05% GO-Co_3O_4 dispersed in 60% Ethylene Glycol and 40% Water, and 0.15% GO-Co_3O_4 dispersed in 60% Ethylene Glycol and 40% Water) with the experimental results. They found that the existing correlations were inaccurate. Therefore, they developed new correlations to study the properties of HyNF. Sundar et al. [162,163] measured the thermophysical properties of the ND-Ni/water HyNF at different volume fractions (0 to 0.3 %) and temperatures (30 to 60 °C). The density and viscosity of the HyNF were found to decrease, and the thermal conductivity and specific heat were found to increase with an increase in temperature.

In summary, the HyNF's thermophysical properties are strongly influenced by the nanoparticle concentration and operating temperature. As temperature rises, the density and viscosity decrease, whereas the thermal conductivity and specific heat increase. It is observed that at high temperatures, the nanoparticles' velocity increases due to the strong Brownian motion development, which results in higher thermal conductivity. As the temperature increases, the viscosity reduces due to the decrease in cohesive force between the molecules; however, a slight increase in viscosity is observed due to the momentum transfer occurring between adjacent layers in the turbulent flow. In contrast to the above general fact, some researchers have reported a reduction in specific heat [40,155,156] and thermal conductivity [152] with temperature.

The thermophysical properties such as density, viscosity, and thermal conductivity increase with nanoparticle concentration, whereas specific heat decreases. Since the thermal conductivity of nanoparticles is much higher than the base fluid, the interaction of nanoparticles with base fluid increases at higher concentrations. It helps in increasing the thermal conductivity of HyNF. The viscosity value increases at higher concentrations due to increased cohesive forces between like and unlike molecules. In contrast to the preceding observations, some literature reported a slight increase in specific heat with concentration [40,155–157].

The variations in thermophysical properties (density, viscosity, specific heat, and thermal conductivity) of different hybrid nanofluids over the base fluid are compared in Figs. 6-9. It is observed that CuO-MWCNT / water (2%; 50°C) HyNF reported higher values of density and viscosity over base fluid. Similarly, ND-Ni/water (0.1%; 60°C) and MWCNT- Fe_3O_4 /water (0.3% and 20°C) reported higher thermal conductivity and specific heat over base fluid, respectively. It is understood that density, viscosity, and the thermal conductivity of the HyNF are higher than that of the base fluid, whereas the specific heat of the HyNF is slightly lower. The thermophysical properties for some of the hybrid nanofluids widely used in heat transfer applications are listed in Table 2.

4. Heat transfer applications

Hybrid nanofluid is extensively used in various heat transfer applications, as shown in Fig. 10. This section comprehensively reviewed the various heat transfer applications, including heat exchangers, heat sinks, heat pipes, photovoltaic modules, natural convection enclosures, refrigeration systems, jet impingement cooling, boiling, and thermal energy storage systems.

4.1. Heat Exchangers

The heat exchanger is a device to exchange the heat between two or more fluids. It is widely used in many industries such as heating, air conditioning, chemical processing, petroleum, automobiles, power plants, waste heat recovery, solar heaters, cryogenic, food, and pharmaceutical [168]. The growing energy demand is reflecting the need for more efficient heat exchangers [169,170]. Heat transfer enhancement in heat exchangers can be achieved by either active or passive methods. Active methods generally require an external power source for heat transfer augmentation, which is comparatively sophisticated and less energy efficient. In the passive methods, the heat transfer rate is increased by minimizing the thermal boundary layer thickness and enhancing the fluid mixing. This can be achieved via introducing artificial roughness, fins, vortex generators, twisted tapes, and coiled wires [171–180]. In addition to this, improvement in the working fluid's thermophysical properties can lead to an increased heat transfer. In the last decade, many researchers extensively investigated the mono nanofluid applications in heat exchangers and showed a considerable improvement in the heat exchangers' performance [181]. In recent years, hybrid nanofluids have attracted the researcher's attention due to their improved thermophysical properties and stability [182].

According to the configuration, the recuperative heat exchanger can be mainly classified into three categories, (1) Tubular heat exchangers, (2) Plate type heat exchangers, and (3) Extended surface heat exchangers [183]. The working fluid passage for most of the heat exchangers is a tubular conduit. Therefore, it is essential to understand the

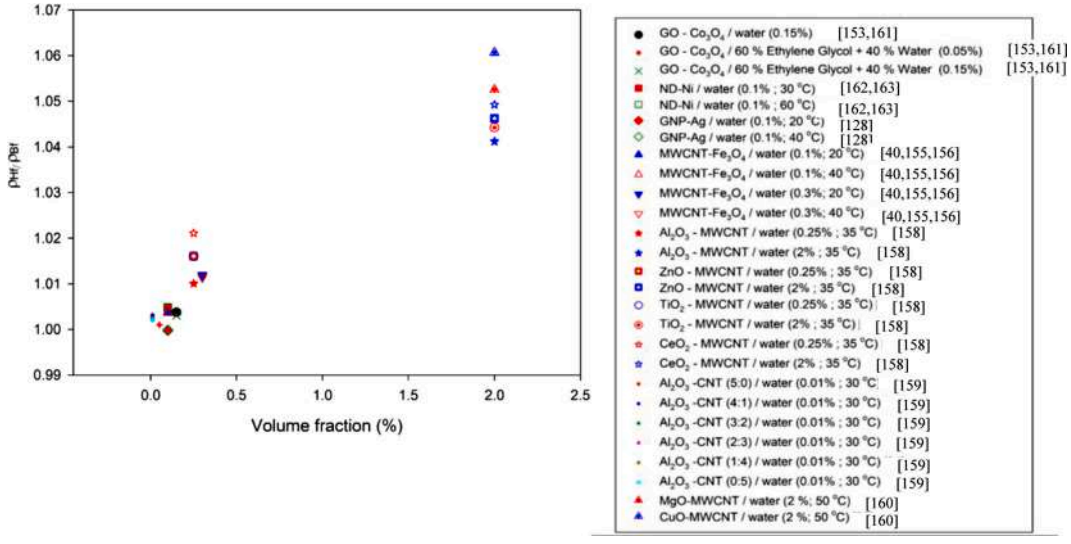

Fig. 6. Comparison of HyNF density over base fluid.

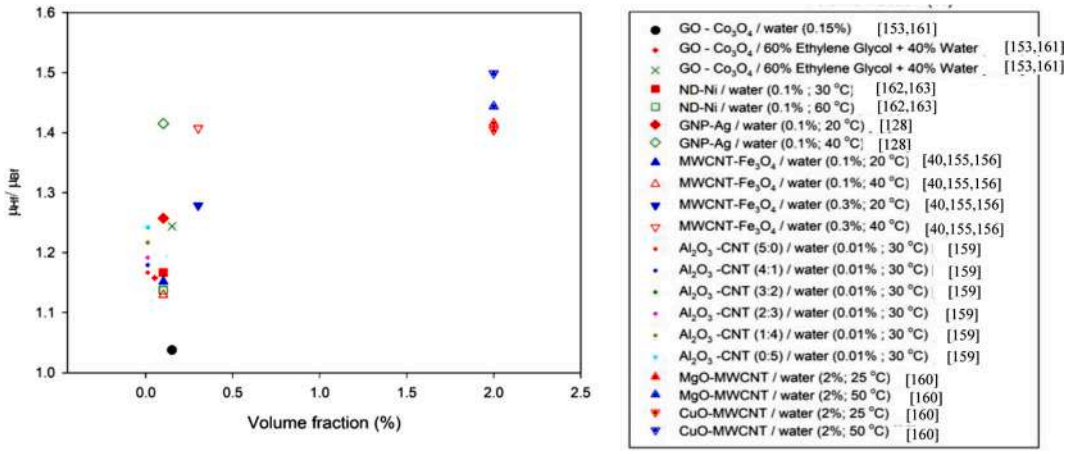

Fig. 7. Comparison of HyNF viscosity over base fluid.

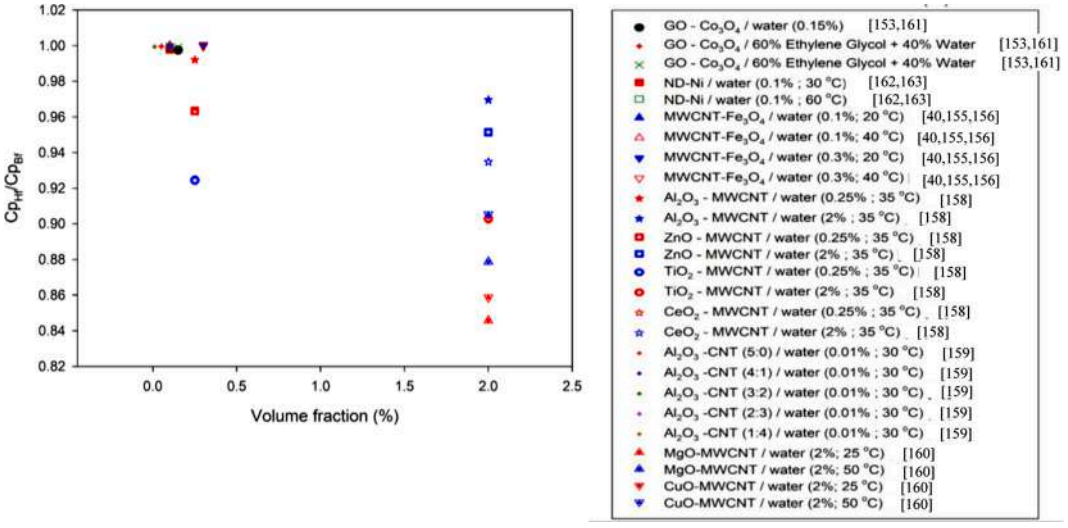

Fig. 8. Comparison of HyNF specific heat over base fluid.

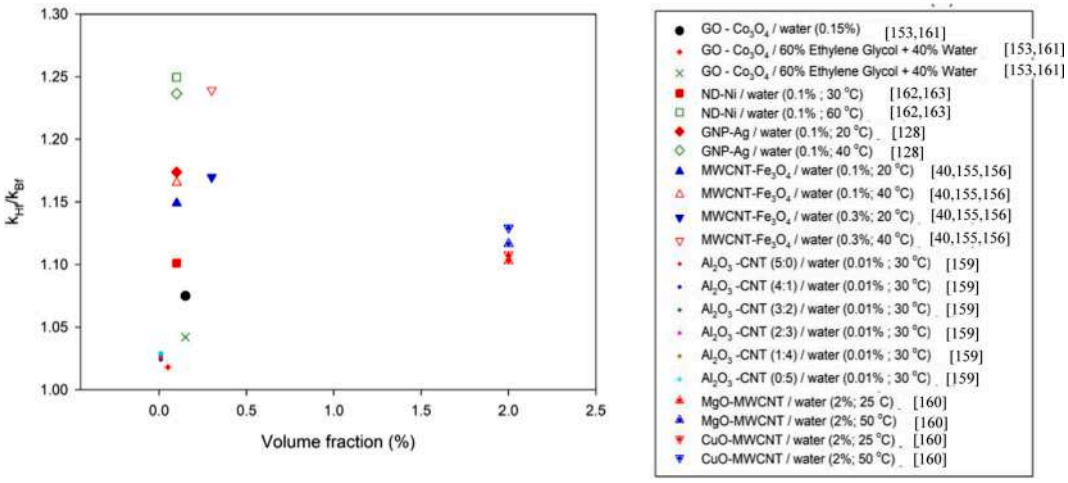

Fig. 9. Comparison of HyNF thermal conductivity over base fluid.

fundamental behavior of the HyNF in various tubular sections such as circular, elliptical, triangular, and rectangular. Hence, the first part of this section mainly discusses the hydrothermal behavior of the HyNF in a bare circular tube, and the related works are summarized in Table 3. The second part of this section focuses on the hydrothermal performance of HyNF on the full-scale heat exchangers, and the associated works are

Table 2
Thermophysical properties of different hybrid nanofluids.

Hybrid Nanofluid specification	Thermophysical properties				Ref.
	Density ($kg\ m^{-3}$)	Viscosity ($kg\ m^{-1}\ s^{-1}$)	Specific heat ($J\ kg^{-1}K^{-1}$)	Thermal conductivity ($W\ m^{-1}K^{-1}$)	
Al_2O_3- Cu /transformer oil (0.1vol. %)	998	$4.49*10^{-3}$	1840	0.32	[164]
Al_2O_3 - Cu / water (0.1vol. %)	1001.3	$9.3*10^{-4}$	4176.8	0.62	[165–167]
Al_2O_3-TiO_2 /water (0.1vol. %)	1029.1	$1.315*10^{-3}$	4044.6	0.64	[151]
TiO_2-ZnO /water (0.1vol. %)	1037.3	$1.315*10^{-3}$	4011.5	0.64	
ZnO - Al_2O_3 /water (0.1vol. %)	1036	$1.315*10^{-3}$	4017.4	0.64	
1.5 % Al_2O_3 -1.5% TiO_2 / oil (300 K)	1024	$9.87*10^{-3}$	1526	0.14	[152]
1.5 % Al_2O_3 -1.5% TiO_2 / oil (650 k)	683	$7.8*10^{-5}$	1951	0.072	
0.15 % GO - Co_3O_4 / water	1001.9	$10.4*10^{-4}$	4172.6	0.63	[153,161]
0.05 % GO - Co_3O_4 / 60 % Ethylene Glycol + 40 % Water	1087.3	$62.3*10^{-4}$	3082.7	0.34	
0.15 % GO - Co_3O_4 / 60 % Ethylene Glycol + 40 % Water	1089.5	$68.9*10^{-4}$	3080.3	0.34	
0.85 g ND - 0.15 g Ni / water (0.1 vol. % & 30 °C)	1000.4	$9.3*10^{-4}$	4174.2	0.66	[162,163]
0.85 g ND - 0.15 g Ni/water (0.1 vol. % & 60 °C)	987.9	$5.3*10^{-4}$	4179.2	0.80	
GNP-Ag / water (0.1 vol. % & 20 °C)	998	$1.26*10^{-3}$	NA	0.68	[128]
GNP-Ag / water (0.1 vol. % & 40 °C)	992	$9.2*10^{-4}$	NA	0.76	
50 % Ag –50 % MgO / water (1.5 vol.%)	1089	$10.25*10^{-4}$	4127.5	0.67	[153,154]
50% Ag – 50% MgO / water (2 vol.%)	1119.2	$10.91*10^{-4}$	4109.4	0.69	
0.26 g MWCNT - 0.74 g Fe_3O_4 / water (0.1 vol. % & 20 °C)	1002	$0.91*10^{-3}$	4182.6	0.67	[40,155,156]
0.26 g MWCNT - 0.74 g Fe_3O_4 / water (0.1 vol. % & 20 °C)	995.8	$0.61*10^{-3}$	4179.6	0.72	
0.26 g MWCNT - 0.74 g Fe_3O_4 /water (0.3 vol. % & 20 °C)	1010.1	$1.01*10^{-3}$	4183.9	0.68	
0.26 g MWCNT - 0.74 g Fe_3O_4 /water (0.3 vol. % & 40 °C)	1003.6	$0.76*10^{-3}$	4180.9	0.76	
Alumina–Cu /water (0.1vol.%)	1002.2	$0.95*10^{-3}$	4176.8	0.62	[157]
Alumina–Cu /water (0.3vol.%)	1002.3	$0.98*10^{-3}$	4176.8	0.63	
Alumina–CNT /water (0.1vol.%)	1001.1	$0.98*10^{-3}$	4174.0	0.63	
Alumina–CNT /water (0.3vol.%)	1004.6	$1.01*10^{-3}$	4174.7	0.64	
Al_2O_3 - MWCNT / water (0.25 vol.% &35 °C)	1004	NA	4150	NA	[158]
Al_2O_3 - MWCNT /water (2 vol.% & 35 °C)	1035	NA	4056	NA	
ZnO - MWCNT / water (0.25 vol.% & 35 °C)	1010	NA	4030	NA	
ZnO - MWCNT / water (2 vol.% & 35 °C)	1040	NA	3980	NA	
TiO_2 - MWCNT / water (0.25 vol. % & 35 °C)	1010	NA	3867	NA	
TiO_2 - MWCNT / water (2 vol.% & 35 °C)	1038	NA	3776	NA	
CeO_2 - MWCNT / water (0.25 vol.% & 35 °C)	1015	NA	4028	NA	
CeO_2 - MWCNT / water (2 vol.% & 35 °C)	1043	NA	3910	NA	
Al_2O_3 -CNT (5:0)/ water (0.01 vol.% & 30 °C)	998.8	$9.3*10^{-4}$	4181	0.61	[159]
Al_2O_3-CNT (4:1) / water (0.01 vol.% & 30 °C)	998.7	$9.4*10^{-4}$	4180.8	0.61	
Al_2O_3-CNT (3:2) / water (0.01 vol.% & 30 °C)	998.2	$9.5*10^{-4}$	4180.4	0.61	
Al_2O_3-CNT (2:3) / water (0.01 vol.% & 30 °C)	998	$9.5*10^{-4}$	4180.3	0.61	
Al_2O_3-CNT (1:4) / water (0.01 vol.% & 30 °C)	997.9	$9.7*10^{-4}$	4180.1	0.61	
Al_2O_3-CNT (0:5) – water (0.01 vol.% & 30 °C)	997.7	$9.9*10^{-4}$	7179.9	0.62	
80% MgO - 20% MWCNT / water (2 vol.% & 25 °C)	NA	$1.26*10^{-3}$	3538	0.65	[160]
80% MgO - 20% MWCNT / water (2 vol.% & 50 °C)	1040	$0.79*10^{-3}$	3674	0.70	
80%CuO - 20% MWCNT / water (2 vol.% & 25 °C)	NA	$1.25*10^{-3}$	3592	0.65	
80%CuO - 20% MWCNT / water (2 vol.% & 50 °C)	1048	$0.82*10^{-3}$	3785	0.71	

listed in Table 6.

Suresh et al. [167] studied the heat transfer behavior of Al_2O_3-Cu/Water (0.1 vol.%) HyNF under the laminar flow regime in a uniformly heated circular pipe. They showed that compared to pure water, a maximum of 13.9% improvement in Nusselt number was obtained for HyNF at Re = 1730, and the average increase in Nusselt number and friction factor obtained was 10.9% and 16.9%, respectively. This study also demonstrated that the increase in Nusselt number attained by Al_2O_3/Water MoNF was 6.0% higher than that of pure water, which indicates that the heat transfer enhancement attained by HyNF was 4.9% higher than that of MoNF. The reason for this improvement is the enhancement of thermal conductivity of HyNF due to the addition of metallic nanoparticles (Cu) into the MoNF. Balla et al. [184] numerically investigated the CuO-Cu/water HyNF behavior in a circular tube and found 30-35% enhancement in Nusselt number compared to water. Labib et al. [135] numerically examined the heat transfer coefficient for the laminar flow of CNT- Al_2O_3/Water HyNF in a circular tube maintained at a constant heat flux. They used a two-phase mixture model for the numerical analysis and reported a maximum increment of 59.9% in the heat transfer coefficient for 0.05 vol.% CNT + 1.6% Al_2O_3/water HyNF compared to 0.05 vol.% CNT/water MoNF. The reduction in boundary layer thickness, caused by the higher shear thinning effect, has been attributed to the heat transfer augmentation. The velocity and temperature profiles of the HyNF are compared with the MoNF, as shown in Fig. 11. The HyNF profiles demonstrated a developing region behavior, whereas the MoNF profiles exhibited a fully developed flow character. Due to this, the HyNF showed better thermal performance over the MoNF.

Sundar et al. [40] observed a 31.1% increase in Nu for 0.3 vol.% MWCNT-Fe_3O_4/Water HyNF with 1.18 times increase in friction factor at Re = 22,000. Moghadassi et al. [166] numerically simulated the experimental work of Suresh et al. [167] using a single-phase model and mixture model. The percentage increase in Nu predicted by the mixture model was 13.4% and 4.7% compared to the water and Al_2O_3/water MoNF, respectively, which is very close to the experimental measurements of Suresh et al. [167]. Hence, they proposed that the mixture model is more suitable for the numerical analysis of hybrid nanofluids. Sundar et al. [155] experimentally investigated the hydrothermal characteristics of CNT- Fe_3O_4/Water HyNF in the plain circular tube and the tube with a twisted tape insert. They observed that in the plain circular tube, the Nusselt number increased by 31.1% with 1.18 times increase in friction factor for 0.3 vol.% CNT-Fe_3O_4/Water HyNF, which is the same as that of the one found for 0.3 vol.%MWCNT-Fe_3O_4/Water HyNF in Sundar et al. [40]. It implies that both CNT-Fe_3O_4/Water and

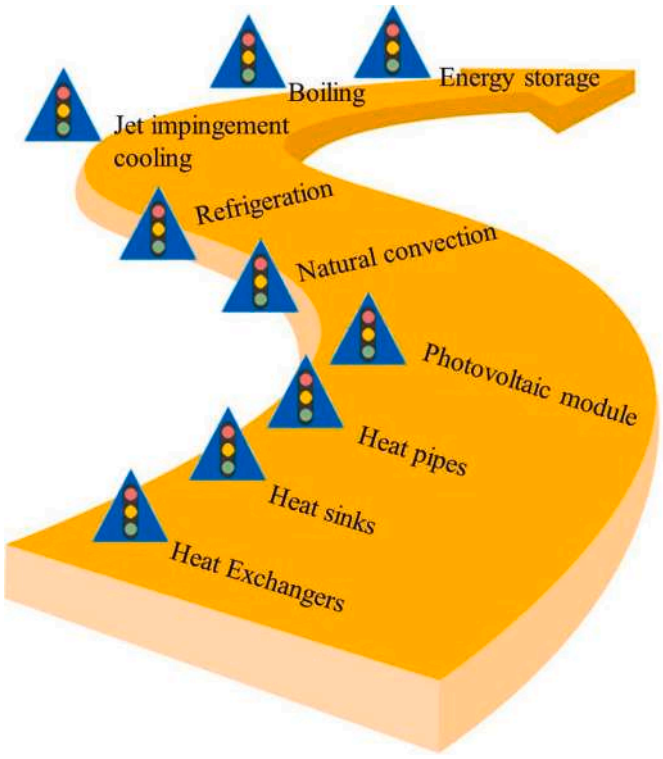

Fig. 10. Heat transfer applications using hybrid nanofluids.

MWCNT-Fe_3O_4/Water exhibit similar thermofluids performance in the turbulent flow regime. Moreover, the use of twisted tapes has further increased the Nusselt number by 42.5% at Re = 22,000. Yarmand et al. [128] examined the role of GNP-Ag/Water HyNF on augmenting the heat transfer performance in the turbulent flow regime. They found that the maximum heat transfer enhancement of 32.7% (Nu) occurred for 0.1 wt.% HyNF at Re = 17,500. However, it was accompanied by 1.1 times increase in friction factor. Takabi et al. [185] concluded a 7.2% improvement of Nusselt number for Al_2O_3-Cu/Water (0.1 vol.%) HyNF, which is about 3% lesser than those reported by Suresh et al. [167] and Moghadassi et al. [166] for the same HyNF. Hussein et al. [186] experimentally studied the behavior of MWCNT-GNP/water HyNF in a mini circular tube (D = 1.1 mm) for the low Reynolds number range of 200 – 500. They found that the maximum (43.4%) increase in heat transfer coefficient was attained at a small Reynolds number of 200. They also showed that the heat transfer coefficient enhancement got reduced in the low Reynolds number flow regime. It is important to mention that this finding is valid only for the mini tube. Whereas, in the large size tubes, other studies showed that for both laminar and turbulent flows, the maximum heat transfer enhancement occurs at higher Reynolds numbers due to the increase in flow inertia [40,128,135,155,166,167]. Megatif et al. [48] studied the heat transfer performance of TiO_2-CNT/water HyNF in a heated circular tube with the following conditions: Re = 1940, T_{in} = 25, 32, and 48 °C with the weight concentrations around 0.1% - 0.2%. They showed that the addition of carbon nanotubes into TiO_2 nanofluid could increase the average heat transfer coefficient up to 33.7%.

The comparison of hybrid nanofluids performance over the base fluid with respect to Nusselt number and friction factor is summarized in Figs. 12 (a) and (b). It can be observed that the Nusselt number and friction factor ratio of HyNF over base fluid were reported to be higher in Al_2O_3-CNT / water – 0.3 vol % at a lower Reynolds number. It was reported that in the laminar regime, the heat transfer enhancement attained via HyNF was almost 10-45% higher than that of the base fluid; however, it was also accompanied by a 10-45% increase in pressure drop. Whereas in the turbulent regime, the attained heat transfer enhancement was 5-40%, but the increase in pressure drop was only 3-20%. The enhancement in heat transfer coefficient is attributed to the interaction of nanoparticles with each other, which is more pronounced in the boundary layer region. However, the increased pressure drop is comparatively higher in the laminar flow regime due to the increased viscosity of HyNF (13%-50% higher than the base fluid), which resulted in a thicker boundary layer. It implies that the use of HyNF is more pronounced in turbulent regimes.

Arunachalam et al. [187] conducted an experimental investigation on Al_2O_3-Cu/Water HyNF to study the hydrodynamic and heat transfer behavior in a plain circular tube and a tube having a V-cut twisted tape insert. They found a maximum enhancement of 42% in Nu for the tubes with V-cut inserts. Hamid et al. [188] studied the effect of various mixing ratios of TiO_2 and SiO_2 (20:80, 40:60, 50:50, 60:40, and 80:20) on heat transfer augmentation with inlet temperature ranging from 30 to 70 °C. They used a mixture of water and ethylene glycol as the base fluid. It was found that the HyNF with a 40:60 mixture ratio provided a 35.3% higher heat transfer coefficient at 70 °C with a negligible pressure drop penalty due to the enhanced thermal conductivity and reduced viscosity, respectively. They reported the least enhancement of 9% for a 50:50 mixture ratio of 1 vol.% HyNF at 30 °C due to the adverse thermo-physical properties. In contrast, Nabil et al. [189] showed that a 50:50 mixture ratio of 1 vol.% TiO_2-SiO_2/water-EG HyNF yielded a 13.6% increase in heat transfer coefficient at 30 °C with a slight increase in pressure drop, and 3 vol.% HyNF provided a maximum improvement of 81% at 70 °C.

To clear this discrepancy, more experimental studies are required on TiO_2-SiO_2/water-EG HyNF for various mixture ratios. For the same HyNF, Hamid et al. [190] demonstrated that for the tube with wire coil inserts, a maximum of 254.4% enhancement in heat transfer was found at a pitch ratio of 0.83 with 6.38 times higher pressure drop. Though the pitch ratio of 0.83 exhibited a higher heat transfer, the pitch ratio of 1.5 was found to be optimum in terms of thermal performance factor. To understand the heat transfer and flow behavior, Sundar et al. [162,163] performed an experimental study on ND-Ni/Water HyNF in the tubes with and without longitudinal stripes. The results revealed that the increase in Nusselt number was 35.4% and 93.3% at Re = 22,000 for tubes with and without longitudinal inserts, respectively. Hussein et al. [191] studied the thermofluids behavior of MWCNT-GNP/Water HyNF in a brass microtube for the low Reynolds number flow regime (Re = 200 – 500). They showed a maximum enhancement of 58.2% in the Nusselt number with a penalty of 12.4% increase in pressure drop. Hussein et al. [192] numerically analyzed the heat transfer characteristics of Al_2O_3.Graphene/water in a mini tube and found that the Nu was increased by 13.7%. Hameed et al. [157] compared the thermal performance of Al_2O_3-Cu/water and Al_2O_3-CNT/water hybrid nanofluids. The results demonstrated that the heat transfer enhancement obtained by Al_2O_3-CNT/water was better than the Al_2O_3-Cu/water due to the improved thermal conductivity of the earlier HyNF. Dalkilic et al. [193] experimentally investigated the heat transfer behavior of graphite-SiO_2/water HyNF in the tube with quad-channel twisted tape inserts (QDCC). They showed a 26% enhancement in heat transfer coefficient for the tube with QDCC.

Table 3 shows that many authors widely studied the circular geometry due to its wider use in industries. However, studies on the effect of HyNF on other tubular sections, such as elliptical, triangular, and rectangular are still limited. In Table 4, Nusselt number and friction factor correlations proposed by many researchers are listed for various hybrid nanofluids.

Usually, hybrid nanofluid comprises two nanocomposites; hence, from each HyNF, two MoNF can be derived. Based on this, the heat transfer performance of various hybrid nanofluids is compared with the corresponding two mono nanofluids, illustrated in Table 5. The heat transfer performance of the various fluids (HyNF, MoNF-1, and MoNF-2) is assessed on a scale of 1-3. For the given fluid, scale 1 denotes the highest heat transfer enhancement compared to the base fluid, whereas

Table 3
Summary on studies related to tubular heat exchangers.

Reference	Method	Hybrid Nano composite	Base fluid	Concentration	Re/ Flow rate	Type of heat exchanger	Comparison of HyNF Heat transfer and Pressure drop Characteristics with base fluid
Suresh et al. [167]	E	Al_2O_3-Cu	Water	0.1 vol.%	Laminar (Re = 700-2300)	Circular tube with constant heat flux	A maximum increase of 13.5% in Nusselt number (Nu) was attained with a penalty of 16.9% increase in friction factor
Balla et al. [184]	N	CuO-Cu	Water	0 - 1 vol.%	Laminar (Re = 100-1100)	Circular tube with constant heat flux	Enhancement of 30-35% in Nu
Labib et al. [135]	N	Al_2O_3-CNT	Water	___	Laminar (Re = 500-2000)	Circular tube with constant heat flux	HyNF (0.05 vol.% CNT+1.6 vol.% Al_2O_3) has provided 59.9% enhancement in heat transfer coefficient when compared to 0.05 vol.% CNT-Water MoNF
Sundar et al. [40]	E	MWCNT-Fe_3O_4	Water	0.1 - 0.3 vol.%	Turbulent (Re = 3000-22000)	Circular tube with constant heat flux	An increase in Nu of up to 31.1% was observed for 0.3 vol.% of HyNF with a penalty of 1.18 times increase in friction factor at a Reynolds number of 22000
Moghadassi et al. [166]	N	Al_2O_3-Cu	Water	0.1 vol.%	Laminar (Re < 2300)	Circular tube with constant heat flux	Average increase in Nusselt number of 13.5% was obtained with an increase of 15.5% in pressure drop
Sundar et al. [155]	E	CNT-Fe_3O_4	Water	0.1 - 0.3 vol.%	Turbulent (Re = 3000-22000)	Circular tube with twisted tape - constant heat flux	Tube with twisted tape has resulted 42.5% enhancement in Nu with a penalty of 1.23 times increase in friction factor
Yarmand et al. [128]	E	GNP-Ag	Water	0.02 - 0.1 wt. %	Turbulent (Re = 5000-17500)	Circular tube with constant heat flux	A maximum of 32.7% enhancement of Nu was attained for 0.1 wt.% HyNF at Re = 17500. Correspondingly, friction factor increased by 8%
Takabi et al. [185]	N	Al_2O_3-Cu	Water	0.1 - 2 vol.%	Laminar (Re 600 - 2300)	Circular tube with constant heat flux	Average increase in Nusselt number of 7.2% was obtained with an increase of 10.9% in pressure drop
Hussein et al. [186]	E	MWCNT-GNP	Water	___	Laminar (Re = 200 -500)	Mini circular tube with constant heat flux	Average heat transfer coefficient enhancement of up to 33.5% was attained for a 0.25 wt.% with a penalty of 11% increase in pressure drop
Megatif et al. [48]	E	TiO_2-CNT	Water	0.1 - 0.2 wt.%	Re = 1940	Circular tube with constant heat flux	Increase in average heat transfer coefficient of 33.7% for 0.2 wt.% was reported
Arunachalam et al. [187]	E	Al_2O_3-Cu	Water	___	Laminar (Re < 2300)	Circular tube with V-cut twisted tape - constant heat flux	HyNF (0.01% Cu + 0.4% Alumina) provided a maximum of 42% improvement in Nusselt number for the circular tube with V-cut tube inserts
Hamid et al. [188]	E	TiO_2-SiO_2	Water+EG (60:40)	1.0 vol.%	Turbulent (Re = 3000 - 24000)	Circular tube with constant heat flux	A maximum enhancement of 35.3% in heat transfer coefficient was reported for 40:60 mixture ratio. Furthermore, it showed a slight increment in friction factor, only 1.02 times higher than base fluid.
Nabil et al. [189]	E	TiO_2-SiO_2	Water+EG (60:40)	0.5 - 3.0 vol.%	Turbulent (Re = 3000 - 24000)	Circular tube with constant heat flux	A maximum of 80.9% improvement in heat transfer coefficient was obtained for 3 vol.% HyNF with a slight increase in friction factor
Hamid et al. [190]	E	TiO_2-SiO_2	Water+EG (60:40)	0.5 - 3.0 vol.%	Turbulent (Re = 2300 - 12000)	Circular tube with wire coil inserts - constant heat flux	A maximum enhancement of 254.4% in Nusselt number was attained for 2.5 vol.% and pitch-diameter (PD) ratio of 0.83 when compared to the plain tube. Furthermore, wire coil insert arrangement provided a 6.38 times higher friction factor for the 0.83 PD ratio
Sundar et al. [162]	E	ND-Ni	Water	0.1 - 0.3 vol.%	Turbulent (Re = 3000 - 22000)	Circular tube with constant heat flux	Nusselt number of HyNF with 0.3 vol.% was increased by 35.4% at Re = 22000. However, for the same Re, the friction factor was increased up to 1.12 times
Sundar et al. [163]	E	ND-Ni	Water	0.1 - 0.3 vol.%	Turbulent (Re = 3000 - 22000)	Circular tube with longitudinal strip inserts - constant heat flux	Tube with longitudinal strip insert (AR = 1.0) has provided a 93.3% enhancement in Nusselt number and a penalty of 1.248 times increase in friction factor compared to plain tubes operated with water.
Hussein et al. [191]	E	MWCNT-GNP	Water	0 - 0.125 wt.%	Laminar (Re = 200 - 500)	Circular micro tube with constant heat flux	Heat transfer coefficient and pressure drop were increased by 58.2% and 12.4%, respectively
Hussein et al. [192]	N	Al_2O_3-Graphene	Water	___	Laminar (Re = 100 - 1600)	Circular mini tube with constant heat flux	Enhancement in Nusselt number of 12.7-13.7% was reported
Hameed et al. [157]	E	Al_2O_3-CNT; Al_2O_3-Cu	Water	0.1 - 0.3 vol.%	Laminar (Re = 700-2300)	Circular tube with constant heat flux	Al_2O_3+CNT and Al_2O_3+Cu HyNFs enhanced the Nusselt number by 26.6% and 16.5%, respectively. However, friction factor was also increased by 38.4% and 30.8% respectively.
Dalkilic et al. [193]	E	Graphite-SiO_2	Water	0.5 - 1 vol.%	Turbulent (Re = 3400 - 11000	Circular tube with quad channel twisted tape insert (QDCC) - constant heat flux	Increase in heat transfer coefficient of 26% was provided by tube with QDCC for 1 vol.% HyNF

*E – Experimental study; N – Numerical study

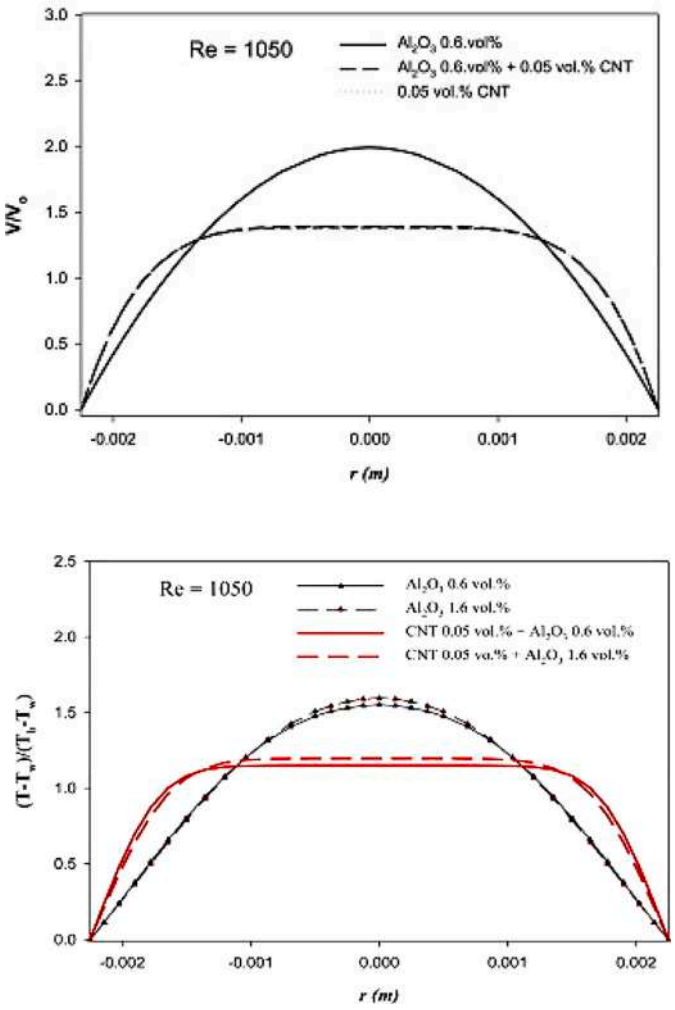

Fig. 11. Comparison of velocity profile and temperature profile of HyNF with MoNF [135].

scale 3 denotes the least enhancement of heat transfer coefficient compared to the base fluid. It is important to note here that for many studies, heat transfer data of the metallic nanofluids (MoNF) are not available in the respective literature for comparison; so, for those cases, only the performance of metal-oxide nanofluids are compared with the HyNF. Table 5 clearly demonstrates that the heat transfer performance of HyNF is better than the metal-oxide MoNF. However, Balla et al. [184] showed that the Cu/Water MoNF (metallic nanofluid) exhibited a higher heat transfer coefficient (HTC) than that of Al_2O_3-Cu/water HyNF. Metallic nanofluid showed a higher HTC due to its improved thermal conductivity. Though the thermal conductivity of metallic mono nanofluid is high, its stability is lacking compared to the metal-oxide mono nanofluids, which contains relatively higher stability. This fact impedes the use of metallic nanofluids in practical applications. To overcome this issue, the metallic mono nanofluids (higher thermal conductivity) and the metal-oxide mono nanofluids (higher stability) are combined to develop hybrid nanofluid. This newly developed HyNF possesses the synergetic effect of both the higher thermal conductivity and stability, which makes the HyNF a potential candidate for various heat transfer applications [194].

So far, the performance of hybrid nanofluids in a single circular tube is discussed. In this section, the applications of HyNF in the full-scale heat exchangers (HX), such as shell and tube HX, tube in tube HX, and plate heat exchangers, are discussed, and the summary is presented in Table 6. Madhesh et al. [43] experimentally determined the Nusselt number and the friction factor for a tube in tube counter-flow heat exchanger using Cu-TiO_2/water HyNF for the volume concentration of 0.1% to 2.0%. The results revealed that the Nusselt number enhancement (49%) was achieved up to a volume concentration of 1.0%, beyond which a considerable degradation in heat transfer enhancement was noticed. However, another similar study conducted by Madhesh et al. [195] showed that the optimum volume concentration for Cu-TiO_2/water HyNF was 0.7%. A maximum increase of 59.3% in the Nusselt number was obtained for 0.7 vol.%. The heat transfer enhancement started to deteriorate beyond 0.7 vol.% due to the increase in viscosity and agglomeration, which in turn reduces the fluid velocity and the interaction between the base fluid and nanoparticles. They also proposed a heat transfer correlation for counter-flow heat exchangers,

$$\mathrm{Nu} = 0.012\, Re\, Pr^{0.333}\, \varphi^{0.032}, 4000 < Re < 8000 \& 0.1 < \varphi < 1.0 \text{ vol.\%} \quad (25)$$

$$\mathrm{Nu} = 0.012\, Re^{1.148}\, Pr^{0.333}\, \varphi^{0.064}, 4000 < Re < 14000 \& 0.1 < \varphi < 1.0 \text{ vol.\%} \quad (26)$$

Phanindra et al. [164] conducted experimental and numerical studies on a counter-flow tube in tube heat exchanger using 0.1 vol.% Al_2O_3-Cu/transformer oil. They showed a 12.1% increase in the Nusselt number at a Reynolds number of 1820. Bahiraei et al. [196] numerically investigated the thermal and hydraulic performances of CNT-Fe_3O_4/water HyNF in a minichannel heat exchanger. They reported an improved heat transfer performance of HyNF over water and mono nanofluids, and a maximum of 53.8% increase in heat transfer coefficient was obtained at a Reynolds number of 500. Heat transfer performance was more influenced by the rise in magnetite concentration (i.e., Fe_3O_4) than the CNTs concentration. This is due to significant improvement in thermal conductivity obtained by adding the magnetite nanoparticles over the CNT. Shahsavar et al. [197] compared the Newtonian and non-Newtonian behavior of CNT-Fe_3O_4/water HyNF in a double pipe heat exchanger. The study concluded that the assumption of Newtonian fluid behavior for HyNF could result in a significant predictive deviation (up to 19.6% deviation was observed for performance evaluation criterion) in pressure drop and pumping power. Whereas the same has a minor impact (less than 2.91%) on the heat transfer calculation. So, this study implies the necessity of considering the HyNF as non-Newtonian fluid.

Singh et al. [198] performed energy and economic analyses for various hybrid nanofluids, such as Al_2O_3-MWCNT/water, Al_2O_3-Ag/water, Al_2O_3-Cu/water, and Al_2O_3-TiO_2/water, in a shell and tube heat exchanger. The results showed that a maximum of 3.2% enhancement in heat transfer was found for Al_2O_3-Ag/water HyNF with a higher pressure drop. Whereas Al_2O_3-MWCNT/water exhibited a 2.9% increase in heat transfer rate with a slight increase in pressure drop. The Al_2O_3-MWCNT/water requires an 11.6% lesser pumping power, whereas the same was 10.9%, 10.2%, and 9.6% for Al_2O_3-TiO_2/water, Al_2O_3-Cu/water, and Al_2O_3-Ag/water HyNFs, respectively. The economic assessment also demonstrated that the Al_2O_3-Ag/water HyNF demands a payback period of 247 years, whereas the payback period for Al_2O_3-TiO_2/water drastically reduced to 9.8 years. Anitha et al. [199] studied the hydraulic and thermal response of shell and tube heat exchanger using Al_2O_3-Cu/water HyNF. The results demonstrated that the heat transfer coefficient obtained by HyNF was 139% and 25% higher than water and Cu/water mono nanofluid, and the obtained Nusselt number was 90% higher than that of Al_2O_3/water MoNF. Hence, it can be firmly stated that the heat transfer performance of the hybrid nanofluid is better than that of mono nanofluid.

Hung et al. [114] adopted hybrid carbon nanofluids in an air-cooled heat exchange system and measured the heat exchange capacity and the system efficiency factor. An increase in the heat exchange capacity (13 %) and the system efficiency factor (11.7 %) were achieved at the inlet temperature of 35 °C and a flow rate of 2 LPM. The enhancement ratio in heat exchange capacity and system efficiency factor was more tangible for higher Re (greater than 8000), below which (but still within the

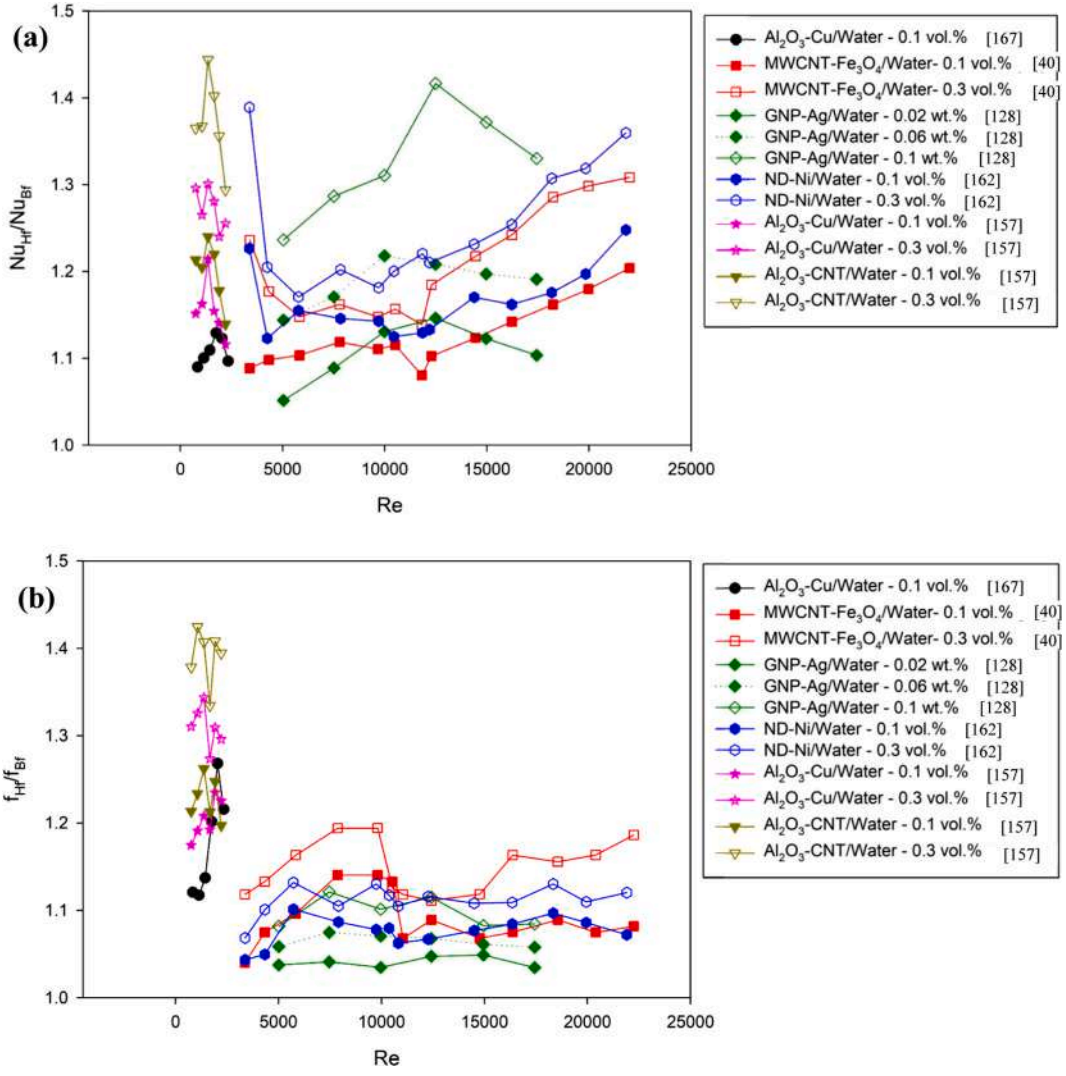

Fig. 12. Comparison of hybrid nanofluids performance over base fluid (a) Nusselt number and (b) Friction factor.

turbulent flow condition) the HyNF has not shown any significant improvement. Nevertheless, other turbulent flow-related studies [40,128,155,162,163,188–190,193] showed that the significant enhancement in heat transfer rate could be attained for the Reynolds number less than 8000. Karimi et al. [200] examined the MgO-MWCNT/EG HyNF in an air-cooled heat exchange system. They showed a maximum enhancement of 20% in Nusselt number at a Reynolds number of 350, volume concentration of 1%, and inlet temperature of 45 °C. The increase in pressure drop was 50% at a Reynolds number of 350, the volume concentration of 0.8%, and inlet temperature of 45 °C. This study reported that the concentration of nanofluids and Reynolds number are the crucial factors affecting the heat transfer and pressure drop characteristics, which is consistent with most of the studies. However, they reported a small effect of fluid inlet temperature on pressure drop and heat transfer rate despite having a higher thermal conductivity of HyNF at higher temperatures, which contradicts the results obtained by other researchers. A detailed discussion of the effect of inlet temperature on thermofluids performance of HyNF is provided later in this section.

Sahoo et al. [201] compared the heat transfer performance of various hybrid nanofluids, including Al_2O_3-Ag/water, Al_2O_3-Cu/water, Al_2O_3-CuO/water, Al_2O_3-Fe_2O_3/water, and Al_2O_3-TiO_2/water in a louvered fin automotive radiator. Similarly, Sahoo et al. [202] numerically analyzed the performance of various HyNFs, including Al_2O_3-Ag/EG, Al_2O_3-Cu/EG, Al_2O_3-SiC/EG, Al_2O_3-CuO/EG, and Al_2O_3-TiO_2/EG in a louvered fin automotive radiator. Both the studies showed that the Al_2O_3-Ag based hybrid nanofluid could provide a higher heat transfer coefficient than the other hybrid nanofluids. However, the pressure drop of Al_2O_3-Ag based hybrid nanofluid was also the highest among other HyNFs. For the fixed flow rate and heat transfer rate, using Al_2O_3-Ag based hybrid nanofluid, the heat exchanger size could be reduced approximately by 3.8% with a 2.9%-3.4% increase in pumping power. Huminic et al. [203] performed a comparative study between MWCNT-Fe_3O_4/water and ND-Fe_3O_4/water HyNFs in a flat tube automobile radiator. The results showed that MWCNT-Fe_3O_4/water HyNF provided a higher heat transfer coefficient than that of the ND-Fe_3O_4/water HyNF. A maximum of 21% and 15% enhancement in the heat transfer coefficient was attained by MWCNT-Fe_3O_4/water and ND-Fe_3O_4/water HyNFs, respectively. Huminic et al. [204] showed a 16.4% enhancement in the heat transfer coefficient using MgO-MWCNT/EG in a flat tube automobile radiator.

Returi et al. [205] performed a numerical analysis on a spiral plate heat exchanger using Al_2O_3-CuO/water and Al_2O_3-TiO_2/water HyNFs. They observed an over 16%-27% increase in heat transfer rate for the volume concentration of 4%. Further, Al_2O_3-CuO/water HyNF yielded a 10% higher heat transfer rate than Al_2O_3-TiO_2/water HyNF. Allahyar et al. [78] showed a 31.58% increase in the Nusselt number using Al_2O_3-Ag/water HyNF in a coiled heat exchanger. Furthermore, Hormozi et al.

Table 4
Summary of the HyNF's Nusselt number and friction factor correlation for circular tubes.

Reference	HyNF	Description	Correlation	Deviation
Suresh et al. [167]	Al_2O_3-Cu/water	$Re < 2300$; $\phi = 0.1$ vol.%	$Nu = 0.031 (Re Pr)^{0.68} (1+\phi)^{95.73}$ $f = 26.44 Re^{-0.8737} (1+\phi)^{156.23}$	-3% and +5% for Nu; -5% and +3% for f
Sundar et al. [40]	MWCNT-Fe_3O_4/water	$3000 < Re < 22000$	$Nu = 0.0215 Re^{0.8} Pr^{0.5} (1+\phi)^{0.78}$; 0 vol.% $< \phi <$ 0.3 vol.%; 4.50 $<$ Pr $<$ 6.13 $f = 0.3108 Re^{-0.245} (1+\phi)^{0.42}$ 0 vol.% $< \phi <$ 0.6 vol.%; 3.72 $<$ Pr $<$ 6.37	Standard deviation of 8% and 2.72% for Nu and f, respectively
Moghadassi et al. [166]	Al_2O_3-Cu/water	$Re < 2300$; $\phi = 0.1$ vol.%	$Nu = 0.125 Re^{0.592} Pr^{0.333} (1+\phi)^{77.13}$ $f = 133.57 Re^{-1.12} (1+\phi)^{112.45}$	±7% for Nu; -5% and +7% for f
Sundar et al. [155]	CNT-Fe_3O_4/water	$3000 < Re < 22000$; $0 < H/D < 15$	$Nu = 0.0223 Re^{0.8} Pr^{0.5} (1+\phi)^{0.58} (1+H/D)^{0.036}$; 0 vol.% $< \phi <$ 0.3 vol.%; 3.75 $<$ Pr $<$ 6.23 $f = 0.31 Re^{-0.245} (1+\phi)^{0.473} (1+H/D)^{0.013}$ 0 vol.% $< \phi <$ 0.3 vol.%;	NA
Yarmand et al. [128]	GNP-Ag/water	$5000 < Re < 17500$; 0 wt.% $< \phi <$ 0.1 wt.%;	$Nu = 0.0017066 Re^{0.9253} Pr^{1.29001}$ $f = 0.567322 Re^{-0.285869} \phi^{0.0271605}$	Maximum deviation of 8.05% and 0.9% for Nu and f, respectively
Hamid et al. [188]	TiO_2-SiO_2/W+EG	$3000 < Re < 24000$; 0 vol.% $< \phi <$ 1.0 vol.%; 30 $<$ T $<$ 70 °C; $0 < R < 0.8$	$Nu = 0.023 Re^{0.8} Pr^{0.4} (1+\phi/100)^{15} (0.1+T/70)^{-0.062} (1+R)^{-0.218}$ $f = 0.3164 Re^{-0.25} (1+\phi/100)^{3.1} (1+R)^{-0.032}$	Standard deviation of 4.88% and 2.12% for Nu and f, respectively
Nabil et al. [213]	TiO_2-SiO_2/W+EG	$3000 < Re < 24000$; 0 vol.% $< \phi <$ 3.0 vol.%; 30 $<$ T $<$ 70 °C;	$Nu = 0.023 Re^{0.8} Pr^{0.4} (1+\phi/100)^{6.9} (0.01+T/70)^{0.05}$ $f = 0.3164 Re^{-0.25} (1+\phi/100)^{2.8}$	Standard deviation of 4.2% and 2.9% for Nu and f, respectively
Hamid et al. [190]	TiO_2-SiO_2/W+EG	$2300 < Re < 12000$; 0 vol.% $< \phi <$ 3.0 vol.%; 0.83 $<$ P/D $<$ 4.17	$Nu = 1.65 \times 10^{-4} Re^{0.705} Pr^{2.64} (1+\phi/100)^{8.58} (P/D_c)^{0.411}$ $f = 4.16 Re^{-0.269} (1+\phi/100)^{3.31} (1+P/D_c)^{-1.17}$	Standard deviation of 6.35% and 4.31% for Nu and f, respectively
Sundar et al. [162]	ND-Ni/water	$3000 < Re < 22000$; 0 vol.% $< \phi <$ 0.3 vol.%; 4.39 $<$ Pr $<$ 5.71	$Nu = 0.022 Re^{0.8} Pr^{0.5} (1+\phi)^{0.86}$ $f = 0.295 Re^{-0.241} (1+\phi)^{0.3097}$	Standard deviation of 5.1% and 2.01% for Nu and f, respectively
Sundar et al. [163]	ND-Ni/water	$3000 < Re < 22000$; 0 vol.% $< \phi <$ 0.3 vol.%; 4.35 $<$ Pr $<$ 5.85 $0 < AR < 4$	$Nu = 0.02433 Re^{0.8} Pr^{0.4} (1+\phi)^{1.193} (1+AR)^{0.0291} (D_h/D_i)^{-0.1532}$ $f = 0.2689 Re^{-0.2312} (1+\phi)^{0.3556} (1+AR)^{-0.0024} (D_h/D_i)^{-0.083}$	Standard deviation of 9.42% and 2.18% for Nu and f, respectively
Hussein et al. [192]	Al_2O_3-Graphene/water	$100 < Re < 1600$	$Nu = 3.33 (Re Pr (D/L))^{0.21} (1+\phi)^{3.12}$	$R^2 = 0.954$
Dalkilic et al. [193]	Al_2O_3-Cu/water	$3400 < Re < 11000$; $\phi = 0.5$ and 1.0 vol.%; L = 14, 28 and 42 cm	$Nu = 0.00012 Re^{1.148294} Pr^{1.596637} (1+\phi)^{9.429766} (l/L+1)^{0.401864}$ $f = 0.646889 Re^{-0.318925639} (1+\phi)^{1.90706352} (l/L+1)^{7.158388067}$	Error margin of ±5% and ±10% for Nu and f, respectively

[206] also conducted an experimental study in a helical coil exchanger using Al_2O_3-Ag/water HyNF added with nonionic Poly Vinyl Pyrrolidone (PVP) and anionic Sodium Dodecyl Sulfate (SDS) surfactants (0.1 – 0.4 wt.%). They concluded that the addition of 0.1 wt.% concentration of SDS anionic surfactant into the Al_2O_3-Ag/water HyNF could increase the stability and enhance the thermal performance of the heat exchanger by 16%.

Safi et al. [207] experimentally investigated the heat transfer performance of MWCNT-TiO_2/water HyNF in a plate heat exchanger and noted a 20.2% increase in heat transfer for 0.08 wt.%. Huang et al. [208] analyzed the convective heat transfer behavior of Al_2O_3-MWCNT/water HyNF in the plate heat exchangers. They observed that the heat transfer enhancement attained by hybrid nanofluid was very less when compared to pure water and mono nanofluids. There is an apparent contradiction between this study observation and other studies, such as [40,186,191,198,200,203,204,207], which showed a significant heat transfer enhancement using MWCNT based hybrid nanofluids. The lower performance improvement might be attributed to the hybrid nanofluid preparation method that produced poor bonding between Al_2O_3 and MWCNT nanocomposites, thereby adversely affecting the thermophysical properties of HyNF. Also, the random motion of nanoparticles in the fluid mixture may, sometimes, align the nanocomposites parallel to the fluid flow direction, which would also deteriorate the heat transfer augmentation. Bhattad et al. [209] demonstrated a 39.2% enhancement in heat transfer rate using Al_2O_3-MWCNT/water HyNF in the plate heat exchangers. Bhattad et al. [210] performed a comparative analysis of various hybrid nanofluids, including Al_2O_3-SiC/water, Al_2O_3-AlN/water, Al_2O_3-MgO/water, Al_2O_3-CuO/water, and Al_2O_3-MWCNT/water, in the plate heat exchangers. They observed that Al_2O_3-MWCNT/water HyNF had provided a maximum heat transfer enhancement of 31.2% with a negligible pressure drop. Whereas another similar study performed by Bhattad et al. [211] on the plate heat exchangers using Al_2O_3-MWCNT/water HyNF showed that the heat transfer performance of MWCNT MoNF was superior to Al_2O_3-MWCNT/water HyNF; yet, this observation is inconsistent with the previous study of Bhattad et al. [209,210]. Bhattad et al. [212] theoretically analyzed the performance of Al_2O_3-Ag and MgO-Ag hybrid nanofluids in the plate heat exchangers applicable for the milk chillers. The analysis used the ethylene glycol (EG)-water and propylene glycol (PG)-water combination as base fluids. The results revealed that the maximum and the minimum heat transfer coefficient improvement of 9.3% and 8.1% were obtained for PG-based Al_2O_3-Ag hybrid nanofluid and EG-based MgO-Ag hybrid nanofluid, respectively.

Based on the above-mentioned comprehensive review, it appears that the results regarding the influence of inlet temperature of HyNF on the heat transfer performance of the heat exchangers are inconclusive. For example, Karimi et al. [200] reported no impact of inlet temperature on heat transfer performance at different volume fractions, as shown in Figs. 13 (a) and 13(b). Whereas Huminic et al. [203,204] and Safi et al. [207] showed that the heat transfer enhancement deteriorates gradually with increased fluid temperature. This is because of the decrease in

Table 5
Heat transfer performance of assessment of HyNF with MoNF.

Reference	HyNF	MoNF-1	MoNF-2	HyNF Vs MoNF		
				HyNF	MoNF-1	MoNF-2
Suresh et al. [167]	Al_2O_3-Cu/water	Al_2O_3/water	Cu/water	1	2	NA
Balla et al. [184]	CuO-Cu/water	CuO/water	Cu/water	2	3	1
Labib et al. [135]	Al_2O_3-CNT/water	Al_2O_3/water	CNT/water	1	3	2
Sundar et al. [40]	MWCNT-Fe_3O_4/water	Fe_3O_4/water	MWCNT/water	1	2	NA
Moghadassi et al. [166]	Al_2O_3-Cu/water	Al_2O_3/water	Cu/water	1	2	NA
Sundar et al. [155]	CNT-Fe_3O_4/water	Fe_3O_4/water	CNT/water	1	2	NA
Yarmand et al. [128]	GNP-Ag/water	GNP/water	Ag/water	1	NA	NA
Takabi et al. [185]	Al_2O_3-Cu/water	Al_2O_3/water	Cu/water	1	2	NA
Hussein et al. [186]	MWCNT-GNP/water	GNP/water	MWCNT/water	1	NA	2
Megatif et al. [48]	TiO_2-CNT/water	TiO_2/water	CNT/water	1	NA	2
Arunachalam et al. [187]	Al_2O_3-Cu/water	Al_2O_3/water	Cu/water	1	2	NA
Hamid et al. [188]	TiO_2-SiO_2/W+EG	TiO_2/W+EG	SiO_2/W+EG	1	2	3
Nabil et al. [189]	TiO_2-SiO_2/W+EG	TiO_2/W+EG	SiO_2/W+EG	1	2	3
Hamid et al. [190]	TiO_2-SiO_2/W+EG	TiO_2/W+EG	SiO_2/W+EG	1	2	3
Sundar et al. [162]	ND-Ni/water	ND/water	Ni/water	1	2	3
Sundar et al. [163]	ND-Ni/water	ND/water	Ni/water	1	2	3
Hussein et al. [191]	MWCNT-GNP/water	GNP/water	MWCNT/water	1	NA	2
Hussein et al. [192]	Al_2O_3-Graphene/water	Al_2O_3/water	Graphene/water	1	2	NA
Hameed et al. [157]	Al_2O_3-Cu/water	Al_2O_3/water	Cu/water	1	2	NA
Hameed et al. [157]	Al_2O_3-CNT/water	Al_2O_3/water	CNT/water	1	2	NA

viscosity and density at higher temperatures, which in turn lead to a rise in Reynolds number. This increase in Reynolds number may align the nanoparticles rapidly and result in a smaller interaction between fluid and particles; thus, the Brownian motion in hybrid nanofluid diminishes and reduces the heat transfer rate, as shown in Figs. 14 (a) and 14(b). It is important to note here that the thermal conductivity of hybrid nanofluid increases with fluid temperature. In this regard, the reduction in heat transfer coefficient is possible only if the reduction in Brownian motion surpasses the effect of increasing thermal conductivity of HyNF. In contrast to Huminic et al. [203,204] and Safi et al. [207], the results of Bhattad et al. [209–211] demonstrated that the heat transfer coefficient increases with fluid inlet temperature due to the increase in thermal conductivity of HyNF, as shown in Fig. 15. To clarify the discrepancy among various studies, detailed experimental investigations on the influence of inlet temperature on the heat transfer performance of various heat exchangers are required for better clarity and understanding.

4.2. Heat sinks

Miniaturized electronic components and semiconductor devices, which are often accompanied with higher power dissipation, pose a challenge on thermal management due to increased heat generation [214,215]. To ensure reliable operation of the electronic equipments, the junction temperature of the electronic components must be below the threshold value of their specifications. The cooling of electronic components can be achieved by air or liquid cooling methods. Owing to the superior cooling capacity, liquid cooling methods are becoming more popular and accepted for high-flux applications [216]. In liquid cooling methods, water is mostly used as a working fluid as it offers outstanding thermophysical properties and widespread availability [217]. For further enhancing the cooling demand in response to the gigantic rise in heat dissipation associated with 5G, HPC, IoT, smart computing, and the like, it is therefore imperative to uplift the performance of liquid cooling. The following techniques have been widely used for augmenting the cooling capacity, such as providing different geometrical configurations of the flow channel (ex., circular, elliptical, triangular, trapezoidal, and rectangular), employing wavy structures in the heat sinks, and introducing porous structure in the channels of heat sinks [218–220]. Although the aforementioned techniques have rendered a better cooling performance, further improvement in heat transfer capacity can be achieved by enhancing the coolant's thermophysical properties. One of such techniques recently developed is nanofluid. Many authors studied the role of mono nanofluids in heat sinks and demonstrated superior performance over water [221–224]. Moreover, hybrid nanofluids are recently developed with higher thermal conductivity and greater stability. This section discusses the thermal and hydraulic performance of hybrid nanofluids in heat sinks and micro/minichannels. The studies related to the micro/minichannel heat sinks concerning the use of hybrid nanofluids are summarized in Table 7.

Nimmagada et al. [225] numerically investigated the heat transfer and flow behavior of Al_2O_3-Ag/water hybrid nanofluid in a rectangular microchannel, using a 2D conjugate heat transfer model. They reported an enhancement of 143% in average heat transfer coefficient for 3 vol.% HyNF (0.6vol.% Al_2O_3 + 2.4vol.% Ag). At the same time, the increase in the average heat transfer coefficient obtained by 3 vol.% Ag/water nanofluid was 135.5%, almost 8% lesser than the one attained by HyNF. Many studies reported that in the core region of the channel, nanoparticles tend to accumulate and increasing the concentration and density [167]. Because of this, the nanofluids provide a flat velocity profile (like the developing region velocity profile) compared to pure fluid such as water and EG. Whereas the velocity profile attained by Nimmagada et al. [225] showed a reverse trend. i.e., the velocity of HyNF was higher than that of pure fluid in the core region. The reason for attaining the higher velocity in the core region could probably be attributed to using the homogeneous conjugate heat transfer model, which assumes the constant thermophysical properties, instead of the multiphase mixture model. Nimmagada et al. [226] numerically studied the hydrothermal performance of SWCNT-Cu/water HyNF in the laminar flow regime of the microchannel. They performed the numerical analysis using a single-phase homogeneous approach and the multiphase mixture model. They showed that the mixture model results are closer to the experimental findings, which is in agreement with the observations of [135,166]. Moreover, the velocity profile attained using the multiphase mixture model was flatter than pure water. And the velocity of HyNF obtained using a single-phase approach was higher than that of pure water due to the increase in kinematic viscosity, which does not match with other studies [135,166,167]. Nimmagada et al. [227] experimentally and numerically analyzed the flow performance of Al_2O_3-Ag/water HyNF in the low Reynolds number (30-50) regime of a rectangular microchannel. The heat transfer enhancement obtained by HyNF (1.5% Al_2O_3 + 1.5% Ag) was equivalent to 3 vol.% Ag/water MoNF. Yet, the cost of Ag nanocomposites is high; thus, the use of Al_2O_3-Ag/water HyNF may be economically viable. Nimmagada et al. [228] investigated the heat transfer and flow behavior of Cu-Al/water HyNF in a rectangular microchannel. They showed a 23.4% increase in the

Table 6
Summary on studies related to full-scale heat exchangers.

Reference	Method	Hybrid nano composite	Base fluid	Concentration	Re/Flow rate	Type of heat exchanger	Comparison of HyNF Heat transfer and Pressure drop Characteristics with base fluid
Madhesh et al. [43]	E	Cu-TiO_2	Water	0.1 - 2.0 vol.%	Re = 4000-8000	Tube in tube counterflow heat exchanger	Nusselt number was increased by 49%, up to the volume fraction of 1.0%. Pressure drop was increased by 14.9%, up to the volume fraction of 2.0%
Madhesh et al. [195]	E	Cu-TiO_2	Water	0.1 - 1.0 vol.%	Re = 4000-14000	Tube in tube counterflow heat exchanger	Increase in Nu of 59.3% was noticed up to the volume fraction of 0.7%. Pressure drop was increased by 5.4%, up to the volume fraction of 1.0%
Phanindra et al. [164]	E+N	Al_2O_3+Cu	Oil	0.1 vol.%	0.5-1.5 LPM	Tube in tube counterflow heat exchanger	Nusselt number was increased by 12.1%
Bahiraei et al. [196]	N	CNT+Fe_3O_4	Water	__	Re = 500 - 2000	Double pipe counterflow minichannel heat exchanger	Increase in heat transfer rate of 53.8% and 28.6% were obtained at Re = 500 and 2000, respectively
Shahsavar et al. [197]	N	CNT+Fe_3O_4	Water	__	Re = 500 - 2000	Double pipe counterflow minichannel heat exchanger	Assumption of Newtonian fluid behavior for HyNF could lead to a large computational error. Whereas, Non-Newtonian fluid assumption for HyNF could predict the experimental results closer
Singh et al. [198]	N	Al_2O_3-MWCNT; Al_2O_3-Ag; Al_2O_3-Cu; Al_2O_3-TiO2	Water	0 - 1 vol.%	__	Shell and tube condenser	Al_2O_3-Ag exhibited a ∡3.2% higher heat transfer coefficient with 4% reduction in pressure drop; whereas, Al_2O_3-MWCNT showed 2.9% improvement in heat transfer with 6.2% reduction in pressure drop
Anitha et al. [199]	E+N	Al_2O_3-Cu	Water	0 - 0.2 vol. %	Re = 800 - 2400	Shell and tube heat exchanger	Al_2O_3-Cu/water with 0.2 vol.% has yielded a 139% increase in heat transfer coefficient
Hung et al. [114]	E	Hybrid carbon nanofluid	Water	0.005 - 0.02 wt.%	0.5 – 2.0 LPM	Air-cooled finned-tube heat exchanger	The heat exchange capacity and system efficiency factor of 0.02 wt.% HCNF were improved by 13% and 11.7%, respectively, at 2 LPM and 35 °C inlet temperature
Karimi et al. [200]	N	MgO-MWCNT	EG	0 - 1 vol.%	Re = 350-1060	Air-cooled heat exchanger	For the inlet temperature of 45 °C, 1% volume concentration, and Re = 350, Nusselt number was increased by 20%.
Sahoo et al. [201]	N	Al_2O_3-Ag; Al_2O_3-Cu; Al_2O_3-CuO; Al_2O_3-Fe_2O_3; Al_2O_3-TiO_2	Water	___	Re = 3500-3800	Louver finned flat tube heat exchanger	Heat transfer rate and pressure drop of Al_2O_3+Ag HyNF were increased by 3% and 7.3% respectively.
Sahoo et al. [202]	N	Al_2O_3-Ag; Al_2O_3-Cu; Al_2O_3-SiC; Al_2O_3-CuO; Al_2O_3-TiO_2	EG	___	___	Louver finned flat tube heat exchanger	A maximum increase in heat transfer rate attained by Al_2O_3-Ag/EG HyNF was 5.4%. As compared to the Al_2O_3 nanofluid, Al_2O_3-Ag/EG HyNF has yielded a 2% higher pressure drop
Huminic et al. [203]	N	MWCNT-Fe_3O_4; ND-Fe_3O_4	Water	0 - 0.3 vol. %	Re = 250-2000	Flattened tube automobile radiator	A maximum of 21% and 15% improvement in heat transfer coefficient was attained by MWCNT-Fe_3O_4/water and ND-Fe_3O_4/water HyNFs respectively
Huminic et al. [204]	N	MgO-MWCNT	EG	0 - 0.4 vol. %	Re = 50-1000	Flattened tube automobile radiator	Heat transfer coefficient was increased by 16.3% at 0.4 vol.%
Returi et al. [205]	N	Al_2O_3-CuO; Al_2O_3-TiO_2	Water	2 - 4 vol.%	Re = 25000 - 65000	Spiral plate heat exchanger	Heat transfer rate attained by Al_2O_3-CuO/water HyNF was 10% higher than that of Al_2O_3-TiO_2/water HyNF
Allahyar et al. [78]	E	Al_2O_3-Ag	Water	0.1 - 0.4 vol.%	Re = 800-5100	Coiled heat exchanger	Nusselt number was increased by 31.6% at Re = 4687 and 0.4 vol.%
Hormozi et al. [206]	E	Al_2O_3-Ag	Water	0.2 vol.%	Re = 800-5100	Coiled heat exchanger	Thermal performance enhancement of 16% was attained using Al_2O_3-Ag/water with 0.1 wt.% concentration of SDS anionic surfactant
Safi et al. [207]	E	MWCNT-TiO_2	Water	0.02 - 0.08 wt.%	2 - 3.5 LPM	Plate heat exchanger	Enhancement in heat transfer rate of 20.2% obtained by 0.08 wt.% HyNF
Huang et al. [208]	E	Al_2O_3-MWCNT	Water	~ 2.0 vol. %	___	Plate heat exchanger	For a given pumping power, hybrid nanofluid provided poor performance than the pure water and Al_2O_3 nanofluid
Bhattad et al. [209]	E+N	Al_2O_3-MWCNT	Water	0.01-0.03 vol.%	2 - 4 LPM	Plate heat exchanger	HyNF provided 39.1% improvement in Nusselt Number with 1.2% increase in pressure drop
Bhattad et al. [210]	E	Al_2O_3+SiC; Al_2O_3+AlN; Al_2O_3+MgO; Al_2O_3+CuO; Al_2O_3+MWCNT	Water	0.1 vol.%	2 - 4 LPM	Plate heat exchanger	Al2O3+MWCNT has provided a maximum of 31.2% increase in heat transfer coefficient with a negligible pressure drop
Bhattad et al. [211]	E	Al_2O_3-MWCNT	Water	0.01 vol.%	2 - 4 LPM	Plate heat exchanger	The heat transfer performance of MoNF (MWCNT (0:5)) was better than the HyNF. Heat transfer coefficient enhancement of 15.2% was produced by MWCNT (0:5) MoNF
Bhattad et al. [212]	T	MgO-Ag; Al_2O_3-Ag	EG-Water; PG-Water (20:80)	0 - 2 vol.%	3 - 7 LPM	Plate heat exchanger	A maximum improvement of 9.3% in heat transfer coefficient was provided by propylene glycol/water based Al_2O_3-Ag HyNF

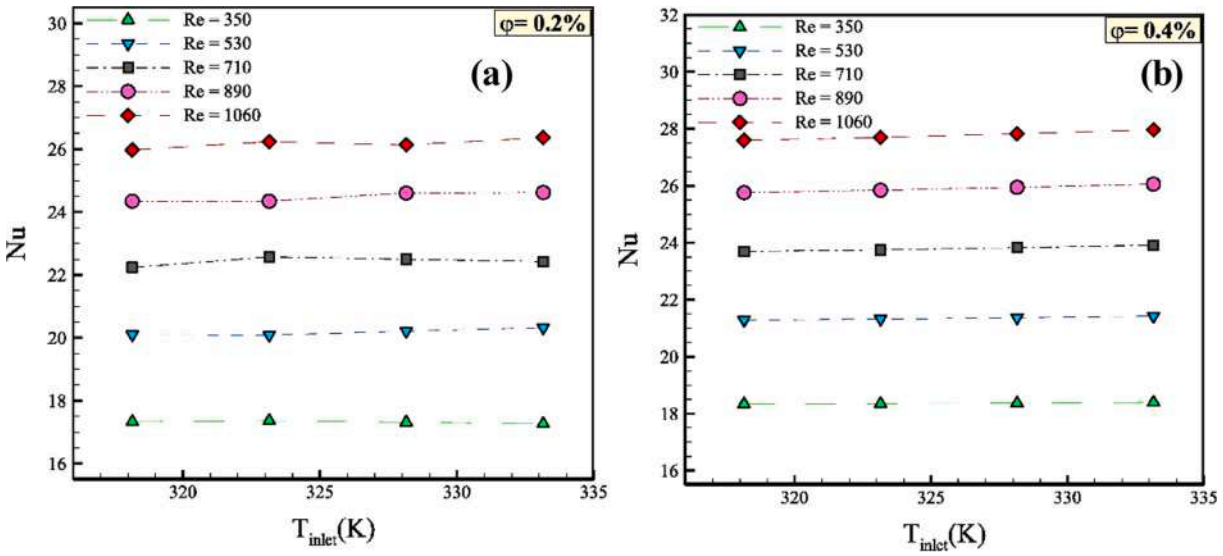

Fig. 13. HyNF's inlet temperature showed negligible influence on Nusselt number (a) volume fraction of 0.2 % and (b) volume fraction of 0.4 % [200].

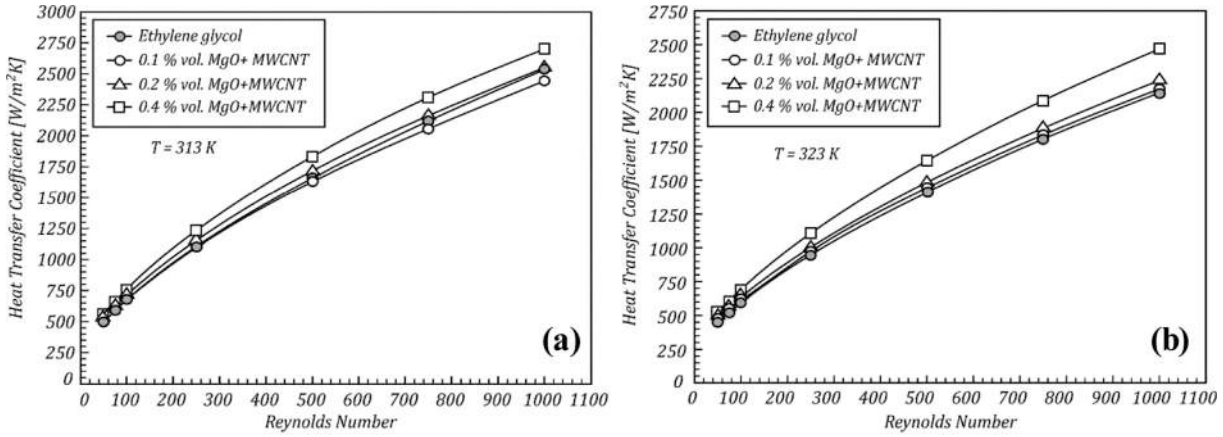

Fig. 14. Reduction of heat transfer coefficient with increasing HyNF's inlet temperature (a) 313 K and (b) 323 K [204].

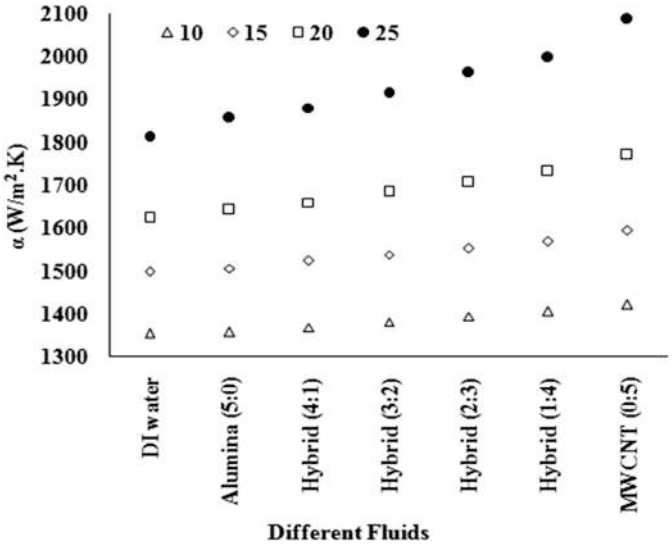

Fig. 15. Effect of HyNF's inlet temperature on heat transfer coefficient [211].

average Nusselt number. But still, the enhancement obtained by HyNF was lower than that of the Cu/water MoNF because of the superior thermal conductivity of Cu/water MoNF. Uysal et al. [229] showed a 30% increase in heat transfer coefficient using Diamond-Fe_3O_4/water HyNF. In addition, they also found that heat transfer coefficient enhancement obtained by HyNF was higher than that of the respective MoNF (i.e., Diamond/water and Fe_3O_4 water).

Ahammed et al. [230] carried out an experimental investigation using Al_2O_3/water MoNF, graphene/water MoNF, and Al_2O_3-Graphene/water HyNF in a multiport minichannel heat sink. They reported that the heat transfer and flow characteristics of graphene/water MoNF were comparatively better than that of the Al_2O_3-Graphene/water HyNF and Al_2O_3/water MoNF due to higher thermal conductivity of graphene ($k_{graphene}$ = 5000 W/m·K). The enhancement in the average heat transfer coefficient obtained by graphene/water MoNF was 88.6%, whereas the same obtained by HyNF and Al_2O_3/water MoNF was 63.1% and 31.9%, respectively. Kumar et al. [231] performed a numerical analysis on the laminar flow of Al_2O_3-MWCNT/water HyNF in a minichannel heat sink using a two-phase mixture model. They showed a maximum 15.6% enhancement in heat transfer coefficient with a negligible increase in pressure drop for 0.01 vol.% Al_2O_3-MWCNT/water (7:3) HyNF. Bahiraei et al. [232] evaluated the influence of secondary channels and ribs in microchannel heat sink using Ag-graphene/water HyNF. They reported a heat transfer improvement of 17% at a Reynolds number of 100 and a

Table 7
Summary on works related to micro/minichannel heat sinks using HyNF

Reference	Method	Hybrid Nano composite	Base fluid	Concentration	Re/ Flow rate	Type	Comparison of HyNF Heat transfer and Pressure drop Characteristics with base fluid
Nimmagada et al. [225]	N	Al_2O_3-Ag	Water	3.0 vol.%	Laminar (Re = 200 -600)	Rectangular microchannel	HyNF (0.6 vol.% Al_2O_3 + 2.4 vol.% Ag) has provided 111-144% enhancement in average convective heat transfer coefficient
Nimmagada et al. [226]	N	SWCNT-Cu	Water	1.0 vol.%	Laminar (Re = 100 -500)	Rectangular microchannel	Increase in average heat transfer coefficient of 11% was achieved by 0.3% Cu +0.7% SWCNT HyNF
Nimmagada et al. [227]	E+N	Al_2O_3-Ag	Water	3.0 vol.%	Laminar (Re = 30 - 50)	Rectangular microchannel	Increase in Nu attained by 3 vol.% HyNF (1.5% Al_2O_3+1.5% Ag) was similar to the one attained by 3 vol.% Ag/water MoNF
Nimmagada et al. [228]	N	Cu-Al	Water	3 vol.%	Laminar (Re = 200 - 600)	Rectangular microchannel	HyNF has provided 23.4% enhancement in average Nusselt number
Uysal et al. [229]	N	Diamond-Fe_3O_4	Water	0.05 - 0.2 vol. %	Laminar (Re = 100 - 1000)	Rectangular minichannel	Improvement of convective heat transfer coefficient of 30% was obtained by 0.2 vol.% HyNF at Re = 1000
Ahammed et al. [230]	E	Al_2O_3-Graphene	Water	0.1 vol.%	Laminar (Re = 200 -1000)	Multiport minichannel	Enhancement in average heat transfer coefficient obtained by graphene/water NF was 88.6%; whereas the same obtained by HyNF and alumina/water NF was 63.1% and 31.9% respectively
Vivek Kumar et al. [231]	N	Al_2O_3+MWCNT	Water	0.01 vol.%	Laminar (Re = 50 - 500)	Minichannel heat sink	Enhancement in heat transfer coefficient of 15.6 % was observed for 0.01 vol% Al_2O_3-MWCNT (7:3) HyNF
Bahiraei et al. [232]	N	Ag-Graphene	Water	0-0.1 vol.%	Laminar (Re = 100 - 500)	Microchannel heat sink	Convective heat transfer coefficient has improved by 17% at 0.1 vol.% and Re = 100
Vivek Kumar et al. [233]	E+N	Al_2O_3-Cu	Water	0.1 vol.%	Laminar (Re = 90 - 500)	Minichannel heat sink	Maximum of 12.8% enhancement in heat transfer coefficient was obtained for Al_2O_3/water MoNF
Vivek Kumar et al. [159]	E	Al_2O_3-MWCNT	Water	0.01 vol.%	Laminar (Re = 140 - 460)	Minichannel heat sink	MWCNT/water mono nanofluid provided a maximum improvement in heat transfer coefficient of 44 % with 51.2% increase in pressure drop
Selva Kumar et al. [234]	E	Al_2O_3-Cu	Water	0.1 vol.%	Turbulent (Re = 2576.56 - 9261.62)	Rectangular channel heat sink	Enhancement in convective heat transfer coefficient of 24.4% was obtained with a 12.6% increase in pumping power
Ambreen et al. [235]	N	Al_2O_3-Cu	Water	1.0 vol.%	—	Micro pin-fin heat sink	HyNF enhanced the Nu by 19.7%, 24% and 25.1% for circular, elliptical, and diamond pin-fins

volume concentration of 0.1%. Kumar et al. [233] further analyzed the influence of various mixing ratios of Al_2O_3 and TiO_2 nanocomposites in Al_2O_3-TiO_2/water hybrid nanofluid. They found that the Al_2O_3/water mono nanofluid has provided a maximum increase of 12.8% in heat transfer coefficient compared to the hybrid nanofluids. Similar to the previous study, Kumar et al. [159] studied the effect of various mixing ratios of Al_2O_3 and MWCNT nanocomposites in Al_2O_3-MWCNT/water hybrid nanofluid. They showed that the MWCNT/water mono nanofluid had yielded a maximum enhancement of 44% in heat transfer coefficient compared to the hybrid nanofluids.

Kumar et al. [234] performed an experimental investigation in the turbulent flow regime of a rectangular channel heat sink using Al_2O_3-Cu/water hybrid nanofluid. They showed a 24.4% improvement in convective heat transfer coefficient with a 12.6% increase in pumping power. Ambreen et al. [235] performed a numerical simulation to compare the heat transfer performance of different shapes of pin-fins such as circular, elliptical, and diamond in micro-pin fin heat sink using Al_2O_3-Cu/water hybrid nanofluid. They used a multiphase Lagrangian and Eulerian approach for the numerical simulation. The results revealed that the HyNF enhanced the Nusselt number by 19.7%, 24%, and 25.1% for circular, elliptical, and diamond pin-fins.

Table 7 shows that the studies using hybrid nanofluids in the turbulent flow regime of micro/minichannel heat sinks are very limited. Future research works can focus on predicting the heat transfer and flow behavior of hybrid nanofluids in the turbulent regime.

4.3. Heat pipe

Heat pipe is a widely used component for cooling applications due to its simple structure and high efficiency. The vacuumed heat pipe has an evaporator (heat source), an adiabatic, and a condenser section (heat sink), and it is filled with fluid. A porous structure such as a screen mesh is placed on the inner periphery of the heat pipe to enable fluid circulation through capillary action. Heat pipe uses the phase change phenomenon of working fluid to transport heat from the source (evaporator) to the sink (condenser). Many studies have shown that the mono nanofluids could enhance heat pipe thermal performance [236,237]. In recent years, researchers focused on applying hybrid nanofluids in heat pipes to improve their performance. Swapnil et al. [238] employed Al_2O_3-BN/water HyNF (1-2 vol.%) in a cylindrical heat pipe and showed an approximately 40% reduction in thermal resistance compared to water. Ramachandran et al. [239] utilized Al_2O_3-CuO/water HyNF in a cylindrical screen mesh heat pipe. The results revealed that the use of HyNF could reduce the thermal resistance up to 44.3% compared to DI water, as shown in Fig. 16. The increased surface roughness and

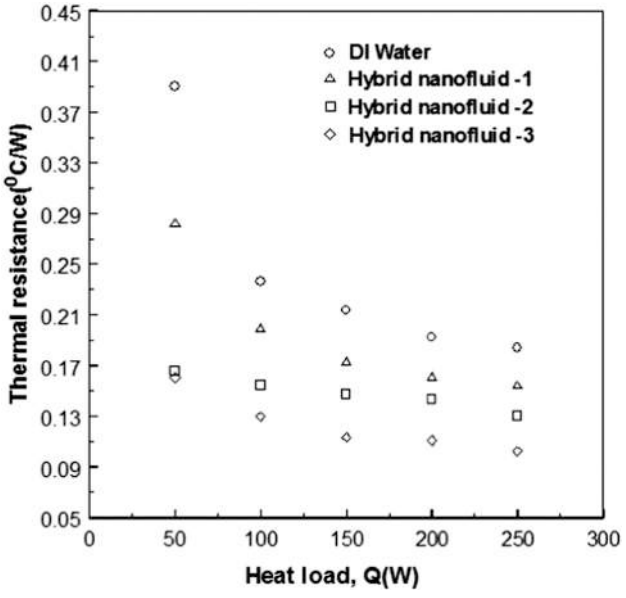

Fig. 16. Heat pipe's thermal resistance comparison for the HyNF and DI water [239].

wettability caused by the adherence of nanoparticles on the wick structure could increase the number of nucleation sites, which could enhance the heat transfer rate and reduce the thermal resistance. They also demonstrated that the use of HyNF in heat pipes could significantly reduce the vapor temperature in the adiabatic section. A maximum 21.4% reduction in vapor temperature was attained at a heat load of 250 W, as shown in Fig. 17. It indicates that HyNF can significantly increase the heat load for the given heat pipe configuration. Chaudhari et al. [240] experimentally studied the performance of cylindrical heat pipe using CuO-BN/water HyNF. They showed that the thermal resistance of the heat pipe decreases with the rise in heat load, inclination angle, and volume concentration of hybrid nanofluid. It was demonstrated that a maximum of 40% reduction in thermal resistance could be achieved at 100 W heat input, 0° inclination angle, and 2 vol.%. Kamble et al. [241] observed a 39.3% reduction in thermal resistance using 2 vol.% Al_2O_3-CuO/water HyNF at 100 W heat input in a heat pipe. All the studies mentioned above substantiated the use of hybrid nanofluid to reduce the thermal resistance of the heat pipe significantly. In contrast to those, Han et al. [242] displayed a 40-50% higher overall thermal resistance in grooved heat pipe (GHP) filled with Al_2O_3-Ag/water HyNF compared to water, suggesting that the use of Al_2O_3-Ag/water HyNF in a GHP could jeopardize the thermal performance.

4.4. Photovoltaic modules

Owing to several advantages, like grid-independent power production, low pollution, and easy installation, the photovoltaic (PV) modules are used in many applications such as PV modules for rooftop power generation, solar collectors, crop dryers, and agriculture water pump [243–245]. The power production and effectiveness of the PV modules can considerably reduce as the temperature of the PV cell increases [246]. Hence, the coolants are used to maintain the temperature of the PV modules [247]. Recently, few studies have focused on the applicability of HyNF in solar panel cooling to improve the system efficiency. Younis et al. [248] used the Al_2O_3-ZnO/water HyNF in PV integrated solar collector system to improve the efficiency. It was observed that by using hybrid nanofluids, total efficiency and exergy efficiency of the system were increased by 4.1% and 4.6%, respectively. The HyNF's optical properties can be tailored in such a way to facilitate absorption of the solar radiation at a particular spectrum range, which can increase

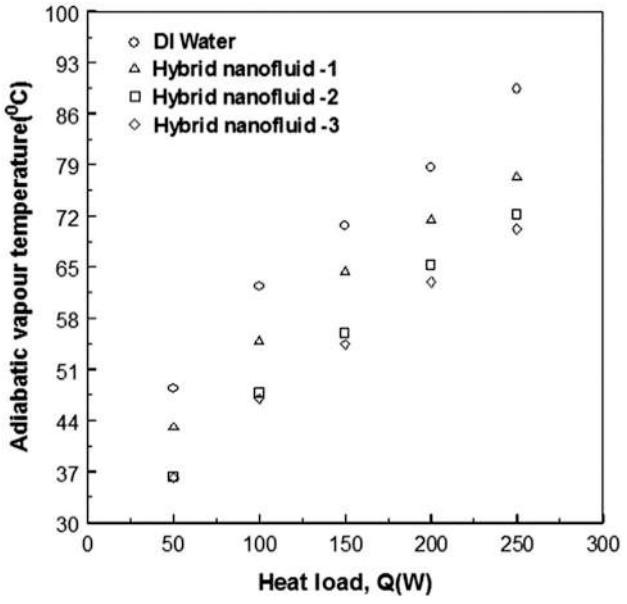

Fig. 17. Comparison of adiabatic vapor temperature of HyNF with DI water [239].

the efficiency considerably. Crisostomo et al. [249] demonstrated that the Ag-SiO_2/water HyNF could improve system efficiency up to 12%. Similarly, Hjerrild et al. [250] utilized the selective spectrum absorption technique in PV/thermal collector. They used the Ag-SiO_2/CNT hybrid nanofluids, which can absorb the radiation at the whole visible spectrum with minimal scattering. It is observed that the combined efficiency of the PV system can be increased by 30%. Sai et al. [251] studied the effect of Go-TiO_2 hybrid nanocomposite in PV cells. The HyNF resulted in increased current output and efficiency, and it reduced the recombination rate. Han et al. [53] used $CoSo_4$ Ag-based hybrid nanofluid to enhance the performance of the PV system. It was observed that the $CoSo_4$Ag-based HyNF has strong absorption in UV and visible spectrum. It was reported that a merit function of 1.37 could be reached by using $CoSo_4$Ag-based HyNF filters in PV systems.

4.5. Heat transfer in various enclosure/cavity

Natural, mixed, or forced convective flow through a channel, chamber, and past a given plate are seen in various applications such as electronic cooling, solar collectors, nuclear reactors, chemical and power industries, geothermal energy, and double pane windows [252]. Many researchers studied the role of hybrid nanofluids in different enclosures such as square, circular, trapezoidal, wavy, and unconventional shapes. The recent studies are listed in Table 8. Takabi and Salehi [146], Goudarzi et al. [253], Tayebi and Chamkha [147], and Tayebi and Chamkha [148] investigated the effect of HyNF on natural convective heat transfer in a sinusoidal corrugated enclosure, sinusoidal wavy enclosure, the annulus between horizontal confocal elliptical cylinders, and eccentric circular annulus, respectively. They found that for the same volume concentration, the Nusselt number of HyNF is higher than the mono nanofluid. The increased heat transfer performance is attributed to the enhanced buoyancy effect. Chamkha et al. [254] showed that the Nu increased with volume concentration for higher Rayleigh numbers ($Ra = 10^6$) in the semicircular cavity. In contrast, Ghalambaz et al. [255] found that in a square cavity, increasing the Ag-MgO/water volume concentration improved the local and average Nusselt number at smaller Rayleigh numbers, while the Nu reduced at higher Ra. Besides, Ghalambaz et al. [256] studied the natural convection heat transfer behavior of Ag-MgO/water in a porous square cavity. They used the local thermal non-linear model and finite element method (FEM) for solving the governing equations obtained by the Darcy model. They observed that the heat transfer rate of the HyNF significantly increases up to $Ra = 600$ and beyond which there is no significant improvement in heat transfer rate is attained. In contrast, Mehryan et al. [257] reported that for the porous enclosure, the heat transfer rate of Ag-MgO/water HyNF is lower than that of the respective MoNF. Al-Srayyih et al. [258] simulated the square cavity partially filled with porous medium using Galerkin FEM and found that the maximum heat transfer rate has occurred at $Ra = 10^5$. Kalidasan and Rajesh Kanna [259] performed the finite difference analysis of natural convection heat transfer behavior of nanodiamond – cobalt oxide/water hybrid nanofluid. The results revealed that the Rayleigh number significantly influences the heat transfer performance. Up to $Ra = 10^5$, the average Nusselt number increased with the Rayleigh number, while it reduced beyond $Ra = 10^5$ due to the weak primary vortex formed at higher Ra. Similarly, Yildiz et al. [260] found that the Al_2O_3-SiO_2/water HyNF showed a higher heat transfer performance at a lower volume concentration than MoNF. Yan et al. [261] compared the heat transfer behavior of tall and narrow enclosures and found that the narrow enclosures are performed better for small Richardson numbers, while the tall enclosures are suitable under large Richardson numbers. Cimpean et al. [262] showed that the performance of porous trapezoidal cavities is more efficient than the square cavities.

Besides the conventional enclosures such as square, triangular, and trapezoidal shapes, few studies examined the performance of unconventional shape enclosures filled with HyNF. Izadi et al. [263]

Table 8
Summary of studies related to enclosure/cavity using HyNF

References	Method	Scheme	HyNF	Range	Geometry	Findings
Takabi and Salehi [146]	Natural convection	FVM	Cu-Al_2O_3/Water	$0\% \leq \varphi \leq 2\%$ $10^3 \leq Ra \leq 10^6$	Sinusoidal corrugated enclosure	Heat transfer rate of HyNF is higher compared to MoNF and it is more profound at higher Rayleigh number (Ra)
Goudarzi et al. [253]	Natural convection	FVM	Ag-MgO/Water	-	Sinusoidal wavy enclosure	Nu increment of 11% is achieved via thermophoresis diffusion
Tayebi and Chamkha [147]	Natural convection	FVM	Cu-Al_2O_3/Water	$0\% \leq \varphi \leq 1.2\%$ $10^3 \leq Ra \leq 3x10^5$	Annulus between confocal elliptical cylinder	At low Ra, the increase of volume concentrations considerably enhanced the average Nu
Tayebi and Chamkha [148]	Natural convection	FVM	Cu-Al_2O_3/Water	$0\% \leq \varphi \leq 1.2\%$ $10^3 \leq Ra \leq 10^6$	Eccentric cylindrical annulus	For the same volume concentration, the Nusselt number increases about 5% at higher Ra
Chamkha et al. [254]	Natural convection	FDM	Cu-Al_2O_3/Water	$0\% \leq \varphi \leq 0.05\%$ $10^4 \leq Ra \leq 10^6$	Semicircular cavity	Up to $Ra = 10^6$, Nu increases with volume concentration
Ghalambaz et al. [255]	Natural convection	FEM	Ag-MgO/Water	$0\% \leq \varphi \leq 2\%$ $10^3 \leq Ra \leq 10^5$	Square cavity	At low Ra, HyNF increases the average Nusselt number, whereas the Nu reduces at high Ra
Ghalambaz et al. [256]	Natural convection	FEM	Ag-MgO/Water	$0\% \leq \varphi \leq 2\%$ $0 \leq Ra \leq 10^3$	Porous square cavity	Nu significantly increases up to $Ra = 600$
Mehryan et al. [257]	Natural convection	FEM	Ag-MgO/Water	$0\% \leq \varphi \leq 2\%$ $10 \leq Ra \leq 10^3$	Porous square cavity	Heat transfer rate of HyNF is lower than that of tMoNF
Al-Srayyih et al. [258]	Natural convection	FEM	Cu-Al_2O_3/Water	$0\% \leq \varphi \leq 0.2\%$ $10^3 \leq Ra \leq 10^7$	Porous square cavity	Maximum heat transfer rate attained at $Ra = 10^5$
Kalidasan and Rajesh Kanna [259]	Natural convection	FDM	Nano diamond-Cobalt Oxide/ Water	$0\% \leq \varphi \leq 6\%$ $10^4 \leq Ra \leq 10^6$	Square cavity	Nu increases up to $Ra = 10^5$ and beyond which it is decreased
Yildiz et al. [260]	Natural convection	FVM	Al_2O_3-SiO_2/ Water	$1\% \leq \varphi \leq 3\%$ $10^4 \leq Ra \leq 10^5$	Square cavity	Compared to MoNF, HyNF enhances the heat transfer performance at lower volume concentration
Yan et al. [261]	Mixed convection	FVM	Cu-TiO_2/water	$0\% \leq \varphi \leq 2\%$ $0.01 \leq Ri \leq 100$	Rectangular enclosure	For narrow and tall enclosures, Nu increases up to 10.4% and 14.5% at $Ri = 0.01$ and 100, respectively
Cimpean et al. [262]	Mixed convection	FDM	Cu-Al_2O_3/Water	$0\% \leq \varphi \leq 0.04\%$ $Ra = 10^6$	Porous trapezoidal chamber	Trapezoidal cavity performance is more efficient than square cavity
Kadhim et al. [278]	Natural convection	FEM	Cu-Al_2O_3/Water	$0\% \leq \varphi \leq 0.2\%$ $10^4 \leq Ra \leq 10^7$	Porous wavy wall	HyNF provided higher Nusselt number compared to MoNF for all inclination angle
Izadi et al. [263]	Natural convection	LBM	MWCNT-Fe_3O_4/ Water	$0\% \leq \varphi \leq 0.003\%$ $10^4 \leq Ra \leq 10^6$	Inverted T shape	Nu decreases with cavity obstruction ratio and increases with heat source aspect ratio
Kalidasan et al. [264]	Natural convection	FDM	Cu-TiO_2/water	$0\% \leq \varphi \leq 5\%$ $10^4 \leq Ra \leq 10^6$	C shaped open cavity	Primary vortex strength reduces at higher Ra
Almeshaal et al. [265]	Natural convection	CVM	CNT-Al_2O_3/ Water	$0\% \leq \varphi \leq 4\%$ $10^3 \leq Ra \leq 10^6$	T shaped cavity	At higher volume concentration and Ra, HyNF demonstrated a 100% increase in heat transfer rate over water
Zahan et al. [266]	MHD natural convection	FEM	Cu-Al_2O_3/Water	$0\% \leq \varphi \leq 0.05\%$ $0.5 \leq Ri \leq 10$	Triangular enclosure with sinusoidal bottom wall	Richardson number greatly influences the flow structure and heat transfer mechanism of HyNF with in the cavity
Tayebi and Chamkha [267]	MHD natural convection	FVM	Cu-Al_2O_3/Water	$0\% \leq \varphi \leq 0.09\%$ $10^3 \leq Ra \leq 10^6$	Square cavity with corrugated conducting block	HyNF increased the heat transfer rate and irreversibility under magnetic effects

(*continued on next page*)

Table 8 (*continued*)

References	Method	Scheme	HyNF	Range	Geometry	Findings
				$0 \leq Ha \leq 50$		
Tayebi and Chamkha [268]	MHD natural convection	FVM	Cu-Al_2O_3/Water	$0\% \leq \varphi \leq 0.09\%$ $10^3 \leq Ra \leq 10^6$ $0 \leq Ha \leq 50$	Square cavity with a conducting hollow cylinder	Entropy generation and heat transfer rate decreased with increasing Hartmann number
Tayebi and Chamkha [269]	MHD natural convection	FVM	Cu-Al_2O_3/Water	$0\% \leq \varphi \leq 0.06\%$ $10^3 \leq Ra \leq 10^6$ $0 \leq Ha \leq 50$	Square cavity with a wavy circular conducting cylinder	Heat transfer rate increased with Rayleigh number, volume fraction, and fluid to solid conductivity ratio, whereas it decreased with Hartmann number
Ashorynejad and Shahriari [270]	MHD natural convection	LBM	Cu-Al_2O_3/Water	$0\% \leq \varphi \leq 0.04\%$ $10^3 \leq Ra \leq 10^5$ $0 \leq Ha \leq 90$	Wavy enclosure	Nu increases with increasing Ra and volume concentration, while it reduces with increasing Ha
Shehzad et al. [271]	MHD natural convection	CVFEM	MWCNT-Fe_3O_4/ Water	$1 \leq Ha \leq 20$	Elliptic porous enclosure	For low Ha values, Nu increases about 7.95 times at higher Ra; whereas it reduces at higher values of Ha
Gorla et al. [273]	MHD natural convection	FDM	Cu-Al_2O_3/Water	$0.03\% \leq \varphi \leq 0.1\%$ $0 \leq Ha \leq 100$	Square porous cavity	Average Nu of hybrid suspension is lower than the Al_2O_3/ water and Cu/water
Izadi et al. [274]	MHD natural convection	FEM	MWCNT-Fe_3O_4/ Water	$0\% \leq \varphi \leq 0.3\%$ $0 \leq Ha \leq 50$	Square porous cavity	Nu reduces with increasing porosity and it increases with Ra under magnetic effect

performed a numerical analysis to predict the performance of an inverted T shape enclosure, as shown in Fig. 18, under natural convection using the Lattice Boltzmann Method (LBM). They studied the influence of HyNF's volume concentration, Rayleigh number, heat source aspect ratio and its position, and cavity obstruction ratio on the heat transfer performance. The results revealed that the Nu decreased with cavity obstruction ratio and increased with heat source aspect ratio. Similarly, Kalidasan et al. [264] predicted the performance of Cu-TiO_2/ water in a C-shaped open cavity, as shown in Fig. 18. They found that the Nu increased with a volume concentration of HyNF for $Ra = 10^4$ and 10^5, whereas it is marginally decreased for $Ra = 10^6$. Almeshaal et al. [265] predicted that the heat transfer rate of CNT-Al_2O_3/water HyNF in

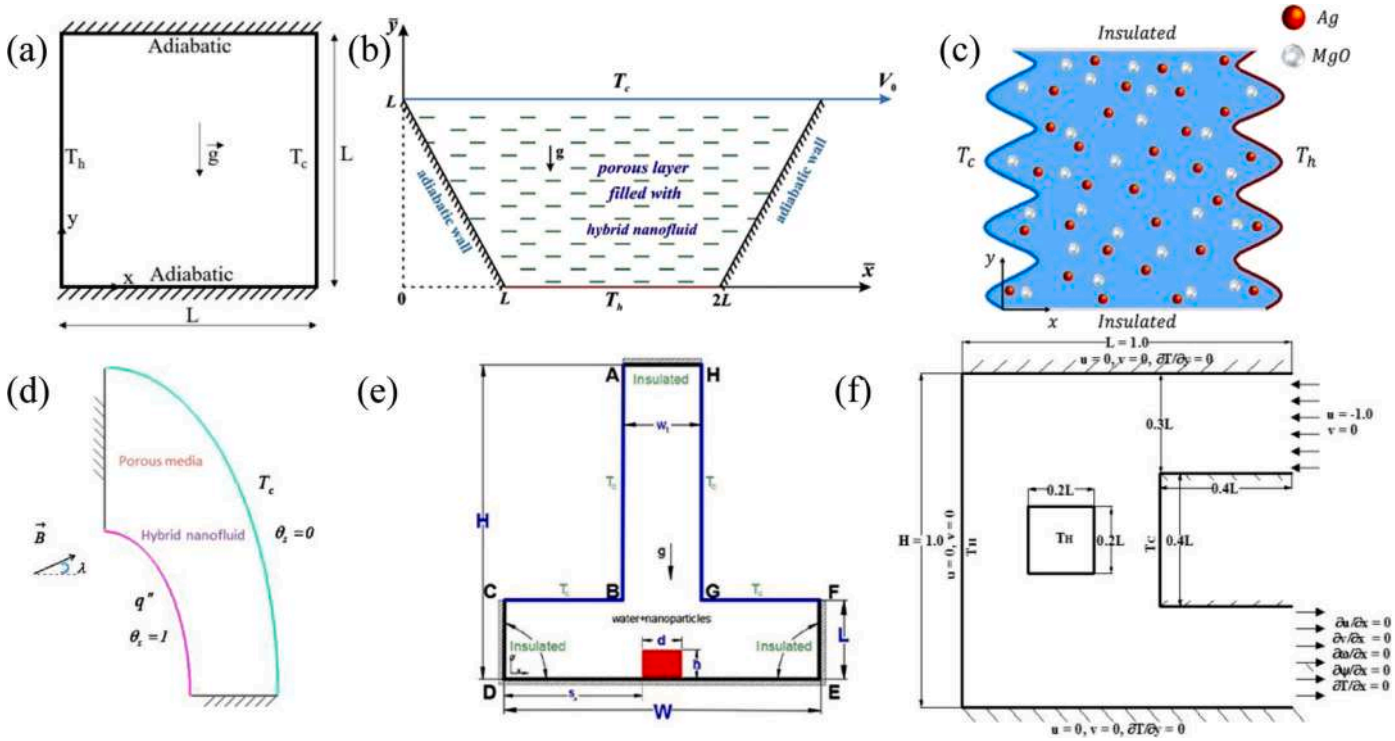

Fig. 18. Shapes of various enclosures used in natural convection studies (a) Square cavity [260], (b) Trapezoidal cavity [262], (c) Sinusoidal wavy enclosure [253], (d) Elliptical enclosure [271], (e) Inverted T cavity [263], and (f) C shaped chamber [264].

a T-shaped enclosure is 100% higher than that of water at high Ra and volume concentrations.

HyNF's heat transfer characteristics in enclosure/cavity under the magnetohydrodynamic (MHD) effect are investigated by many researchers. Zahan et al. [266] investigated the Cu- Al_2O_3/water performance in the triangular enclosure with a sinusoidal bottom wall under the MHD effect. They found that the HyNF showed modest enhancement of Nusselt number compared to MoNF. Besides, they concluded that the flow structure and heat transfer mechanism are greatly affected by the Richardson number (Ri). Tayebi and Chamkha [267–269] examined the heat transfer performance and entropy generation during MHD natural convection in the square enclosure with a corrugated conducting block, conducting hollow cylinder, and wavy circular conducting cylinder. Ashorynejad and Shahriari [270] found that the Nu increases with increasing Ra and volume concentration, and it reduces with increasing Hartmann number in the wavy open cavity. Similarly, the MHD effects on natural convection heat transfer of hybrid nanofluids in various porous enclosures such as elliptical [271], octagonal [272], and square [273,274] are investigated, and the important outcomes are presented in Table 8. A detailed description of the numerical modeling and simulation of nanofluids can be found in [275–277].

Based on the above discussion, it is understood that most of the studies on natural convection are numerically based. In this regard, more experimental studies in the future are suggested for a deep understanding of the buoyancy flow and thermal behavior in cavities. Moreover, several studies were focused on 2D numerical analysis, and future studies can be extended to 3D analysis. The existing literatures mainly focused on predicting the natural convection effects of various enclosures under horizontal and vertical orientation; whereas, the studies concerning the inclination effects are rare. Besides, the works on unconventional enclosure shapes such as L and H are minimal.

4.6. Miscellaneous applications

The research works on the use of HyNF in heat exchangers, heat sinks, heat pipes, natural convetion applications, and solar panels are numerous. However, the studies related to other heat transfer applications such as HVAC systems, pool boiling, jet impingement cooling, and latent heat thermal energy storage systems are still limited. In this section, reports on those miscellaneous applications are reviewed.

4.6.1. Vapor compression refrigeration system

Ahmed and Ashraf [279] compared the performance of mono nanofluids (Al_2O_3/water and TiO_2/water) with the hybrid nanofluids (Al_2O_3-TiO_2/water) in a chilled water air conditioning system. The experimental results revealed that the COP of the vapor compression refrigeration cycle was 22.9% higher for the MoNF (i.e., Al_2O_3/water) compared to pure water. However, COP enhancement attained using HyNF (Al_2O_3-TiO_2/water) was comparatively lower than MoNF (i.e., Al_2O_3/water). For the same mass fraction, the viscosity of HyNF is much higher than MoNF. The increased viscosity of HyNF, which can directly affect the heat transfer, is attributed to the lower performance improvement.

4.6.2. Jet Impingement cooling

Sun et al. [280] studied the convective heat transfer behavior of a conventional impinging jet and swirling impinging jet cooling system using Ag-MWCNT/water nanofluid. Due to the improved eddies and diffusion in the fluid flow, the swirling impinging jet system has provided a 120.5% improvement in heat transfer coefficient for 0.05% Ag-MWCNT/water HyNF compared to pure water. In contrast, the same for the conventional impinging jet was 116.7%. They also reported that the heat transfer coefficient of MoNF was significantly lower than that of HyNF.

4.6.3. Boiling

Reported research works on the use of HyNF in nucleate boiling and convective boiling are limited. Anil Reddy and Venkatachalapathy [281] experimentally investigated the effect of Al_2O_3-CuO/water hybrid nanofluid (0.01-0.1 vol.%) under pool boiling conditions. Compared to pure water, the critical heat flux (CHF) of HyNF was 19.3%, 27.3%, and 49.8% higher for 0.01 vol.%, 0.03 vol.%, and 1.0 vol.%, respectively. Compared to CuO MoNF, HyNF showed 6.6% and 8.2% higher CHF for 0.01 vol.% and 0.03 vol.%, respectively. An increase of 7.1% in the heat transfer coefficient (HTC) was observed for 0.01 vol.% of HyNF; whereas, the HTC deteriorates at the higher concentrations. In pool boiling, the surface roughness and the number of nucleation sites control the bubble departure. At higher concentrations, a layer of nanoparticles tends to settle on the nucleation sites and thus deteriorates the bubble departure frequency, reducing the HTC. Aizzat et al. [282] conducted a pool boiling study using a low concentration Al_2O_3-SiO_2/water HyNF (0.001 vol.%). They reported that for the first 30 min, the HTC increases tremendously for HyNF. However, the HTC deteriorates over time due to the deposition of SiO_2 nanoparticles (lower thermal conductivity) on the surface, which can form a thin layer and can considerably increase the thermal resistance.

4.6.4. Latent heat thermal energy storage system

In the latent heat thermal energy storage system (LHTESS), the energy released during the phase change process is stored. The phase change materials (PCM) used in LHTESS possess very low thermal conductivity, which can slow down the phase change process, and thus, the energy extracted. The use of nanoparticles in PCM can increase its thermal conductivity and can accelerate the phase change process. Hosseinzadeh et al. [283] used Al_2O_3-Go hybrid nanoparticles in PCM. They found that the addition of hybrid nanoparticles in PCM increased the solidification rate by 1.75 and 2.69 times for the 2.5% and 5% volume fractions, respectively.

5. Conclusions, challenges, and future research scope

This study presents a comprehensive review on recent developments in the hybrid nanofluids synthesis, characterization, thermophysical properties evaluation, and then its application in heat exchangers, heat sinks, heat pipes, solar panels, natural convection enclosures, HVAC systems, jet impingement cooling, boiling, and latent heat thermal energy storage systems. Overall, the hybrid nanofluids showed a significant improvement in heat transfer performance; however, it was also accompanied by a pressure drop penalty due to increased viscosity. The main reason for obtaining the improved heat transfer performance is the improvement in the thermal conductivity of HyNF. However, the lack of longer stability challenges its usage in industrial applications. The thermophysical properties are the key parameters that control the heat transfer and flow behavior of the HyNF. The thermophysical properties of the hybrid nanofluids are mainly affected by the types of nanoparticles, nanoparticles concentration, nanoparticles size and shape, base fluid, operating temperature, preparation methods, and the use of surfactants. For future research directions, the following observations are proposed.

- Among the various types of nanoparticles, Al_2O_3 and CNT/MWCNT based nanoparticles have widely been studied by many researchers. The suitability of other hybrid nanofluids, which are already developed, requires extensive experimental and numerical research on various heat transfer applications.
- Concurrently, the development of new hybrid nanofluids needs to be carried out to fulfill the future energy requirement. However, developing the new kind of HyNF poses a compatibility limitation. Since the hybrid nanocomposites comprise more than two different kinds of nanoparticles, examining and developing the compatible hybrid nanocomposite is challenging.

- The use of HyNF in industrial applications is limited due to the stability issues. Therefore, the development of new synthesis and preparation techniques is required for improving stability. Besides developing the new synthesis and preparation techniques, these techniques must be standardized for repeatability and mass production.
- Water is the commonly used base fluid for developing hybrid nanofluids. Future research might focus on the development of HyNF using other base fluids such as ethylene glycol (EG), EG mixture, and oil.
- The conclusion on the rheological behavior of HyNF is inconsistent. Some studies claim that HyNF exhibits a Newtonian behavior, whereas other studies display a non-Newtonian behavior. To develop a better numerical model, the rheological behavior needs to be further investigated.
- Numerical studies have widely adopted a single-homogeneous approach and the multiphase mixture model. The Brownian motion, which is a crucial factor determining the heat transfer augmentation, is not accounted for in the single-phase homogeneous approach. At the same time, the Brownian motion effects are considered in the multiphase mixture model. The previous studies also suggested that the multiphase model is more suitable for analyzing the hydrothermal behavior of HyNF. Still, the analysis concerning the multiphase mixture model is minimal.
- HyNF's thermophysical properties are highly dependent on the operating temperature. Hence, the heat transfer and the flow behavior of a system could be significantly affected by the change in operating temperature. However, most of the numerical studies considered constant thermophysical properties. The temperature dependency behavior needs to be considered in future numerical simulations.
- Thermophysical properties analysis reveals that HyNF's thermal conductivity is a strong function of temperature and increases with temperature. Hence, it is expected to have higher heat transfer performance at a high temperature. However, some studies reported a reverse trend of no effect or reduction in heat transfer performance with an increase in temperature. More experimental studies are required to understand the effect of fluid inlet temperature in heat transfer performance to clear this discrepancy. The reason for the above discrepancy might be due to the randomness associated with the Brownian motion. The nanoparticles' motion in the base fluid could probably be different at various temperature ranges. Therefore, some flow visualization studies (using laser doppler velocimetry or other viable techniques) are required to understand the motion of nanoparticles at various temperatures and the effect of temperature on HyNF's performance.
- The heat transfer and flow behavior of HyNF's can further be extended under the influence of magnetic and electrical effects, which might affect the motion of the nanoparticles in base fluid.
- Most of the studies reported the heat transfer and the pressure drop behavior of HyNF's in different applications. However, the major issues associated with the HyNF's are the sedimentation and corrosion occurring in the thermal system after prolonged usage. The studies dealt with these topics are extremely rare.
- The heat transfer and friction factor correlations are only available for few types of hybrid nanofluids. More experimental studies are needed to develop these correlations for different HyNF's at various operating conditions.
- The studies related to the micro/minichannel heat sinks using HyNF are restricted to the laminar flow regime only. The studies on turbulent flow region are very limited. Future research might focus more on the transition and turbulent flow regimes.
- HyNF is comparatively well studied in heat exchangers. Still, it is minimal on other applications such as mini/microchannel heat sinks, heat pipes, solar panels, refrigeration and air conditioning, boiling, and impingement cooling.

Authorship statement

I am the corresponding author (Chi-Chuan Wang) and I certify that all authors have participated sufficiently in the work to take public responsibility for the content. Their contributions have been specified as follows:

Muneeshwaran M: Conceptualization and writing original draft
Srinivasan G: Writing original draft
Muthukumar P: Reviewing and revising
Chi-Chuan Wang*: Supervision, reviewing and revising

Declaration of Competing Interest

None.

Acknowledgment

The financial support from the Ministry of science and technology, Taiwan under contract No. 109-2622-E-009-006-CC2 is acknowledged.

References

[1] F. Selimefendigil, H.F. Öztop, Thermoelectric generation from vented cavities with a rotating conic object and highly conductive CNT nanofluids for renewable energy systems, Int. Communicat. Heat Mass Transfer 122 (2021) 105139.
[2] A. Rezania, L. Rosendahl, S.J. Andreasen, Experimental investigation of thermoelectric power generation versus coolant pumping power in a microchannel heat sink, Int. Communicat. Heat Mass Transfer 39 (8) (2012) 1054–1058.
[3] M. Ghanbarpour, R. Khodabandeh, K. Vafai, An investigation of thermal performance improvement of a cylindrical heat pipe using Al 2 O 3 nanofluid, Heat Mass Transf. 53 (3) (2017) 973–983.
[4] M. Shafahi, V. Bianco, K. Vafai, O. Manca, An investigation of the thermal performance of cylindrical heat pipes using nanofluids, Int. J. Heat Mass Transf. 53 (1-3) (2010) 376–383.
[5] K. Khanafer, K. Vafai, Analysis of turbulent two-phase flow and heat transfer using nanofluid, Int. Communicat. Heat Mass Transfer 124 (2021) 105219.
[6] K. Khanafer, K. Vafai, A critical synthesis of thermophysical characteristics of nanofluids, Int. J. Heat Mass Transf. 54 (19-20) (2011) 4410–4428.
[7] G. Srinivasan, M. Muneeshwaran, B. Raja, Numerical investigation of heat and mass transfer behavior of freeze drying of milk in vial, Heat Mass Transf. 55 (8) (2019) 2073–2081.
[8] M. Muneeshwaran, G. Srinivasan, B. Raja, C.-C. Wang, Investigation of heat and mass transfer behavior of mannitol during vial freeze-drying, J. Therm. Anal. Calorim. (2021) 1–12.
[9] J. Bi, K. Vafai, D.M. Christopher, Heat transfer characteristics and CHF prediction in nanofluid boiling, Int. J. Heat Mass Transf. 80 (2015) 256–265.
[10] V. Karlapalem, S.K. Dash, Design of perforated branching fins in laminar natural convection, Int. Communicat. Heat Mass Transfer 120 (2021) 105071.
[11] D. Mohankumar, Y. Pazhaniappan, R. N. Kumar, R. Ragul, P. M. Kumar, and P. N. Babu, "Computational study of heat-transfer in extended surfaces with various geometries," in *IOP Conference Series: Materials Science and Engineering*, 2021, vol. 1059, no. 1: IOP Publishing, p. 012055.
[12] U. Kashyap, K. Das, B.K. Debnath, U. Kashyap, S.K. Saha, Numerical study on effect of secondary surface on rectangular vortex generator, J. Thermal Sci. Eng. Applicat. 13 (1) (2021).
[13] L. Godson, B. Raja, D. Mohan Lal, S. Wongwises, Convective heat transfer characteristics of silver-water nanofluid under laminar and turbulent flow conditions, J. Thermal Sci. Eng. Applicat. 4 (3) (2012).
[14] V. Umesh, S.B. Vignesh, B. Raja, A study on nucleate boiling heat transfer characteristics of acetone on smooth and indented surfaces, Exper. Heat Transfer 29 (3) (2016) 414–425.
[15] A. Peddu, S. Chakraborty, P.K. Das, Visualization and flow regime identification of downward air–water flow through a 12 mm diameter vertical tube using image analysis, Int. J. Multiphase Flow 100 (2018) 1–15.
[16] A. Rajalingam, S. Chakraborty, Effect of micro-structures in a microchannel heat sink–A comprehensive study, Int. J. Heat Mass Transf. 154 (2020) 119617.
[17] A. Albojamal, K. Vafai, Analysis of particle deposition of nanofluid flow through porous media, Int. J. Heat Mass Transf. 161 (2020) 120227.
[18] K. Khanafer, K. Vafai, M. Lightstone, Buoyancy-driven heat transfer enhancement in a two-dimensional enclosure utilizing nanofluids, Int. J. Heat Mass Transf. 46 (19) (2003) 3639–3653.
[19] H. Hamzah, A. Albojamal, B. Sahin, K. Vafai, Thermal management of transverse magnetic source effects on nanofluid natural convection in a wavy porous enclosure, J. Therm. Anal. Calorim. 143 (3) (2021) 2851–2865.
[20] R.L. Hamilton, O. Crosser, Thermal conductivity of heterogeneous two-component systems, Ind. Eng. Chem. Fundam. 1 (3) (1962) 187–191.
[21] S.U. Choi, J.A. Eastman, Enhancing thermal conductivity of fluids with nanoparticles, Argonne National Lab, IL (United States), 1995.

[22] A. Rostami, K. Hosseinzadeh, D. Ganji, Hydrothermal analysis of ethylene glycol nanofluid in a porous enclosure with complex snowflake shaped inner wall, Waves Random Complex Media (2020) 1–18.

[23] A.R. Mogharrebi, A.R.D. Ganji, K. Hosseinzadeh, S. Roghani, A. Asadi, A. Fazlollahtabar, Investigation of magnetohydrodynamic nanofluid flow contain motile oxytactic microorganisms over rotating cone, Int. J. Num. Methods Heat & Fluid Flow (2021), https://doi.org/10.1108/HFF-08-2020-0493.

[24] L. Godson, B. Raja, D.M. Lal, S. Wongwises, Experimental investigation on the thermal conductivity and viscosity of silver-deionized water nanofluid, Exper. Heat Transfer 23 (4) (2010) 317–332.

[25] L.G. Asirvatham, B. Raja, D.M. Lal, S. Wongwises, Convective heat transfer of nanofluids with correlations, Particuology 9 (6) (2011) 626–631.

[26] D.D. Kumar, A.V. Arasu, A comprehensive review of preparation, characterization, properties and stability of hybrid nanofluids, Renew. Sust. Energ. Rev. 81 (2018) 1669–1689.

[27] L.S. Sundar, K. Sharma, M.K. Singh, A. Sousa, Hybrid nanofluids preparation, thermal properties, heat transfer and friction factor–a review, Renew. Sust. Energ. Rev. 68 (2017) 185–198.

[28] S. Chakraborty, P.K. Panigrahi, Stability of nanofluid: A review, Appl. Therm. Eng. (2020) 115259.

[29] N.S. Pandya, H. Shah, M. Molana, A.K. Tiwari, Heat transfer enhancement with nanofluids in plate heat exchangers: A comprehensive review, Eur. J. Mech. B/Fluids 81 (2020) 173–190.

[30] A. Arshad, M. Jabbal, Y. Yan, D. Reay, A review on graphene based nanofluids: preparation, characterization and applications, J. Mol. Liq. 279 (2019) 444–484.

[31] S. Angayarkanni, J. Philip, Review on thermal properties of nanofluids: Recent developments, Adv. Colloid Interf. Sci. 225 (2015) 146–176.

[32] J.R. Babu, K.K. Kumar, S.S. Rao, State-of-art review on hybrid nanofluids, Renew. Sust. Energ. Rev. 77 (2017) 551–565.

[33] G. Huminic, A. Huminic, Hybrid nanofluids for heat transfer applications–a state-of-the-art review, Int. J. Heat Mass Transf. 125 (2018) 82–103.

[34] M.H. Ahmadi, M. Ghazvini, M. Sadeghzadeh, M.A. Nazari, M. Ghalandari, Utilization of hybrid nanofluids in solar energy applications: A review, Nano-Struct. Nano-Objects 20 (2019) 100386.

[35] G. Huminic, A. Huminic, Entropy generation of nanofluid and hybrid nanofluid flow in thermal systems: A review, J. Mol. Liq. (2020) 112533.

[36] M. Baghbanzadeh, A. Rashidi, D. Rashtchian, R. Lotfi, A. Amrollahi, Synthesis of spherical silica/multiwall carbon nanotubes hybrid nanostructures and investigation of thermal conductivity of related nanofluids, Thermochim. Acta 549 (2012) 87–94.

[37] M. Baghbanzadeh, A. Rashidi, A.H. Soleimanisalim, D. Rashtchian, Investigating the rheological properties of nanofluids of water/hybrid nanostructure of spherical silica/MWCNT, Thermochim. Acta 578 (2014) 53–58.

[38] L. Chen, W. Yu, H. Xie, Enhanced thermal conductivity of nanofluids containing Ag/MWNT composites, Powder Technol. 231 (2012) 18–20.

[39] B. Munkhbayar, M.R. Tanshen, J. Jeoun, H. Chung, H. Jeong, Surfactant-free dispersion of silver nanoparticles into MWCNT-aqueous nanofluids prepared by one-step technique and their thermal characteristics, Ceram. Int. 39 (6) (2013) 6415–6425.

[40] L.S. Sundar, M.K. Singh, A.C. Sousa, Enhanced heat transfer and friction factor of MWCNT–Fe3O4/water hybrid nanofluids, Int. Communicat. Heat Mass Transfer 52 (2014) 73–83.

[41] S. Suresh, K. Venkitaraj, P. Selvakumar, Synthesis, characterisation of Al2O3-Cu nano composite powder and water based nanofluids, Adv. Mater. Res. 328 (2011) 1560–1567. Trans Tech Publ.

[42] S. Suresh, K. Venkitaraj, P. Selvakumar, M. Chandrasekar, Synthesis of Al2O3–Cu/water hybrid nanofluids using two step method and its thermo physical properties, Colloids Surf. A Physicochem. Eng. Asp. 388 (1-3) (2011) 41–48.

[43] D. Madhesh, R. Parameshwaran, S. Kalaiselvam, Experimental investigation on convective heat transfer and rheological characteristics of Cu–TiO2 hybrid nanofluids, Exp. Thermal Fluid Sci. 52 (2014) 104–115.

[44] S.J. Aravind, S. Ramaprabhu, Graphene–multiwalled carbon nanotube-based nanofluids for improved heat dissipation, RSC Adv. 3 (13) (2013) 4199–4206.

[45] W.S. Hummers Jr., R.E. Offeman, Preparation of graphitic oxide, J. Am. Chem. Soc. 80 (6) (1958) 1339.

[46] S. Jana, A. Salehi-Khojin, W.-H. Zhong, Enhancement of fluid thermal conductivity by the addition of single and hybrid nano-additives, Thermochim. Acta 462 (1-2) (2007) 45–55.

[47] S.M. Abbasi, A. Rashidi, A. Nemati, K. Arzani, The effect of functionalisation method on the stability and the thermal conductivity of nanofluid hybrids of carbon nanotubes/gamma alumina, Ceram. Int. 39 (4) (2013) 3885–3891.

[48] L. Megatif, A. Ghozatloo, A. Arimi, M. Shariati-Niasar, Investigation of laminar convective heat transfer of a novel TiO2–carbon nanotube hybrid water-based nanofluid, Exper. Heat Transfer 29 (1) (2016) 124–138.

[49] L. Li, et al., The fabrication of CNTs/TiO2 photoanodes for sensitive determination of organic compounds, Nanotechnology 21 (48) (2010) 485503.

[50] T.T. Baby, S. Ramaprabhu, Experimental investigation of the thermal transport properties of a carbon nanohybrid dispersed nanofluid, Nanoscale 3 (5) (2011) 2208–2214.

[51] G. Paul, J. Philip, B. Raj, P.K. Das, I. Manna, Synthesis, characterization, and thermal property measurement of nano-Al95Zn05 dispersed nanofluid prepared by a two-step process, Int. J. Heat Mass Transf. 54 (15–16) (2011) 3783–3788.

[52] C. Ho, J. Huang, P. Tsai, Y. Yang, Preparation and properties of hybrid water-based suspension of Al2O3 nanoparticles and MEPCM particles as functional forced convection fluid, Int. Communicat. Heat Mass Transfer 37 (5) (2010) 490–494.

[53] Z. Han, B. Yang, S. Kim, M. Zachariah, Application of hybrid sphere/carbon nanotube particles in nanofluids, Nanotechnology 18 (10) (2007) 105701.

[54] T.T. Baby, S. Ramaprabhu, Synthesis and nanofluid application of silver nanoparticles decorated graphene, J. Mater. Chem. 21 (26) (2011) 9702–9709.

[55] N.A.C. Sidik, I.M. Adamu, M.M. Jamil, G. Kefayati, R. Mamat, G. Najafi, Recent progress on hybrid nanofluids in heat transfer applications: a comprehensive review, Int. Communicat. Heat Mass Transfer 78 (2016) 68–79.

[56] L.S. Sundar, E.V. Ramana, M. Graça, M.K. Singh, A.C. Sousa, Nanodiamond-Fe3O4 nanofluids: preparation and measurement of viscosity, electrical and thermal conductivities, Int. Communicat. Heat Mass Transfer 73 (2016) 62–74.

[57] C. Suryanarayana, B. Prabhu, Synthesis of nanostructured materials by inert-gas condensation methods, in: Nanostructured Materials, Elsevier, 2007, pp. 47–90.

[58] T. Wong, P. John, Advances in spray drying technology for nanoparticle formation, in: Handbook of Nanoparticles, *Springer International Publishing, Cham, Switzerland*, 2015, pp. 1–16.

[59] X. Li, N. Anton, C. Arpagaus, F. Belleteix, T.F. Vandamme, Nanoparticles by spray drying using innovative new technology: The Büchi Nano Spray Dryer B-90, J. Control. Release 147 (2) (2010) 304–310.

[60] D.-J. Lee, F.-L. Jin, S.-J. Park, Preparation of Cu nanoparticles by a pulsed wire evaporation process for conductive ink applications, Bull. Mater. Sci. 42 (2) (2019) 1–8.

[61] S. Park, J. Her, D. Cho, M.M. Haque, J.H. Park, C.S. Lee, Preparation of conductive nanoink using pulsed-wire-evaporated copper nanoparticles for inkjet printing, Mater. Trans. (2012) M2012137.

[62] J.-W. Song, D.-J. Lee, F. Yilmaz, S.-J. Hong, Effect of variation in voltage on the synthesis of Ag nanopowder by pulsed wire evaporation, J. Nanomater. 2012 (2012) 24.

[63] H. Chang, et al., A study of nanoparticle manufacturing process using vacuum submerged arc machining with aid of enhanced ultrasonic vibration, J. Mater. Sci. 40 (4) (2005) 1005–1010.

[64] T.-P. Teng, W.-P. Wang, Y.-C. Hsu, Fabrication and characterization of nanocarbon-based nanofluids by using an oxygen–acetylene flame synthesis system, Nanoscale Res. Lett. 11 (1) (2016) 288.

[65] R.L. Vander Wal, Flame synthesis of substrate-supported metal-catalyzed carbon nanotubes, Chem. Phys. Lett. 324 (1–3) (2000) 217–223.

[66] U.S. Shenoy, A.N. Shetty, A simple single-step approach towards synthesis of nanofluids containing cuboctahedral cuprous oxide particles using glucose reduction, Front. Mater. Sci. 12 (1) (2018) 74–82.

[67] R.W. Siegel, Cluster-assembled nanophase materials, Annu. Rev. Mater. Sci. 21 (1) (1991) 559–578.

[68] P. Grammatikopoulos, S. Steinhauer, J. Vernieres, V. Singh, M. Sowwan, Nanoparticle design by gas-phase synthesis, Adv. Phys.: X 1 (1) (2016) 81–100.

[69] C.-H. Yu, K. Tam, E.S. Tsang, Chemical methods for preparation of nanoparticles in solution, Handbook Metal Phys. 5 (2008) 113–141.

[70] J.A. Eastman, S. Choi, S. Li, W. Yu, L. Thompson, Anomalously increased effective thermal conductivities of ethylene glycol-based nanofluids containing copper nanoparticles, Appl. Phys. Lett. 78 (6) (2001) 718–720.

[71] Y. Heo, M. Antoaneta Bratescu, D. Aburaya, N. Saito, A phonon thermodynamics approach of gold nanofluids synthesized in solution plasma, Appl. Phys. Lett. 104 (11) (2014) 111902.

[72] H.-t. Zhu, Y.-s. Lin, Y.-s. Yin, A novel one-step chemical method for preparation of copper nanofluids, J. Colloid Interface Sci. 277 (1) (2004) 100–103.

[73] T.X. Phuoc, Y. Soong, M.K. Chyu, Synthesis of Ag-deionized water nanofluids using multi-beam laser ablation in liquids, Opt. Lasers Eng. 45 (12) (2007) 1099–1106.

[74] T. Zhao, et al., Size-controlled preparation of silver nanoparticles by a modified polyol method, Colloids Surf. A Physicochem. Eng. Asp. 366 (1-3) (2010) 197–202.

[75] G.-J. Lee, C.K. Kim, M.K. Lee, C.K. Rhee, S. Kim, C. Kim, Thermal conductivity enhancement of ZnO nanofluid using a one-step physical method, Thermochim. Acta 542 (2012) 24–27.

[76] J. Tavares, S. Coulombe, Dual plasma synthesis and characterization of a stable copper–ethylene glycol nanofluid, Powder Technol. 210 (2) (2011) 132–142.

[77] H. Babar, H.M. Ali, Towards hybrid nanofluids: preparation, thermophysical properties, applications, and challenges, J. Mol. Liq. 281 (2019) 598–633.

[78] H. Allahyar, F. Hormozi, B. ZareNezhad, Experimental investigation on the thermal performance of a coiled heat exchanger using a new hybrid nanofluid, Exp. Thermal Fluid Sci. 76 (2016) 324–329.

[79] A. Parsian, M. Akbari, New experimental correlation for the thermal conductivity of ethylene glycol containing Al 2 O 3–Cu hybrid nanoparticles, J. Therm. Anal. Calorim. 131 (2) (2018) 1605–1613.

[80] M.S. Kumar, V. Vasu, A.V. Gopal, Thermal conductivity and rheological studies for Cu–Zn hybrid nanofluids with various basefluids, J. Taiwan Inst. Chem. Eng. 66 (2016) 321–327.

[81] S. Mechiri, V. Vasu, A. Venu Gopal, Investigation of thermal conductivity and rheological properties of vegetable oil based hybrid nanofluids containing Cu–Zn hybrid nanoparticles, Exper. Heat Transfer 30 (3) (2017) 205–217.

[82] A. Asadi, M. Asadi, A. Rezaniakolaei, L.A. Rosendahl, M. Afrand, S. Wongwises, Heat transfer efficiency of Al2O3-MWCNT/thermal oil hybrid nanofluid as a cooling fluid in thermal and energy management applications: An experimental and theoretical investigation, Int. J. Heat Mass Transf. 117 (2018) 474–486.

[83] M.H. Esfe, et al., Thermal conductivity of Cu/TiO2–water/EG hybrid nanofluid: Experimental data and modeling using artificial neural network and correlation, Int. Communicat. Heat Mass Transfer 66 (2015) 100–104.

[84] B. Wei, C. Zou, X. Yuan, X. Li, Thermo-physical property evaluation of diathermic oil based hybrid nanofluids for heat transfer applications, Int. J. Heat Mass Transf. 107 (2017) 281–287.
[85] M.H. Esfe, S. Esfandeh, S. Saedodin, H. Rostamian, Experimental evaluation, sensitivity analyzation and ANN modeling of thermal conductivity of ZnO-MWCNT/EG-water hybrid nanofluid for engineering applications, Appl. Therm. Eng. 125 (2017) 673–685.
[86] S.H. Qing, W. Rashmi, M. Khalid, T. Gupta, M. Nabipoor, M.T. Hajibeigy, Thermal conductivity and electrical properties of hybrid SiO2-graphene naphthenic mineral oil nanofluid as potential transformer oil, Mater. Res. Express 4 (1) (2017) 015504.
[87] M. Nabil, W. Azmi, K.A. Hamid, R. Mamat, F.Y. Hagos, An experimental study on the thermal conductivity and dynamic viscosity of TiO2-SiO2 nanofluids in water: ethylene glycol mixture, Int. Communicat. Heat Mass Transfer 86 (2017) 181–189.
[88] M. Afrand, K.N. Najafabadi, M. Akbari, Effects of temperature and solid volume fraction on viscosity of SiO2-MWCNTs/SAE40 hybrid nanofluid as a coolant and lubricant in heat engines, Appl. Therm. Eng. 102 (2016) 45–54.
[89] M.H. Esfe, M. Afrand, S.H. Rostamian, D. Toghraie, Examination of rheological behavior of MWCNTs/ZnO-SAE40 hybrid nano-lubricants under various temperatures and solid volume fractions, Exp. Thermal Fluid Sci. 80 (2017) 384–390.
[90] A.M. Hussein, Thermal performance and thermal properties of hybrid nanofluid laminar flow in a double pipe heat exchanger, Exp. Thermal Fluid Sci. 88 (2017) 37–45.
[91] D.C. Gregg, in: I. Vogel Arthur (Ed.), Practical Organic Chemistry, ACS Publications, 1952.
[92] S. Chakraborty, P.K. Panigrahi, Stability of nanofluid: A review, Appl. Therm. Eng. 174 (2020) 115259.
[93] H.W. Xian, N.A.C. Sidik, S.R. Aid, T.L. Ken, Y. Asako, Review on preparation techniques, properties and performance of hybrid nanofluid in recent engineering applications, J. Adv. Res. Fluid Mech. Thermal Sci. 45 (1) (2018) 1–13.
[94] S. Sharma, S.M. Gupta, Preparation and evaluation of stable nanofluids for heat transfer application: a review, Exp. Thermal Fluid Sci. 79 (2016) 202–212.
[95] S. Chakraborty, I. Sarkar, K. Haldar, S.K. Pal, S. Chakraborty, Synthesis of Cu–Al layered double hydroxide nanofluid and characterization of its thermal properties, Appl. Clay Sci. 107 (2015) 98–108.
[96] S. Chakraborty, I. Sarkar, A. Ashok, I. Sengupta, S.K. Pal, S. Chakraborty, Thermo-physical properties of Cu-Zn-Al LDH nanofluid and its application in spray cooling, Appl. Therm. Eng. 141 (2018) 339–351.
[97] V.O. Aseyev, H. Tenhu, F.M. Winnik, Temperature dependence of the colloidal stability of neutral amphiphilic polymers in water, Conformat. Dependent Des. Seq. Copolymers II (2006) 1–85.
[98] Y. Xuan, Q. Li, Heat transfer enhancement of nanofluids, Int. J. Heat Fluid Flow 21 (1) (2000) 58–64.
[99] B.C. Pak, Y.I. Cho, Hydrodynamic and heat transfer study of dispersed fluids with submicron metallic oxide particles, Exper. Heat Transfer Int. J. 11 (2) (1998) 151–170.
[100] N. Ahammed, L.G. Asirvatham, S. Wongwises, Effect of volume concentration and temperature on viscosity and surface tension of graphene–water nanofluid for heat transfer applications, J. Therm. Anal. Calorim. 123 (2) (2016) 1399–1409.
[101] M. Sabiha, R. Mostafizur, R. Saidur, S. Mekhilef, Experimental investigation on thermo physical properties of single walled carbon nanotube nanofluids, Int. J. Heat Mass Transf. 93 (2016) 862–871.
[102] S. Mukherjee, P.C. Mishra, P. Chaudhuri, Stability of heat transfer nanofluids–a review, ChemBioEng Rev. 5 (5) (2018) 312–333.
[103] S. Lee, S.-S. Choi, S. Li, J. Eastman, Measuring Thermal Conductivity of Fluids Containing Oxide Nanoparticles, 1999.
[104] C. Cao, L. Zhang, X.-X. Zhang, F.-P. Du, Effect of gum arabic on the surface tension and surface dilational rheology of trisiloxane surfactant, Food Hydrocoll. 30 (1) (2013) 456–462.
[105] L. Jiang, L. Gao, J. Sun, Production of aqueous colloidal dispersions of carbon nanotubes, J. Colloid Interface Sci. 260 (1) (2003) 89–94.
[106] X. Li, D. Zhu, X. Wang, N. Wang, J. Gao, H. Li, Thermal conductivity enhancement dependent pH and chemical surfactant for Cu-H2O nanofluids, Thermochim. Acta 469 (1-2) (2008) 98–103.
[107] M. Assael, I. Metaxa, J. Arvanitidis, D. Christofilos, C. Lioutas, Thermal conductivity enhancement in aqueous suspensions of carbon multi-walled and double-walled nanotubes in the presence of two different dispersants, Int. J. Thermophys. 26 (3) (2005) 647–664.
[108] S.H. Kim, S.R. Choi, D. Kim, Thermal Conductivity of Metal-Oxide Nanofluids: Particle Size Dependence and Effect of Laser Irradiation, 2007.
[109] Y.-j. Hwang, et al., Stability and thermal conductivity characteristics of nanofluids, Thermochim. Acta 455 (1-2) (2007) 70–74.
[110] D. Zhu, X. Li, N. Wang, X. Wang, J. Gao, H. Li, Dispersion behavior and thermal conductivity characteristics of Al2O3–H2O nanofluids, Curr. Appl. Phys. 9 (1) (2009) 131–139.
[111] B. Wei, C. Zou, X. Li, Experimental investigation on stability and thermal conductivity of diathermic oil based TiO2 nanofluids, Int. J. Heat Mass Transf. 104 (2017) 537–543.
[112] S. Aberoumand, A. Jafarimoghaddam, Experimental study on synthesis, stability, thermal conductivity and viscosity of Cu–engine oil nanofluid, J. Taiwan Inst. Chem. Eng. 71 (2017) 315–322.
[113] L. Vandsburger, Synthesis and covalent surface modification of carbon nanotubes for preparation of stabilized nanofluid suspensions, 2009.
[114] Y.-H. Hung, W.-P. Wang, Y.-C. Hsu, T.-P. Teng, Performance evaluation of an air-cooled heat exchange system for hybrid nanofluids, Exp. Thermal Fluid Sci. 81 (2017) 43–55.
[115] C. Nguyen, et al., Viscosity data for Al2O3–water nanofluid—hysteresis: is heat transfer enhancement using nanofluids reliable? Int. J. Therm. Sci. 47 (2) (2008) 103–111.
[116] E.V. Timofeeva, W. Yu, D.M. France, D. Singh, J.L. Routbort, Nanofluids for heat transfer: an engineering approach, in: Nanoscale Research Letters 6, 2011, p. 182, no. 1.
[117] M. Elias, et al., Experimental investigation on the thermo-physical properties of Al2O3 nanoparticles suspended in car radiator coolant, Int. Communicat. Heat Mass Transfer 54 (2014) 48–53.
[118] M. Pantzali, A. Kanaris, K. Antoniadis, A. Mouza, S. Paras, Effect of nanofluids on the performance of a miniature plate heat exchanger with modulated surface, Int. J. Heat Fluid Flow 30 (4) (2009) 691–699.
[119] V. Kumaresan, R. Velraj, Experimental investigation of the thermo-physical properties of water–ethylene glycol mixture based CNT nanofluids, Thermochim. Acta 545 (2012) 180–186.
[120] R. Mostafizur, R. Saidur, A.A. Aziz, M. Bhuiyan, Thermophysical properties of methanol based Al2O3 nanofluids, Int. J. Heat Mass Transf. 85 (2015) 414–419.
[121] I. Mahbubul, I. Shahrul, S. Khaleduzzaman, R. Saidur, M. Amalina, A. Turgut, Experimental investigation on effect of ultrasonication duration on colloidal dispersion and thermophysical properties of alumina–water nanofluid, Int. J. Heat Mass Transf. 88 (2015) 73–81.
[122] M.H. Esfe, S. Saedodin, M. Mahmoodi, Experimental studies on the convective heat transfer performance and thermophysical properties of MgO–water nanofluid under turbulent flow, Exp. Thermal Fluid Sci. 52 (2014) 68–78.
[123] Y. Yang, Z.G. Zhang, E.A. Grulke, W.B. Anderson, G. Wu, Heat transfer properties of nanoparticle-in-fluid dispersions (nanofluids) in laminar flow, Int. J. Heat Mass Transf. 48 (6) (2005) 1107–1116.
[124] Y. He, Y. Jin, H. Chen, Y. Ding, D. Cang, H. Lu, Heat transfer and flow behaviour of aqueous suspensions of TiO2 nanoparticles (nanofluids) flowing upward through a vertical pipe, Int. J. Heat Mass Transf. 50 (11-12) (2007) 2272–2281.
[125] J. Mewis, N.J. Wagner, Colloidal suspension rheology, Cambridge University Press, 2012.
[126] G. Batchelor, The effect of Brownian motion on the bulk stress in a suspension of spherical particles, J. Fluid Mech. 83 (1) (1977) 97–117.
[127] C. Nguyen, et al., Temperature and particle-size dependent viscosity data for water-based nanofluids–hysteresis phenomenon, Int. J. Heat Fluid Flow 28 (6) (2007) 1492–1506.
[128] H. Yarmand, et al., Graphene nanoplatelets–silver hybrid nanofluids for enhanced heat transfer, Energy Convers. Manag. 100 (2015) 419–428.
[129] S.U. Devi, S.A. Devi, Heat transfer enhancement of cu− $ al_ {2} o_ {3} $/water hybrid nanofluid flow over a stretching sheet, J. Nigerian Math Soc. 36 (2) (2017) 419–433.
[130] H. Brinkman, The viscosity of concentrated suspensions and solutions, J. Chem. Phys. 20 (4) (1952) 571.
[131] S.D. Pandey, V. Nema, Experimental analysis of heat transfer and friction factor of nanofluid as a coolant in a corrugated plate heat exchanger, Exp. Thermal Fluid Sci. 38 (2012) 248–256.
[132] J. Choi, Y. Zhang, Numerical simulation of laminar forced convection heat transfer of Al2O3–water nanofluid in a pipe with return bend, Int. J. Therm. Sci. 55 (2012) 90–102.
[133] A. Mohebbi, Prediction of specific heat and thermal conductivity of nanofluids by a combined equilibrium and non-equilibrium molecular dynamics simulation, J. Mol. Liq. 175 (2012) 51–58.
[134] E. De Robertis, et al., Application of the modulated temperature differential scanning calorimetry technique for the determination of the specific heat of copper nanofluids, Appl. Therm. Eng. 41 (2012) 10–17.
[135] M.N. Labib, M.J. Nine, H. Afrianto, H. Chung, H. Jeong, Numerical investigation on effect of base fluids and hybrid nanofluid in forced convective heat transfer, Int. J. Therm. Sci. 71 (2013) 163–171.
[136] M. Chandrasekar, S. Suresh, T. Senthilkumar, Mechanisms proposed through experimental investigations on thermophysical properties and forced convective heat transfer characteristics of various nanofluids–A review, Renew. Sust. Energ. Rev. 16 (6) (2012) 3917–3938.
[137] A. Ghadimi, R. Saidur, H. Metselaar, A review of nanofluid stability properties and characterization in stationary conditions, Int. J. Heat Mass Transf. 54 (17-18) (2011) 4051–4068.
[138] S.S. Harandi, A. Karimipour, M. Afrand, M. Akbari, A. D'Orazio, An experimental study on thermal conductivity of F-MWCNTs–Fe3O4/EG hybrid nanofluid: effects of temperature and concentration, Int. Communicat. Heat Mass Transfer 76 (2016) 171–177.
[139] S. Tavman, I. Tavman, Measurement of effective thermal conductivity of wheat as a function of moisture content, Int. Communicat. Heat Mass Transfer 25 (5) (1998) 733–741.
[140] P. Vadász, Nanofluid suspensions and bi-composite media as derivatives of interface heat transfer modeling in porous media, in: Emerging Topics in Heat and Mass Transfer in Porous Media, Springer, 2008, pp. 283–326.
[141] T.-P. Teng, Y.-H. Hung, T.-C. Teng, H.-E. Mo, H.-G. Hsu, The effect of alumina/water nanofluid particle size on thermal conductivity, Appl. Therm. Eng. 30 (14-15) (2010) 2213–2218.
[142] A. Einstein, Investigations on the Theory of the Brownian Movement, Courier Corporation, 1956.
[143] J.C. Maxwell, A treatise on electricity and magnetism, Clarendon press, 1881.

[144] D. Bruggeman, Calculation of different physical constants of heterogen substances I Dielectric constants and conductibility of mixtures from isotrop substances, Ann. Phys. 24 (8) (1935) 665–679.
[145] J. Koo, C. Kleinstreuer, A new thermal conductivity model for nanofluids, J. Nanopart. Res. 6 (6) (2004) 577–588.
[146] B. Takabi, S. Salehi, Augmentation of the heat transfer performance of a sinusoidal corrugated enclosure by employing hybrid nanofluid, Adv. Mech. Eng. 6 (2014) 147059.
[147] T. Tayebi, A.J. Chamkha, Free convection enhancement in an annulus between horizontal confocal elliptical cylinders using hybrid nanofluids, Num. Heat Transfer, Part A: Applicat. 70 (10) (2016) 1141–1156.
[148] T. Tayebi, A.J. Chamkha, Natural convection enhancement in an eccentric horizontal cylindrical annulus using hybrid nanofluids, Num. Heat Transfer, Part A: Applicat. 71 (11) (2017) 1159–1173.
[149] T. Tayebi, H.F. Öztop, A.J. Chamkha, Natural convection and entropy production in hybrid nanofluid filled-annular elliptical cavity with internal heat generation or absorption, Thermal Sci. Eng. Progress 19 (2020) 100605.
[150] T. Tayebi, A.J. Chamkha, Buoyancy-driven heat transfer enhancement in a sinusoidally heated enclosure utilizing hybrid nanofluid, Computat. Thermal Sci. 9 (5) (2017).
[151] K. Farhana, K. Kadirgama, M. Noor, M. Rahman, D. Ramasamy, A. Mahamude, CFD modelling of different properties of nanofluids in header and riser tube of flat plate solar collector, in: IOP Conference Series: Materials Science and Engineering 469, IOP Publishing, 2019, p. 012041, no. 1.
[152] E. Bellos, C. Tzivanidis, Thermal analysis of parabolic trough collector operating with mono and hybrid nanofluids, Sustainable Energy Technologies and Assessments 26 (2018) 105–115.
[153] A.A. Minea, W.M. El-Maghlany, Influence of hybrid nanofluids on the performance of parabolic trough collectors in solar thermal systems: recent findings and numerical comparison, Renew. Energy 120 (2018) 350–364.
[154] M.H. Esfe, A.A.A. Arani, M. Rezaie, W.-M. Yan, A. Karimipour, Experimental determination of thermal conductivity and dynamic viscosity of Ag–MgO/water hybrid nanofluid, Int. Communicat. Heat Mass Transfer 66 (2015) 189–195.
[155] L. Syam Sundar, A. Sousa, M.K. Singh, Heat transfer enhancement of low volume concentration of carbon nanotube-Fe3O4/water hybrid nanofluids in a tube with twisted tape inserts under turbulent flow, J. Thermal Sci. Eng. Applicat. 7 (2) (2015).
[156] L.S. Sundar, G. Otero-Irurueta, M.K. Singh, A.C. Sousa, Heat transfer and friction factor of multi-walled carbon nanotubes–Fe3O4 nanocomposite nanofluids flow in a tube with/without longitudinal strip inserts, Int. J. Heat Mass Transf. 100 (2016) 691–703.
[157] M.S. Hameed, S. Suresh, R.K. Singh, Comparative study of heat transfer and friction characteristics of water-based Alumina–copper and Alumina–CNT hybrid nanofluids in laminar flow through pipes, J. Therm. Anal. Calorim. 136 (1) (2019) 243–253.
[158] V. Kumar, A.K. Tiwari, S.K. Ghosh, Exergy analysis of hybrid nanofluids with optimum concentration in a plate heat exchanger, Mater. Res. Express 5 (6) (2018) 065022.
[159] V. Kumar, J. Sarkar, Particle ratio optimization of Al2O3-MWCNT hybrid nanofluid in minichannel heat sink for best hydrothermal performance, Appl. Therm. Eng. 165 (2020) 114546.
[160] S.K. Verma, A.K. Tiwari, S. Tiwari, D.S. Chauhan, Performance analysis of hybrid nanofluids in flat plate solar collector as an advanced working fluid, Sol. Energy 167 (2018) 231–241.
[161] L.S. Sundar, M.K. Singh, M. Ferro, A.C. Sousa, Experimental investigation of the thermal transport properties of graphene oxide/Co3O4 hybrid nanofluids, Int. Communicat. Heat Mass Transfer 84 (2017) 1–10.
[162] L.S. Sundar, M.K. Singh, A.C. Sousa, Turbulent heat transfer and friction factor of nanodiamond-nickel hybrid nanofluids flow in a tube: an experimental study, Int. J. Heat Mass Transf. 117 (2018) 223–234.
[163] L.S. Sundar, M.K. Singh, A.C. Sousa, Heat transfer and friction factor of nanodiamond-nickel hybrid nanofluids flow in a tube with longitudinal strip inserts, Int. J. Heat Mass Transf. 121 (2018) 390–401.
[164] Y. Phanindra, S. Kumar, S. Pugazhendhi, Experimental investigation on Al2O3 & Cu/Oil hybrid nano fluid using concentric tube heat exchanger, Mater. Today 5 (5) (2018) 12142–12150.
[165] G.G. Momin, Experimental investigation of mixed convection with water-Al2O3 & hybrid nanofluid in inclined tube for laminar flow, Int. J. Sci. Technol. Res. 2 (2013) 195–202.
[166] A. Moghadassi, E. Ghomi, F. Parvizian, A numerical study of water based Al2O3 and Al2O3–Cu hybrid nanofluid effect on forced convective heat transfer, Int. J. Therm. Sci. 92 (2015) 50–57.
[167] S. Suresh, K. Venkitaraj, P. Selvakumar, M. Chandrasekar, Effect of Al2O3–Cu/water hybrid nanofluid in heat transfer, Exp. Thermal Fluid Sci. 38 (2012) 54–60.
[168] T. Alam, M.-H. Kim, A comprehensive review on single phase heat transfer enhancement techniques in heat exchanger applications, Renew. Sust. Energ. Rev. 81 (2018) 813–839.
[169] S. Jayavel, Influence of flow shedding frequency on convection heat transfer from bank of circular tubes in heat exchangers under cross flow, Int. J. Heat Mass Transf. 105 (2017) 376–393.
[170] R. Deepakkumar, S. Jayavel, Air side performance of finned-tube heat exchanger with combination of circular and elliptical tubes, Appl. Therm. Eng. 119 (2017) 360–372.
[171] S. Saha, P. Langille, Heat transfer and pressure drop characteristics of laminar flow through a circular tube with longitudinal strip inserts under uniform wall heat flux, J. Heat Transf. 124 (3) (2002) 421–432.
[172] S.-S. Hsieh, I.-W. Huang, Heat transfer and pressure drop of laminar flow in horizontal tubes with/without longitudinal inserts, J. Heat Transf. 122 (3) (2000) 465–475.
[173] S.-S. Hsieh, M.-Y. Wen, Developing three-dimensional laminar mixed convection in a circular tube inserted with longitudinal strips, Int. J. Heat Mass Transf. 39 (2) (1996) 299–310.
[174] B. Prasad, A. Kumar, K. Singh, Optimization of thermo hydraulic performance in three sides artificially roughened solar air heaters, Sol. Energy 111 (2015) 313–319.
[175] B. Prasad, Thermal performance of artificially roughened solar air heaters, Sol. Energy 91 (2013) 59–67.
[176] A. Sadeghianjahromi, S. Kheradmand, H. Nemati, C.-C. Wang, Heat transfer enhancement of wavy fin-and-tube heat exchangers via innovative compound designs, Int. J. Therm. Sci. 149 (2020) 106211.
[177] S. Unger, M. Beyer, S. Gruber, R. Willner, U. Hampel, Experimental study on the air-side thermal-flow performance of additively manufactured heat exchangers with novel fin designs, Int. J. Therm. Sci. 146 (2019) 106074.
[178] R. Kumar, M.A. Rosen, Performance evaluation of a double pass PV/T solar air heater with and without fins, Appl. Therm. Eng. 31 (8–9) (2011) 1402–1410.
[179] I. Kotcioglu, S. Caliskan, V. Ozdemir, S. Baskaya, Sizing problem for a cross flow heat exchanger with wing-type vortex generator, Heat Mass Transf. 45 (10) (2009) 1239–1246.
[180] W. Hu, L. Wang, Y. Guan, W. Hu, The effect of shape of winglet vortex generator on the thermal–hydrodynamic performance of a circular tube bank fin heat exchanger, Heat Mass Transf. 53 (9) (2017) 2961–2973.
[181] A.H. Pordanjani, S. Aghakhani, M. Afrand, B. Mahmoudi, O. Mahian, S. Wongwises, An updated review on application of nanofluids in heat exchangers for saving energy, Energy Convers. Manag. 198 (2019) 111886.
[182] L. Yang, W. Ji, M. Mao, J.-n. Huang, An updated review on the properties, fabrication and application of hybrid-nanofluids along with their environmental effects, J. Clean. Prod. (2020) 120408.
[183] R.K. Shah, D.P. Sekulic, Fundamentals of heat exchanger design, John Wiley & Sons, 2003.
[184] H.H. Balla, S. Abdullah, W. MohdFaizal, R. Zulkifli, K. Sopian, Numerical study of the enhancement of heat transfer for hybrid CuO-Cu nanofluids flowing in a circular pipe, J. Oleo Sci. 62 (7) (2013) 533–539.
[185] B. Takabi, A.M. Gheitaghy, P. Tazraei, Hybrid water-based suspension of Al2O3 and Cu nanoparticles on laminar convection effectiveness, J. Thermophys. Heat Transf. (2016) 523–532, no. null.
[186] A.A. Hussien, M.Z. Abdullah, N.M. Yusop, A. Moh'd, M.A. Atieh, M. Mehrali, et al., Int. J. Heat Mass Transf. 115 (2017) 1121–1131.
[187] U. Arunachalam, M. Edwin, Experimental studies on laminar flow heat transfer in nanofluids flowing through a straight circular tube with and without V-cut twisted tape insert, Heat Mass Transf. 54 (3) (2018) 673–683.
[188] K.A. Hamid, W. Azmi, M. Nabil, R. Mamat, Experimental investigation of nanoparticle mixture ratios on TiO2–SiO2 nanofluids heat transfer performance under turbulent flow, Int. J. Heat Mass Transf. 118 (2018) 617–627.
[189] M. Nabil, W. Azmi, K. Hamid, R. Mamat, Heat transfer and friction factor of composite TiO2–SiO2 nanofluids in water-ethylene glycol (60: 40) mixture, in: IOP Conference Series: Materials Science and Engineering 257, IOP Publishing, 2017, p. 012066, no. 1.
[190] K.A. Hamid, W. Azmi, R. Mamat, K. Sharma, Heat transfer performance of TiO2–SiO2 nanofluids in a tube with wire coil inserts, Appl. Therm. Eng. 152 (2019) 275–286.
[191] A.A. Hussien, M.Z. Abdullah, N.M. Yusop, W. Al-Kouz, E. Mahmoudi, M. Mehrali, Heat transfer and entropy generation abilities of MWCNTs/GNPs hybrid nanofluids in microtubes, Entropy 21 (5) (2019) 480.
[192] A.A. Hussien, N.M. Yusop, A. Moh'd, M.Z. Abdullah, A.A. Janvekar, M. H. Elnaggar, Numerical study of heat transfer enhancement using Al 2 O 3–graphene/water hybrid nanofluid flow in mini tubes, Iranian J. Sci. Technol. Transact. 43 (4) (2019) 1989–2000.
[193] A.S. Dalkılıç, O.A. Türk, H. Mercan, S. Nakkaew, S. Wongwises, An experimental investigation on heat transfer characteristics of graphite-SiO2/water hybrid nanofluid flow in horizontal tube with various quad-channel twisted tape inserts, Int. Communicat. Heat Mass Transfer 107 (2019) 1–13.
[194] J. Sarkar, P. Ghosh, A. Adil, A review on hybrid nanofluids: recent research, development and applications, Renew. Sust. Energ. Rev. 43 (2015) 164–177.
[195] D. Madhesh, S. Kalaiselvam, Experimental study on heat transfer and rheological characteristics of hybrid nanofluids for cooling applications, J. Exp. Nanosci. 10 (15) (2015) 1194–1213.
[196] M. Bahiraei, A. Godini, A. Shahsavar, Thermal and hydraulic characteristics of a minichannel heat exchanger operated with a non-Newtonian hybrid nanofluid, J. Taiwan Inst. Chem. Eng. 84 (2018) 149–161.
[197] A. Shahsavar, A. Godini, P.T. Sardari, D. Toghraie, H. Salehipour, Impact of variable fluid properties on forced convection of Fe 3 O 4/CNT/water hybrid nanofluid in a double-pipe mini-channel heat exchanger, J. Therm. Anal. Calorim. 137 (3) (2019) 1031–1043.
[198] S.K. Singh, J. Sarkar, Energy, exergy and economic assessments of shell and tube condenser using hybrid nanofluid as coolant, Int. Communicat. Heat Mass Transfer 98 (2018) 41–48.
[199] S. Anitha, T. Thomas, V. Parthiban, M. Pichumani, What dominates heat transfer performance of hybrid nanofluid in single pass shell and tube heat exchanger? Adv. Powder Technol. 30 (12) (2019) 3107–3117.
[200] A. Karimi, M. Afrand, Numerical study on thermal performance of an air-cooled heat exchanger: effects of hybrid nanofluid, pipe arrangement and cross section, Energy Convers. Manag. 164 (2018) 615–628.

[201] R.R. Sahoo, P. Ghosh, J. Sarkar, Performance analysis of a louvered fin automotive radiator using hybrid nanofluid as coolant, Heat Transfer Asian Res. 46 (7) (2017) 978–995.
[202] R.R. Sahoo, J. Sarkar, Heat transfer performance characteristics of hybrid nanofluids as coolant in louvered fin automotive radiator, Heat Mass Transf. 53 (6) (2017) 1923–1931.
[203] G. Huminic, A. Huminic, The heat transfer performances and entropy generation analysis of hybrid nanofluids in a flattened tube, Int. J. Heat Mass Transf. 119 (2018) 813–827.
[204] G. Huminic, A. Huminic, The influence of hybrid nanofluids on the performances of elliptical tube: Recent research and numerical study, Int. J. Heat Mass Transf. 129 (2019) 132–143.
[205] M.C. Returi, R. Konijeti, A. Dasore, Heat transfer enhancement using hybrid nanofluids in spiral plate heat exchangers, Heat Transfer Asian Res. 48 (7) (2019) 3128–3143.
[206] F. Hormozi, B. ZareNezhad, H. Allahyar, An experimental investigation on the effects of surfactants on the thermal performance of hybrid nanofluids in helical coil heat exchangers, Int. Communicat. Heat Mass Transfer 78 (2016) 271–276.
[207] M. Safi, A. Ghozatloo, A. Hamidi, M. Shariaty-Niassar, Calculation of heat transfer coefficient of MWCNT-TiO2 nanofluid in plate heat exchanger, Int. J. Nanosci. Nanotechnol. 10 (3) (2014) 153–162.
[208] D. Huang, Z. Wu, B. Sunden, Effects of hybrid nanofluid mixture in plate heat exchangers, Exp. Thermal Fluid Sci. 72 (2016) 190–196.
[209] A. Bhattad, J. Sarkar, P. Ghosh, Discrete phase numerical model and experimental study of hybrid nanofluid heat transfer and pressure drop in plate heat exchanger, Int. Communicat. Heat Mass Transfer 91 (2018) 262–273.
[210] A. Bhattad, J. Sarkar, P. Ghosh, Hydrothermal performance of different alumina hybrid nanofluid types in plate heat exchanger, J. Therm. Anal. Calorim. (2019) 1–11.
[211] A. Bhattad, J. Sarkar, P. Ghosh, Experimentation on effect of particle ratio on hydrothermal performance of plate heat exchanger using hybrid nanofluid, Appl. Therm. Eng. 162 (2019) 114309.
[212] A. Bhattad, J. Sarkar, P. Ghosh, Energetic and exergetic performances of plate heat exchanger using brine-based hybrid nanofluid for milk chilling application, Heat Transfer Eng. (2019) 1–14.
[213] M. Nabil, W. Azmi, K. Hamid, R. Mamat, Experimental investigation of heat transfer and friction factor of TiO2-SiO2 nanofluids in water: ethylene glycol mixture, Int. J. Heat Mass Transf. 124 (2018) 1361–1369.
[214] R.S. Kumar, S. Jayavel, Forced convective air-cooling effect on electronic components of different geometries and orientations at flow shedding region, IEEE Trans. Compon. Packag. Manuf. Technol. 8 (4) (2018) 597–605.
[215] M. Muneeshwaran, C.-C. Wang, Thermal design aspects for improving temperature homogeneity of silicon wafer during thermal processing in microlithography, Appl. Therm. Eng. 171 (2020) 115118.
[216] P.-H. Tseng, K.-T. Tsai, A.-L. Chen, C.-C. Wang, Performance of novel liquid-cooled porous heat sink via 3-D laser additive manufacturing, Int. J. Heat Mass Transf. 137 (2019) 558–564.
[217] D. Sathishkumar and S. Jayavel, Effect of Channel Confinement and Hydraulic Diameter on Heat Transfer in a Micro-channel, Singapore, 2019: Springer Singapore, Numerical Heat Transfer and Fluid Flow, pp. 441 448.
[218] H. Shen, G. Xie, C.-C. Wang, The numerical simulation with staggered alternation locations and multi-flow directions on the thermal performance of double-layer microchannel heat sinks, Appl. Therm. Eng. 163 (2019) 114332.
[219] M.I. Hasan, A.A. Rageb, M. Yaghoubi, H. Homayoni, Influence of channel geometry on the performance of a counter flow microchannel heat exchanger, Int. J. Therm. Sci. 48 (8) (2009) 1607–1618.
[220] J. Yong, C. Teo, Mixing and heat transfer enhancement in microchannels containing converging-diverging passages, J. Heat Transf. 136 (4) (2014).
[221] R. Chein, G. Huang, Analysis of microchannel heat sink performance using nanofluids, Appl. Therm. Eng. 25 (17-18) (2005) 3104–3114.
[222] J. Koo, C. Kleinstreuer, Laminar nanofluid flow in microheat-sinks, Int. J. Heat Mass Transf. 48 (13) (2005) 2652–2661.
[223] S.P. Jang, S.U. Choi, Cooling performance of a microchannel heat sink with nanofluids, Appl. Therm. Eng. 26 (17–18) (2006) 2457–2463.
[224] L. Godson, B. Raja, D.M. Lal, S. Wongwises, Enhancement of heat transfer using nanofluids—an overview, Renew. Sust. Energ. Rev. 14 (2) (2010) 629–641.
[225] R. Nimmagadda, K. Venkatasubbaiah, Conjugate heat transfer analysis of micro-channel using novel hybrid nanofluids (Al2O3+ Ag/Water), Eur. J. Mech. B/Fluids 52 (2015) 19–27.
[226] R. Nimmagadda, K. Venkatasubbaiah, Multiphase approach on heat transfer performance of micro-channel using hybrid carbon nanofluid, in: ASME 2015 13th international conference on nanochannels, microchannels, and minichannels collocated with the ASME 2015 international technical conference and exhibition on packaging and integration of electronic and photonic microsystems, American Society of Mechanical Engineers Digital Collection, 2015.
[227] R. Nimmagadda, K. Venkatasubbaiah, Experimental and multiphase analysis of nanofluids on the conjugate performance of micro-channel at low Reynolds numbers, Heat Mass Transf. 53 (6) (2017) 2099–2115.
[228] R. Nimmagadda, K. Venkatasubbaiah, Two-phase analysis on the conjugate heat transfer performance of microchannel with Cu, Al, SWCNT, and hybrid nanofluids, J. Thermal Sci. Eng. Applicat. 9 (4) (2017).
[229] C. Uysal, E. Gedik, A. Chamkha, A numerical analysis of laminar forced convection and entropy generation of a diamond-Fe3O4/water hybrid nanofluid in a rectangular minichannel, J. Appl. Fluid Mech. 12 (2) (2019) 391–402.
[230] N. Ahammed, L.G. Asirvatham, S. Wongwises, Entropy generation analysis of graphene–alumina hybrid nanofluid in multiport minichannel heat exchanger coupled with thermoelectric cooler, Int. J. Heat Mass Transf. 103 (2016) 1084–1097.
[231] V. Kumar, J. Sarkar, Two-phase numerical simulation of hybrid nanofluid heat transfer in minichannel heat sink and experimental validation, Int. Communicat. Heat Mass Transfer 91 (2018) 239–247.
[232] M. Bahiraei, M. Jamshidmofid, M. Goodarzi, Efficacy of a hybrid nanofluid in a new microchannel heat sink equipped with both secondary channels and ribs, J. Mol. Liq. 273 (2019) 88–98.
[233] V. Kumar, J. Sarkar, Numerical and experimental investigations on heat transfer and pressure drop characteristics of Al2O3-TiO2 hybrid nanofluid in minichannel heat sink with different mixture ratio, Powder Technol. 345 (2019) 717–727.
[234] P. Selvakumar, S. Suresh, Use of ${\rm Al} _ {2}{\rm O} _ {3}\hbox {–}{\rm Cu} $/Water Hybrid Nanofluid in an Electronic Heat Sink, IEEE Trans. Compon. Packag. Manuf. Technol. 2 (10) (2012) 1600–1607.
[235] T. Ambreen, A. Saleem, H.M. Ali, S.A. Shehzad, C.W. Park, Performance analysis of hybrid nanofluid in a heat sink equipped with sharp and streamlined micro pin-fins, Powder Technol. 355 (2019) 552–563.
[236] B.D. Kusure, R. Warkhedkar, P.R. Harde, P. Shirke, Heat transfer enhancement by using nanofluids in heat pipe-a review, in: Applied Mechanics and Materials 592, Trans Tech Publ, 2014, pp. 932–938.
[237] R.K. Bumataria, N. Chavda, H. Panchal, Current research aspects in mono and hybrid nanofluid based heat pipe technologies, Heliyon 5 (5) (2019) e01627.
[238] K. Swapnil, P. Dhananjay, Z. Gaurav, R. Anand, Heat transfer enhancement of circular heat pipe with AL2O3 BN/water hybrid nanofluid, Int. J. Curr, Eng. Technol (2016) 138–143.
[239] R. Ramachandran, K. Ganesan, M. Rajkumar, L. Asirvatham, S. Wongwises, Comparative study of the effect of hybrid nanoparticle on the thermal performance of cylindrical screen mesh heat pipe, Int. Communicat. Heat Mass Transfer 76 (2016) 294–300.
[240] A. Chaudhari, S. Bhosale, Performance evaluation of circular heat pipe using (CuO+ BN)/H2O hybrid nanofluid, Int. J. Eng. Manag. Res. (IJEMR) 6 (4) (2016) 315–321.
[241] D. Kamble, P. Gadhave, M. Anwar, Enhancement of thermal performance of heat pipe using hybrid nanofluid, Int. J. Eng. Trends Technol. 17 (9) (2014) 425–428.
[242] W.-S. Han, S.-H. Rhi, Thermal characteristics of grooved heat pipe with hybrid nanofluids, Therm. Sci. 15 (1) (2011) 195–206.
[243] J.P. Ekka, K. Bala, P. Muthukumar, D.K. Kanaujiya, Performance analysis of a forced convection mixed mode horizontal solar cabinet dryer for drying of black ginger (Kaempferia parviflora) using two successive air mass flow rates, Renew. Energy 152 (2020) 55–66.
[244] G. Sureandhar, G. Srinivasan, P. Muthukumar, S. Senthilmurugan, Performance analysis of arc rib fin embedded in a solar air heater, Thermal Sci. Eng. Progress 23 (2021) 100891.
[245] D. Lakshmi, P. Muthukumar, P.K. Nayak, Experimental investigations on active solar dryers integrated with thermal storage for drying of black pepper, Renew. Energy 167 (2021) 728–739.
[246] M. Muneeshwaran, U. Sajjad, T. Ahmed, M. Amer, H.M. Ali, C.-C. Wang, Performance improvement of photovoltaic modules via temperature homogeneity improvement, Energy (2020) 117816.
[247] A. Hassan, et al., Thermal management and uniform temperature regulation of photovoltaic modules using hybrid phase change materials-nanofluids system, Renew. Energy 145 (2020) 282–293.
[248] A. Younis, E. Elsarrag, Y. Alhorr, M. Onsa, The influence of Al2O3-ZnO-H2O nanofluid on the thermodynamic performance of photovoltaic-thermal hybrid solar collector system, Innov Ener Res 7 (187) (2018), 2576-1463.1000187.
[249] F. Crisostomo, N. Hjerrild, S. Mesgari, Q. Li, R.A. Taylor, A hybrid PV/T collector using spectrally selective absorbing nanofluids, Appl. Energy 193 (2017) 1–14.
[250] N.E. Hjerrild, S. Mesgari, F. Crisostomo, J.A. Scott, R. Amal, R.A. Taylor, Hybrid PV/T enhancement using selectively absorbing Ag–SiO2/carbon nanofluids, Sol. Energy Mater. Sol. Cells 147 (2016) 281–287.
[251] P.S.T. Sai, K. Sharma, K. Devarayapalli, J.R. Rao, GO-TiO2 nano composites for silicon PV cell application, Mater. Today 2 (9) (2015) 4557–4562.
[252] M. Benkhedda, T. Boufendi, T. Tayebi, A.J. Chamkha, Convective heat transfer performance of hybrid nanofluid in a horizontal pipe considering nanoparticles shapes effect, J. Therm. Anal. Calorim. 140 (1) (2020) 411–425.
[253] S. Goudarzi, M. Shekaramiz, A. Omidvar, E. Golab, A. Karimipour, A. Karimipour, Nanoparticles migration due to thermophoresis and Brownian motion and its impact on Ag-MgO/Water hybrid nanofluid natural convection, Powder Technol. 375 (2020) 493–503.
[254] A.J. Chamkha, I.V. Miroshnichenko, M.A. Sheremet, Numerical analysis of unsteady conjugate natural convection of hybrid water-based nanofluid in a semicircular cavity, J. Thermal Sci. Eng. Applicat. 9 (4) (2017).
[255] M. Ghalambaz, A. Doostani, E. Izadpanahi, A.J. Chamkha, Conjugate natural convection flow of Ag–MgO/water hybrid nanofluid in a square cavity, J. Therm. Anal. Calorim. 139 (3) (2020) 2321–2336.
[256] M. Ghalambaz, M.A. Sheremet, S. Mehryan, F.M. Kashkooli, I. Pop, Local thermal non-equilibrium analysis of conjugate free convection within a porous enclosure occupied with Ag–MgO hybrid nanofluid, J. Therm. Anal. Calorim. 135 (2) (2019) 1381–1398.
[257] S. Mehryan, M. Ghalambaz, A.J. Chamkha, M. Izadi, Numerical study on natural convection of Ag–MgO hybrid/water nanofluid inside a porous enclosure: A local thermal non-equilibrium model, Powder Technol. 367 (2020) 443–455.
[258] B.M. Al-Srayyih, S. Gao, S.H. Hussain, Natural convection flow of a hybrid nanofluid in a square enclosure partially filled with a porous medium using a thermal non-equilibrium model, Phys. Fluids 31 (4) (2019) 043609.

[259] K. Kalidasan, P.R. Kanna, Natural convection on an open square cavity containing diagonally placed heaters and adiabatic square block and filled with hybrid nanofluid of nanodiamond-cobalt oxide/water, Int. Communicat. Heat Mass Transfer 81 (2017) 64–71.
[260] Ç. Yıldız, M. Arıcı, H. Karabay, Comparison of a theoretical and experimental thermal conductivity model on the heat transfer performance of Al2O3-SiO2/water hybrid-nanofluid, Int. J. Heat Mass Transf. 140 (2019) 598–605.
[261] S.-R. Yan, R. Kalbasi, A. Parvin, X.-X. Tian, A. Karimipour, Comparison of Nusselt number and stream function in tall and narrow enclosures in the mixed convection of hybrid nanofluid, J. Therm. Anal. Calorim. (2020) 1–11.
[262] D. Cimpean, M. Sheremet, I. Pop, Mixed convection of hybrid nanofluid in a porous trapezoidal chamber, Int. Communicat. Heat Mass Transfer 116 (2020) 104627.
[263] M. Izadi, R. Mohebbi, D. Karimi, M.A. Sheremet, Numerical simulation of natural convection heat transfer inside a$^{\perp}$ shaped cavity filled by a MWCNT-Fe3O4/water hybrid nanofluids using LBM, Chem. Eng. Process. Process Intensificat. 125 (2018) 56–66.
[264] K. Kalidasan, R. Velkennedy, P.R. Kanna, Laminar natural convection of Copper-Titania/Water hybrid nanofluid in an open ended C-shaped enclosure with an isothermal block, J. Mol. Liq. 246 (2017) 251–258.
[265] M.A. Almeshaal, K. Kalidasan, F. Askri, R. Velkennedy, A.S. Alsagri, L. Kolsi, Three-dimensional analysis on natural convection inside a T-shaped cavity with water-based CNT–aluminum oxide hybrid nanofluid, J. Therm. Anal. Calorim. 139 (3) (2020) 2089–2098.
[266] I. Zahan, R. Nasrin, M. Alim, Hybrid nanofluid flow in combined convective lid-driven sinusoidal triangular enclosure, in: AIP Conference Proceedings 2121, AIP Publishing LLC, 2019, p. 070001, no. 1.
[267] T. Tayebi, A.J. Chamkha, Entropy generation analysis during MHD natural convection flow of hybrid nanofluid in a square cavity containing a corrugated conducting block, Int. J. Num. Methods Heat & Fluid Flow 30 (2019) 1115–1136.
[268] T. Tayebi, A.J. Chamkha, Entropy generation analysis due to MHD natural convection flow in a cavity occupied with hybrid nanofluid and equipped with a conducting hollow cylinder, J. Therm. Anal. Calorim. 139 (3) (2020) 2165–2179.
[269] T. Tayebi, A.J. Chamkha, Magnetohydrodynamic natural convection heat transfer of hybrid nanofluid in a square enclosure in the presence of a wavy circular conductive cylinder, J. Thermal Sci. Eng. Applicat. 12 (3) (2020).
[270] H.R. Ashorynejad, A. Shahriari, MHD natural convection of hybrid nanofluid in an open wavy cavity, Results Phys. 9 (2018) 440–455.
[271] S. Shehzad, M. Sheikholeslami, T. Ambreen, A. Shafee, Convective MHD flow of hybrid-nanofluid within an elliptic porous enclosure, Phys. Lett. A 384 (28) (2020) 126727.
[272] K. Hosseinzadeh, S. Roghani, A. Mogharrebi, A. Asadi, D. Ganji, Optimization of hybrid nanoparticles with mixture fluid flow in an octagonal porous medium by effect of radiation and magnetic field, J. Therm. Anal. Calorim. 143 (2) (2021) 1413–1424.
[273] R.S.R. Gorla, S. Siddiqa, M. Mansour, A. Rashad, T. Salah, Heat source/sink effects on a hybrid nanofluid-filled porous cavity, J. Thermophys. Heat Transf. 31 (4) (2017) 847–857.
[274] M. Izadi, R. Mohebbi, A.A. Delouei, H. Sajjadi, Natural convection of a magnetizable hybrid nanofluid inside a porous enclosure subjected to two variable magnetic fields, Int. J. Mech. Sci. 151 (2019) 154–169.
[275] O. Mahian, et al., Recent advances in modeling and simulation of nanofluid flows-Part I: Fundamentals and theory, Phys. Rep. 790 (2019) 1–48.
[276] H. Niazmand, Recent advances in modeling and simulation of nanofluid flows—Part II: Applications, Phys. Rep. 791 (2019).
[277] A. Albojamal, K. Vafai, Analysis of single phase, discrete and mixture models, in predicting nanofluid transport, Int. J. Heat Mass Transf. 114 (2017) 225–237.
[278] H.T. Kadhim, F.A. Jabbar, A. Rona, Cu-Al2O3 hybrid nanofluid natural convection in an inclined enclosure with wavy walls partially layered by porous medium, Int. J. Mech. Sci. 186 (2020) 105889.
[279] M.S. Ahmed, A.M. Elsaid, Effect of hybrid and single nanofluids on the performance characteristics of chilled water air conditioning system, Appl. Therm. Eng. 163 (2019) 114398.
[280] B. Sun, Y. Zhang, D. Yang, H. Li, Experimental study on heat transfer characteristics of hybrid nanofluid impinging jets, Appl. Therm. Eng. 151 (2019) 556–566.
[281] A.R. Yagnem, S. Venkatachalapathy, Heat transfer enhancement studies in pool boiling using hybrid nanofluids, Thermochim. Acta 672 (2019) 93–100.
[282] M. Aizzat, M. Sulaiman, K. Enoki, T. Okawa, Heat transfer coefficient of nucleate boiling in low concentration level of single and hybrid Al2O3-SiO2 water-based nanofluids, in: IOP Conference Series: Materials Science and Engineering 469, IOP Publishing, 2019, p. 012109, no. 1.
[283] K. Hosseinzadeh, M. Alizadeh, M. Tavakoli, D. Ganji, Investigation of phase change material solidification process in a LHTESS in the presence of fins with variable thickness and hybrid nanoparticles, Appl. Therm. Eng. 152 (2019) 706–717.